DE TTK

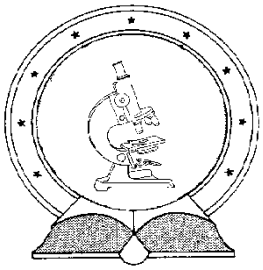

1949

The oxidation of tris(phenanthroline)iron(II) and bis(terpyridine)iron(II) complexes and the corresponding ligands by peroxomonosulfate ion: kinetics and mechanism

Ph. D. thesis

Gábor Bellér

Supervisor: *Dr. István Fábián*

University of Debrecen

PhD Program in Chemistry

Debrecen, 2015.

DE TTK

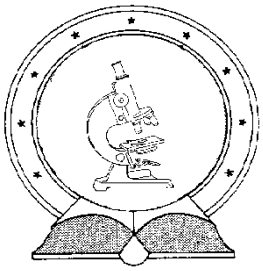

1949

The oxidation of tris(phenanthroline)iron(II) and bis(terpyridine)iron(II) complexes and the corresponding ligands by peroxomonosulfate ion: kinetics and mechanism

Ph. D. thesis

Gábor Bellér

Supervisor: *Dr. István Fábián*

University of Debrecen

PhD Program in Chemistry

Debrecen, 2015.

Ezen értekezést a Debreceni Egyetem Természettudományi Doktori Tanács Kémiai Doktori Iskola Koordinációs Kémia (K/2) programja keretében készítettem a Debreceni Egyetem természettudományi doktori (PhD) fokozatának elnyerése céljából.
Debrecen, 2015. október

Bellér Gábor

Tanúsítom, hogy Bellér Gábor doktorjelölt 2010-2015. között a fent megnevezett Doktori Iskola Koordinációs Kémia (K/2) programjának keretében irányításommal végezte munkáját. Az értekezésben foglalt eredményekhez a jelölt önálló alkotó tevékenységével meghatározóan hozzájárult. Az értekezés elfogadását javasolom.

Debrecen, 2015. október

Dr. Fábián István

The oxidation of tris(phenanthroline)iron(II) and bis(terpyridine)iron(II) complexes and the corresponding ligands by peroxomonosulfate ion: kinetics and mechanism

Értekezés a doktori (Ph.D.) fokozat megszerzése érdekében
a Kémia tudományágban

Írta: ***Bellér Gábor*** okleveles vegyész–angol-magyar szakfordító

Készült a Debreceni Egyetem Kémiai doktori iskolája
(Koordinációs kémiai, K/2 programja) keretében

Témavezető: ***Dr. Fábián István*** egyetemi tanár

A doktori szigorlati bizottság:
elnök: Dr. Bányai István egyetemi tanár (DE)
tagok: Dr. Turányi Tamás egyetemi tanár (ELTE)
Dr. Tóth Imre egyetemi tanár (DE)

A doktori szigorlat időpontja: 2013. okt. 11.

Az értekezés bírálói:
Dr. Rábai Gyula egyetemi tanár (DE)
Dr. Horváth Attila egyetemi docens (PTE)

A bírálóbizottság:
elnök: Dr. .....
tagok: Dr. .....
Dr. .....
Dr. .....
Dr. .....

Az értekezés védésének időpontja: 2015… . …… … .

“If age teaches you anything, then one of its lessons is certainly not to hurry if you're already late.”

Sergei Lukyanenko

Acknowledgements

I express my heartfelt gratitude to Prof. István Fábián and Prof. Gábor Lente for being my mentors for more than 10 years. I owe many thanks to my supervisor: István Fabián, for his great patience, unique thinking and tolerance of helping me to solve every problem even though I might not have always been a dream student during the last couple of years. I am also very grateful to Gábor Lente for introducing me into the mysteries of physical chemistry and for his constant help throughout my career.

I would also like to thank:

- Dr. József Kalmár and Dr. Árpád Kovács for their friendship and for being there for me in good and bad times.
- My family and my friends for their love, care and unconditional support.
- All the present and former members of my research group for the technical help and the friendly atmosphere.
- Zsófia Antal, Júlia Kurucz and József Darázs, undergraduate students for their contributions to the experimental work.
- Dr. Bernadett Kalmár-Biri and Tibor Nagy for their assistance in the mass spectrometric measurements.
- Richter Gedeon Tálentum Alapítvány for financially supporting my graduate studies.

I am thankful because this research was also supported by the European Union and the State of Hungary, co-financed by the European Social Fund in the framework of TÁMOP 4.2.4. A/2-11-1-2012-0001 ‘National Excellence Program’.

TABLE OF CONTENT

1) Introduction

The kinetics and mechanisms of the redox reactions of various inorganic species have extensively been studied in the Environmental Redox Mechanisms Research Group at the Department of Inorganic and Analytical Chemistry of the University of Debrecen over the last two decades. Exploring the redox features of sulfur-containing species has been one of the main objectives of these studies. Within the frame of this research program, the oxidation reactions of peroxomonosulfate ion with various substrates have been studied: metal ions (Fe^{2+}, Ce^{3+}, VO^{2+}),[1] halides or pseudohalides (Cl^-, Br^-, I^-, SCN^-),[1,2] simple biomolecules (tryptophan and its derivatives, dopamine and its derivatives), drugs (isoniazid, ethambutol, pyrazinamide) and molecules relevant in environmental chemistry (chlorophenols, trichloroethylene) have been oxidized. Lately, the use of peroxomonosulfate ion has increased rapidly in organic preparations[3] and also in industrial applications such as wastewater treatment,[4,5] bleaching,[6] microetching[7] etc. The main reasons behind its popularity are favorable features such as stability, simple handling, nontoxic nature, good solubility in water, versatility of the reagent and low costs.

During the oxidation of aqueous Fe(II), unexpectedly complex kinetic phenomena were found partly due to the noncomplementary and inner-sphere features of the redox process.[1] In order to get more insight into the intimate nature of such reactions, it seemed reasonable to study further iron(II) complexes that are more difficult to oxidize and whose oxidation is expected to proceed via outer-sphere electron transfer. Keeping this in mind, the aim of this work is the kinetic and mechanistic study of the oxidation of coordinatively saturated iron complexes and the corresponding N-heteroaromatic ligands (1,10-phenanthroline and 2,2':6',2"-terpyridine, Scheme 1) by peroxomonosulfate ion. The investigation of the oxidation of the ligands was motivated by the preliminary experiments, in which it was found that the ligands are oxidized by peroxomonosulfate ion during the course of the reactions of the complexes.

Complexes containing iron and N-heteroaromatic ligands are of huge importance in analytical, coordination chemistry, as well as in biochemistry. They are often used for modeling the interactions between substrates and iron-containing

metalloproteins. These complexes are good candidates as functional models of both heme enzymes, such as cytochrome c oxidase,[8] and nonheme iron enzymes i.e. intradiol-cleaving catechol dioxygenase.[9]

The study of the oxidation of the ligands can also be the subject of wide interest because N-heteroaromatic substrates readily form N-oxides with peroxo derivatives (hydrogen peroxide, peracetic acid, meta-chloroperoxybenzoic acid, peroxomonosulfate ion etc.). N-Oxides of heterocycles have received much attention due to their applicability as important intermediates in organic syntheses,[10,11] as protecting groups,[12] ligands in metal complexes,[13] energetic materials[14,15] and biologically relevant molecules.[16]

Abbreviated names of the studied compounds and ions:

PMS: peroxomonosulfate ion
phen: 1,10-phenanthroline
tpy: 2,2':6',2"-terpyridine
$Fe(phen)_3^{2+}$: tris(phenanthroline)iron(II) complex cation, ferroin
$Fe(phen)_3^{3+}$: tris(phenanthroline)iron(III) complex cation, ferriin
$Fe(tpy)_2^{2+}$: bis(terpyridine)iron(II) complex cation
$Fe(tpy)_2^{3+}$: bis(terpyridine)iron(III) complex cation

1,10-phenanthroline, phen

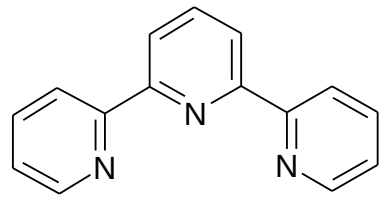

2,2':6',2"-terpyridine, tpy

Scheme 1. Structural formulae of the studied ligands

2) Literature overview

2.1 *Peroxomonosulfate ion*

Peroxomonosulfate ion,[*] primarily used in its monoprotonated form (HSO_5^-), is the anion of Caro's acid (peroxomonosulfuric acid, H_2SO_5). The pure acid is highly explosive and its large scale production is usually done on site, due to its instability. A possible way of producing this compound is reacting >85% sulfuric acid with <50% hydrogen peroxide to form a strongly acidic, highly oxidizing mixture, which is also known as "piranha solution" and frequently used to remove organic residues from glassware in the laboratory and make the surfaces hydrophilic.

Many of its salts are also instable and decompose spontaneously. Because of their explosive character, they were avoided in organic synthesis for a long time. Today, potassium peroxomonosulfate is commercially available in the form of a stable triple salt ($2KHSO_5 \cdot KHSO_4 \cdot K_2SO_4$), and marketed by Evonik under the trade name Caroat and DuPont under the trade name Oxone.

Apart from its wide industrial and consumer applications (such as decolorizing agent in denture cleansers, microetchant in electronics, shock-oxidizer for swimming pools, repulping agent in papermaking or oxidizer in wool treatment), the use of PMS is very common in organic reactions.[3,17] It was shown to be a convenient and efficient oxidant for a great variety of synthetic purposes. Numerous inexpensive, high-yield and simple procedures have been developed, which make PMS an important tool in organic chemistry (Scheme 2).

Generally, the oxidations are performed in water or water-miscible solvents such as methanol, acetone, DMF, or a mixture including one of these solvents. To overcome the need for aqueous conditions, ionic liquids were used as solvents[18] and several tetraalkylammonium salts of peroxomonosulfate have been synthesized for such purposes.[19,20]

[*] In aqueous solution, peroxomonosulfate ion is involved in acid-base equilibria. H_2SO_5 may only exist under very acidic conditions, and the equilibrium concentrations of HSO_5^- and SO_5^{2-} are determined by the actual pH. The abbreviation PMS corresponds to the total concentration of the oxidant throughout the dissertation, distinction between the protonated forms is only made when it is required by the clarity of the presentation.

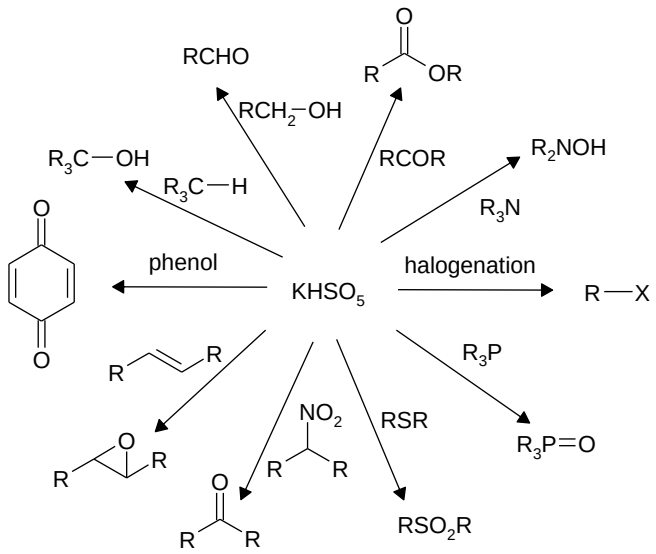

Scheme 2. Examples of the organic oxidation reactions with PMS

There are several particularly interesting reactions of PMS: oxidation of alkanes in the absence of organic solvents,[21] phase-transfer catalysis in the free-radical polymerization of acrylonitrile[22] or autocatalytic oxidations of amino acids[23] and citrate ion.[24]

With respect to this thesis, the most relevant reaction of PMS is the oxidation of nitrogen-containing heteroaromatic compounds. Several reports are found in the literature on the syntheses of N-oxides by the conversion of the derivatives of pyridine,[25] pyrazine,[26,27] quinoxaline,[27] acridine[28] or tetrazole.[29]

However, there are only limited kinetic data on these reactions.[30] It was found that the N-oxidation of nicotinic acid by PMS follows overall second order kinetics and the order with respect to both reactants is one. The rate of the reaction increases with increasing pH in acetate buffer, which was interpreted by the acid-base equilibrium of nicotinic acid and the smaller reactivity of its protonated form. The large negative activation entropy (–98 $Jmol^{-1}K^{-1}$) implies oxygen atom transfer,[1] which is expected in the case of N-oxidation.

PMS is often used as an environmentally friendly replacement of other peroxo species such as H_2O_2 or $S_2O_8^{2-}$. Its main advantage over hydrogen peroxide is easier handling and higher stability. With respect to the peroxodisulfate ion, although it has a higher standard potential: $E°(S_2O_8^{2-}/2HSO_4^-)$ = 2,12 V;[31]

$E°$ (HSO_5^-/HSO_4^-) = 1.82 V;[32] many oxidation reactions of PMS proceed faster than those of $S_2O_8^{2-}$ because the rate limiting homolysis of the latter one (1) has a large activation energy.[33]

$$S_2O_8^{2-} \rightarrow 2SO_4^{-\bullet} \quad (1)$$

There is ample kinetic information on various redox reactions of PMS. It may react via two distinct pathways. More frequently, PMS acts as a two-electron oxidant that involves the heterolytic cleavage of the peroxo bond i.e. the oxidations of bromide to hypobromite ion,[1] thiocyanate ion to hypothiocyanate ion,[2] azide ion to nitrous oxide,[34] dimethyl sulfide to dimethyl sulfoxide[35] or secondary amines to nitrones (2):[36]

$$HSO_5^- + A \rightarrow HSO_4^- + OA \quad (2)$$

In this equation, A is a reagent with an oxygen acceptor site.

In the other type of oxidation, PMS is proposed to be a one-electron oxidant forming sulfate ion radical i.e. the oxidations of Fe(II) to Fe(III)[37] or V(IV) to V(V) (3):[38]

$$HSO_5^- + e^- \rightarrow SO_4^{-\bullet} + OH^- \quad (3)$$

This process is analogous to the first step of the Fenton type reactions of hydrogen peroxide. Although the use of activation parameters as mechanistic indicators is not without problems in general, it was shown that the activation entropy may be helpful in distinguishing between the two pathways:[1] the one-electron oxidation reactions with HSO_5^- usually have relatively small negative activation entropies ($\Delta S^{\ddagger} > -50$ $Jmol^{-1}K^{-1}$), whereas two-electron oxidation steps have $\Delta S^{\ddagger}$ at around -100 $Jmol^{-1}K^{-1}$.

Although the acidic aqueous solution of the pure reagent in distilled water is relatively stable, whenever the kinetics of the reactions of PMS is studied, its spontaneous or metal catalyzed decomposition should be considered as a potential interfering reaction. Peroxomonosulfuric acid[39] and peroxycarboxilic acids (i.e. peroxyacetic acid, peroxypivalic acid or monoperoxyphthalic acid) were found to decompose to give sulfuric acid, the corresponding carboxyilic acids, and

oxygen.[40,41] When precautions were taken to eliminate metal ion catalysis, essentially quantitative yields of singlet oxygen ($^1O_2$) were obtained.[41]

The rate of the spontaneous decomposition of PMS (4) is second order with respect to the total peroxide concentration and does not proceed by a free radical mechanism. The pH dependence shows that the rate has a maximum at the pH equal to the pK_a of HSO_5^-, which indicates the presence of the mononegative (HSO_5^-) and the dinegative (SO_5^{2-}) anions in the activated complex and the rate law can be given as follows:[39]

$$HSO_5^- + SO_5^{2-} \rightarrow 2SO_4^{2-} + O_2 + H^+ \qquad (4)$$

$$v = -\frac{1}{2} \times \frac{d[\mathrm{PMS}]}{dt} = k_4'[\mathrm{PMS}]^2 = \frac{k_4[\mathrm{H^+}][\mathrm{PMS}]^2}{K_a\left(1 + \frac{[\mathrm{H^+}]}{K_a}\right)^2}$$

The decomposition is susceptible to catalysis by transition metal ions such as Co(II)[42] and Cu(I),[43] but their effect can be largely eliminated by adding a chelating agent. It was also proposed that Fe(III) can catalyze the decomposition of PMS,[44] but more recent results challenged this finding.[45]

2.2 *1,10-Phenanthroline*

1,10-Phenanthroline (phen) is a well-known bidentate ligand for transition metals,[46] it has been utilized extensively in analytical procedures and enjoys undiminished popularity as a building block in supramolecular chemistry[47] and versatile starting compound in organic chemistry.[48,49]

Although phen has two basic nitrogen atoms, it behaves as a weak monoprotic base. The acid dissociation constant of $Hphen^+$ (pK_a) has been determined by several groups, the reported values vary between 4.7 and 5.8 depending on the ionic strength.[50,51,52] Spectrophotometric evidence for the existence of a diprotonated species, H_2phen^{2+}, in strongly acidic medium ($[H^+] > 1M$) has been also published.[53] Furthermore, there are literature reports on the dimer species $H(phen)_2^+$. However, its molar fraction is relevant only in relatively concentrated solutions (higher than 7 mM).[50,51,52]

Phen is a planar, rigid, hydrophobic and electron-poor N-heteroaromatic ligand and its structural features control its coordination abilities and provide various application fields. Phen derivatives and their metal complexes have been used, for example, for cleaving DNA,[54] as antimicrobial agents,[55] catalyst for photochemical processes[56] or photoswitchable molecular devices.[57] In these systems, the mechanisms and products of the reactions of phen are of outmost relevance.

The oxidation of phen has been of interest for nearly 70 years.[58] Chemical[59,60,61] and electrochemical[62] oxidations typically lead to the dearomatization or opening of the middle ring. However, the use of peroxo compounds usually results in the N-oxidation of one of the nitrogen atoms.[48,63] Although exhaustive procedures using H_2O_2 in acetic acid (peracetic acid) or meta-chloroperoxybenzoic acid (mCPBA) readily give the di-N-oxide and tri-N-oxide of 2,2'-bipyridine[64,65] and 2,2':6',2"-terpyridine,[66] respectively, similar methods only give the mono-N-oxide (phenO) in the case of phen. The first report on the existence of 1,10-phenanthroline-N,N'-dioxide ($phenO_2$) dates back to 1946,[58] but later it was shown that the synthesis only results in the formation of phenO. Other research groups also failed to prepare $phenO_2$ for a long time.[65,67] The unsuccessful attempts and false reports on $phenO_2$ as a chelating ligand in metal complexes convinced Gillard to publish two notes concluding that „the N,N'-dioxide of 1,10-phenanthroline has not yet been made"[68] and its complexes „cannot be as described, and the claims to their existence and the descriptions of their properties should be withdrawn".[69]

The specific behavior of phen in N-oxidation was explained by its rigid structure compared to the bipyridine derivatives and the limited space in the bay area of the molecule that cannot accommodate two oxygen atoms. At last, Rozen and Dayan succeeded in forcing phen out of planarity and prepared the N,N'-dioxide by using the mixture of F_2, H_2O and CH_3CN in 1999.[70] Since the first synthesis, a couple of $phenO_2$ derivatives have been prepared.[71] However, up to now, the only published method for the synthesis is the one described by Rozen and Dayan, and it is still the prevailing opinion that $phenO_2$ cannot be produced by the use of peroxo compounds.

Although the aforementioned reports on the oxidations of phen lack the mechanistic details of the reactions, there are some kinetic studies published. The oxidation of phen by alkaline MnO_4^- shows complex kinetic behavior with fractional order dependence with respect to the organic substrate.[72] The data suggest that the oxidation proceeds via the formation of a complex between the reactants which decomposes in a slow step to yield a free radical of phen, followed by a fast step to give 2,2'-bipyridyl-3,3'-dicarboxaldehyde. This reaction is catalyzed by Cr(III) resulting in the formation of the same oxidation product.[73] In the mechanism, the formation of a complex between the phen and the Cr(III) was proposed, which reacts with MnO_4^- in the rate-determining step, resulting in the formation of a free radical, which reacts in subsequent fast steps to yield the products.

2.3 *2,2':6',2"-Terpyridine*

2,2':6',2"-Terpyridine (tpy) is one of the most prominent representative of those N-heteroaromatics that have been utilized frequently in supramolecular chemistry and helped this area to evolve from basic research into daily-life applications. A monograph has been published recently giving examples for the utilization of terpyridine-based materials in the fields of polymer science, optoelectronic devices, medicinal chemistry, nanotechnology and molecular catalysis.[74]

Tpy is a molecule with three pyridine rings connected together through the α positions of the nitrogen atoms. Because of its more hydrophobic character, it has lower solubility in water (S = 5.4 mM) than phen (S = 18.8 mM).[52] Despite the three nitrogen atoms, the addition of three protons is very difficult and the first pK_a would be negative.[75] Instead, it acts as a diprotic base with macroconstants of pK_{a1} ~ 3.5 and pK_{a2} ~ 4.5.[52,76] According to the literature, the asymmetric doubly protonated form is assumed to have no appreciable formation and tpy can bond two protons only when they are in nonadjacent positions. The symmetric form dissociates to give the asymmetric monoprotonated $Htpy^+_a$, which is in tautomeric equilibrium with the symmetric form, $Htpy^+_s$. Both singly protonated species dissociate to give the free base, tpy.[77] Obviously, it is impossible to determine the

microconstants by using only spectrophotometry or potentiometry, and the two monoprotic forms cannot be distinguished without additional information or assumptions.

Tpy has also been extensively studied as a chelating agent and it readily reacts with M^{n+} metal ions to give octahedral $[M(tpy)_2]^{n+}$ complexes, which differ structurally from the related $M(bipy)_3^{n+}$ or $M(phen)_3^{n+}$ complexes in being achiral which becomes important when considering multinuclear systems.[78] Although tpy commonly acts as a terdentate donor, rare examples of the ligand acting as a bidentate or monodentate donor have been also reported.[79] Both phen and tpy are π-acceptors and tend to stabilize metals in lower oxidation states. This is demonstrated, for instance, by the high standard electrode potential (both about 1.1 V) of the phen ($Fe(phen)_3^{3+}/Fe(phen)_3^{2+}$)[80] and tpy systems ($Fe(tpy)_2^{3+}/Fe(tpy)_2^{2+}$),[81] compared to the Fe^{3+}/Fe^{2+} = 0.77 V redox pair.

In oxidation reactions with peroxo type oxidants, tpy behaves similarly to phen and gives N-oxides. Whereas the preparation of the tri-N-oxide ($tpyO_3$) was described more than 50 years ago,[66] the mono-and di-N-oxides remained unknown for a while. The tri-N-oxide has efficiently been prepared by the reaction of tpy with 30% hydrogen peroxide in acetic acid at 80 °C, but the lower N-oxides were not observed in this reaction. On the other hand, the use of mCPBA provided both the mono-N-oxide (tpyO) and the di-N-oxide ($tpyO_2$).[82] It was found that the formation of tpyO and $tpyO_2$ can be controlled by using a suitable ratio of the reactants, with an optimum reaction time. The indirect N-oxidation of tpy by PMS was also reported with the formation of the di-N-oxide derivative.[26] In this procedure, the actual oxidant was dimethyldioxirane which was prepared in the reaction of PMS with acetone.

Similarly to the mono- and deprotonated forms of tpy, there are asymmetric and symmetric isomers of both the mono-($tpyO_a$ and $tpyO_s$) and di-N-oxides ($tpyO_{2a}$ and $tpyO_{2s}$). The above mentioned syntheses only gave $tpyO_a$ and $tpyO_{2s}$. The first example of a tpy containing N-oxide at the central pyridine ring was prepared by a Stille coupling reaction of 2,6-dibromopyridine with tributyl(pyridin-2-yl)stannane. The oxidation of $tpyO_s$ by a stoichiometric amount of mCPBA resulted in the formation of $tpyO_{2a}$.[83] Since then, new families of chiral tpy mono-

N-oxide and di-N-oxide ligands were successfully synthesized in simple oxidation reactions by mCPBA and their copper(II) complexes were found to be highly effective catalysts for asymmetric cyclopropanation.[84]

2.4 *1,10-Phenanthroline complexes of iron*

The intensely red colored tris complex of iron(II) and phen is used extensively for the colorimetric determination of iron and as an oxidation-reduction indicator. The indicator use of this compound is due to the rather fast and reversible transformation to the corresponding blue-colored iron(III) complex and the interconversion between the two species is often used to visualize otherwise less obvious changes in reactions showing exotic kinetic phenomena.

The reduced complex has high thermodynamic stability ($\lg\beta$ = 21.4)[85,86] which is primarily connected to a high-spin to low-spin transition in the electronic structure during the stepwise complex formation between the bis and tris complexes (7). In this reaction sequence, 7 is the rate-determining step, while 5 and 6 represent rapidly established equilibria:

$$Fe^{2+} + phen \rightleftharpoons Fe(phen)^{2+} \quad (5)$$

$$Fe(phen)^{2+} + phen \rightleftharpoons Fe(phen)_2^{2+} \quad (6)$$

$$Fe(phen)_2^{2+} + phen \rightleftharpoons Fe(phen)_3^{2+} \quad (7)$$

Apart from the tris complex, the equations for the formation of $Fe(phen)_3^{2+}$, indicate two additional iron-phenanthroline species: $Fe(phen)^{2+}$ and $Fe(phen)_2^{2+}$. Early colorimetric investigation of the iron(II)-phen reaction had indicated only $Fe(phen)_3^{2+}$ in solution under the usual analytical conditions. This is essentially true. However, the existence of $Fe(phen)^{2+}$ under special conditions was observed (high iron(II) concentration and high acidity are favorable for the formation of iron complexes containing less than three molecules of the ligand).[86] The monophenanthroline complex is of pale yellow color and has a $\lg\beta$ = 5.9.[87] The ion $Fe(phen)_2^{2+}$ apparently does not exist in appreciable concentrations in solutions.

The Fe(III) – phen system is somewhat more difficult to study. Direct mixing of the reagents does not result in the formation of the complex, it can only be synthesized by oxidizing $Fe(phen)_3^{2+}$.[88] The standard electrode potential

between the two forms is 1.06 V in 1.0 M H_2SO_4,[89] so it actually takes a strong oxidizing agent to prepare the iron(III) complex, for instance, lead(IV) oxide, chlorine or cerium(IV) are suitable for this purpose. Knowing the stability constant of the iron(II) complex and the redox potentials of the ferrous/ferric and ferroin/ferriin systems, it was possible to calculate the stability constant of $Fe(phen)_3^{3+}$, $\lg\beta$ = 15 in 1 M H_2SO_4.[85] The stability constant of Fe(III) complex increases with increasing sulfuric acid concentration.[85] This unexpected finding was interpreted by assuming that the complex possesses a proton in solutions of high acidity, $FeH(phen)_3^{4+}$.

Both tris complexes undergo proton-assisted dissociation under acidic conditions. The Fe(II) complex is stable in aqueous solution in the pH range 3–9. Below this range, there is noticeable dissociation of the complex, but only the removal of the third phen molecule proceeds at a measurable rate (reverse step of 7). Thus, the dissociation of $Fe(phen)_3^{2+}$ is a first order reaction with respect to the complex and independent of the acid concentration. The dissociation has a half-life of about 2.5-3 hours.[86,90]

The rate of dissociation of $Fe(phen)_3^{3+}$ was determined by measuring the rate of decrease of the electromotive force of a cell containing the ferrous/ferric and ferroin/ferriin systems. In 1 M H_2SO_4, the half-life was found to be about 4 hours.[86] Later, the dissociation was reinvestigated by a spectrophotometric method, which seems more reliable, and a half-life of approximately 8 hours was determined.[91] Both groups clearly agree on that the rate constant for the first order reaction decreases with increasing acid concentration.

The $Fe(phen)_3^{3+}$ complex is often used as a coordinatively saturated, strong, one-electron oxidant.[92,93,94] In some cases, the N-oxide of the ligand (phenO) was found among the primary oxidation products either in acidic[95] or basic solutions.[96] The iron(III) complex can also oxidize ferrous ion in a fast process resulting in the formation of the iron(II) complex and ferric ion.[97,98,99]

The oxidation reactions of $Fe(phen)_3^{2+}$ have been extensively studied. Based on the results of several redox reactions, a general classification was suggested whether or not $Fe(phen)_3^{3+}$ is formed as a product.[100]

The reactions of the first group are first order with respect to the reactants and usually require acidic solutions. These reactions, which involve one equivalent of the oxidizing agents, proceed via an outer-sphere path since electron transfer takes place rapidly and the first coordination sphere of the iron complex remains unchanged throughout the process. Oxidations by ClO_2,[100] Cl_2,[101] Co(III),[102] Ce(IV),[103] and Mn(III)[104] fall into this group.

The reactions of the second group usually take place in a wider pH range, their rates are controlled by the dissociation of one ligand (reverse step of 7), and are often independent of the oxidant concentration. These reactions involve multiequivalent oxidants. Reactions with chlorite ion,[100] peroxodisphosphate ion[105] and hydrogen peroxide[106] are in the second group since they are slower and do not give the corresponding Fe(III) complex.

Some multielectron oxidants such as Cr(VI),[107] lead dioxide and peroxodisulfate ion[108] react with $Fe(phen)_3^{2+}$ to form $Fe(phen)_3^{3+}$. These noncomplementary redox reactions belong to the first group, and their mechanism must involve single-equivalent processes. For example, Cr(V) has been postulated as an intermediate in the $Fe(phen)_3^{2+}$-Cr(VI) reaction.[107] Although no kinetic studies have been reported on the $Fe(phen)_3^{2+}$-PbO_2 reaction, formation of Pb(III) as an intermediate could be assumed since $Fe(phen)_3^{3+}$ is the product. Sulfate radical is also proposed as an intermediate in the $Fe(phen)_3^{2+}$-peroxodisulfate ion reaction.[108] In this oxidation, ion pair formation of the reactants was assumed, which undergoes decomposition producing the Fe(III) complex, sulfate ion and the sulfate radical.[109] The re-investigation of the reaction did not rule out the possibility of ion pairing but questioned the effect due to the limited evidence found.[110]

The oxidation by bromate ion features duality in the behavior depending on the ratios of the reactants and acidity: at $[BrO_3^-] \sim [Fe(phen)_3^{2+}]$, the rate-determining step is the removal of a ligand molecule from the tris(phenanthroline)iron(II),[111] whereas at $[BrO_3^-] >> [Fe(phen)_3^{2+}]$ the reaction is autocatalytic and produces $Fe(phen)_3^{3+}$ fast.[112] Trigger waves were also described in the acidic bromate oxidation of the iron(II) complex.[113] In an unstirred thin film of solution, a single trigger wave of chemical reactivity may develop and subsequently propagate, converting the reaction mixture from the reduced state to

the oxidized state. Because the reaction is nonoscillatory, the trigger wave behavior in the $Fe(phen)_3^{2+}$ – bromate system is a spatial analogue of bistability in the CSTR experiments and thus the coexistence of kinetic states and spatial bistability are considered.

The knowledge of the kinetics and mechanism of reactions between bromate ion and one-electron reductants with formal redox potentials higher than 1 V, e.g. Ce(III), $Fe(phen)_3^{2+}$ is fundamental to the understanding of the Belousov-Zhabotinskii oscillating systems. The iron-phen complexes play an important role in the history of the BZ reaction: a small amount of the Fe(II) complex was often added to a BZ mixture in order to visualize the periodic changes better. Later, it was observed that $Fe(phen)_3^{2+}$ itself can also catalyze the reaction.[114]

There are also reports when the concentration of the iron(II)phenanthroline complex exhibits nonmonotonous temporal dependence in relatively simple chemical or electrochemical oxidation reactions.[115] Such is the case in the present thesis, too. The study of this unusual temporal dependence of $Fe(phen)_3^{2+}$ as a reactant could contribute to the elucidation of the complex dynamic behavior of systems containing the ferroin-ferriin redox couple.

Some kinetic results on the reaction of PMS with $Fe(phen)_3^{2+}$ have already been published.[116] However, our experiments failed to reproduce the findings reported in that work, which described very simple kinetics. One of the aims of this thesis is to give a consistent mechanism for the process.

2.5 *2,2':6',2"-Terpyridine complexes of iron*

The iron – tpy system has been studied less than the closely related iron – bipyridine and iron – phenanthroline systems. The bis(terpyridine)iron(II) complex is characterized by an intense purple color and a high thermodynamic stability ($\lg\beta = 20.4$).[75] The stability of this type of complex can be explained by the strong metal–ligand (d–π^*) back donation. Furthermore, a strong chelate effect is present.

Its use as an analytical reagent dates back to the 1930s when a method was described for the determination of iron in sea water and in marine plankton.[117] More recently, the tpy complexes of transition metal ions such as iron(II), ruthenium(II) or nickel(II), have been applied in metallo-supramolecular chemistry,

where the metal centers are used to control self-organization processes or used for photophysical purposes.[118]

Although there are crystallographic and magnetic data on halide monoterpyridine iron(II) complexes,[119,120] they undergo disproportionation rapidly in water[121] and the information on $Fe(tpy)^{2+}$ in aqueous solutions is very limited.[75,122] However, the derivatives of the mono complex are found to be selective and efficient catalysts for hydrosilylation of olefins in organic solvents.[123,124]

Similarly to the iron(III) tris complex of phen, direct addition of terpyridine to Fe(III) salts does not result in the formation of $Fe(tpy)_2^{3+}$. In acidic medium, on the other hand, oxidizing agents, such as chlorine, cerium(IV) and lead(IV) oxide, are able to produce $Fe(tpy)_2^{3+}$ from the corresponding iron(II) complex and change the color from purple to green or yellow depending on the counter anion and the acidity.[125]

Concerning the redox properties, the iron(III)bisterpyridine behaves similarly to the corresponding phenanthroline and bipyridine complexes and reduction occurs in solutions except in strongly acidic conditions. The instability of the oxidized form excludes the use of this compound as oxidation-reduction indicator.

In acidic solutions, the bis complexes of both oxidation states dissociate to give the protonated ligand and noncomplexed metal ions. The pH dependence of the rate of acid dissociation of $Fe(tpy)_2^{2+}$ has been well studied.[126,127] Rates of the proton-assisted dissociation of the complexes containing bidentate nitrogen-donor ligands generally vary with acid concentration when the leaving group is flexible, for example bipyridine or ethylenediamine, as a result of reaction paths involving species containing unidentate protonated ligands. But when the bidentate ligand is rigid, like in the case of phenanthroline, dissociation rates are independent of acid concentration because it is not possible to protonate the ligand while it is bonded to the metal ion. The rate of proton-assisted dissociation of the $Fe(tpy)_2^{2+}$ depends, as expected, on the acid concentration. The observed first order rate constant increases as the concentration of acid increases until a limiting rate in a *ca*. 4 M acid. According to the literature, the iron(III)bisterpyridine dissociates significantly

faster than the corresponding phenanthroline and bipyridine complexes, and the half-life of the first order decomposition in 0.5 M H_2SO_4 is 6.4 minutes.[128]

There are several reports in the literature on the kinetics of the oxidation of the bis complex both in strongly and mildly (in acetate buffer) acidic conditions.

With O_3,[129] Ce(IV),[130] Mn(IV),[131] Mn(III),[132] and Co(III)[133] the oxidation is fast. The stopped-flow technique was used for monitoring the absorbance change and the reaction is first order with respect to both reactants, second order overall, except for the O_3 oxidation. In the latter case, the kinetics with excess ozone does not obey a simple first order rate equation, but became nearly first order with respect to $Fe(tpy)_2^{2+}$ if NaCl was added to the solutions. According to the proposed mechanism, a one electron transfer reaction occurs between $Fe(tpy)_2^{2+}$ and O_3, forming ozonide ion, O_3^-, which decomposes rapidly to form OH radical in acidic solutions. The role of Cl^- is interpreted to scavenge the OH radical, and the resulting Cl_2^- radical causes additional oxidation of $Fe(tpy)_2^{2+}$. All of these oxidations were run under strongly acidic conditions (pH < 2), the corresponding iron(III) complex was identified as the oxidation product and the reactions were fast enough to neglect the proton-assisted dissociations of both complexes.

However, in the case of the oxidations by BrO_3^- and IO_4^-, the reactions are significantly slower.[134] At the applied acidity ($[H^+]$ = 0.02 M), the iron(II) complex hardly dissociates. On the other hand, both the previous literature reports[99,128] and our own experiments indicate that the iron(III) complex does decompose at a significant rate (k_{obs} ~ 0.1 min^{-1}), whereas the pseudo-first order constants of the oxidations are in the range of 0.01–0.1 min^{-1}. Still, the proton-induced dissociation was not considered in the mechanism at all.

The Ru(III)-catalyzed oxidation by bromate ion[135] and the Ag(I)-catalyzed oxidation by peroxodisulfate ion[136] were studied in acetate buffer. In both systems, rather simple rate equations were found and the reactions follow first order kinetics with respect to the substrate, the oxidant and Ru(III), meanwhile the order with respect to Ag(I) is fractional. In both oxidations, the reported product is the corresponding iron(III) complex. According to the authors, the main difference between the two reactions is that the undissociated iron(II) complex is the reactive species in the BrO_3^--oxidation, whereas the dissociation of $Fe(tpy)_2^{2+}$ is an essential

prerequisite for the oxidation by peroxodisulfate ion and the product formed (the mono tpy complex of Fe^{3+}) is labile and readily converts to $Fe(terpy)_2^{3+}$. The latter assumption for iron(III)-polypyridyl (such as phenanthroline, bipyridine, terpyridine etc.) complexes is rather improbable because, unlike the corresponding iron(II) complexes, their formations do not tend to occur via stepwise coordination of the ligands. Instead, the oxidation of the undissociated Fe(II) complex is the feasible way. For instance, once the partially dissociated bis(phenanthroline)iron(II) complex is formed, the final oxidation product is very unlikely to be $Fe(phen)_3^{3+}$.[100]

3) Objectives

In recent decades, peroxomonosulfate ion has been enjoying increasing popularity in oxidation processes due to its favorable properties. Detailed stoichiometric and kinetic studies on the redox reactions of this powerful nonchlorine oxidizing agent and elucidation of the often complex mechanisms of these reactions may contribute to the wider industrial application of PMS and help to gain a better understanding of advanced oxidation processes.

Some kinetic results on the reaction of PMS with $Fe(phen)_3^{2+}$ has already been published.[116] However, our experiments could not reproduce the findings reported in that work, which described very simple kinetics. One of the aims of this study is to give a consistent mechanism for the process.

The ferroin-ferriin redox couple is widely considered as an innocent redox indicator but decomposition reactions of these complexes may be a major source of unwanted interference and are of primary importance in any analytical applications. These processes also offer some fundamental insight into the redox chemistry of metal complexes. In certain reactions, $Fe(phen)_3^{2+}$ exhibits nonmonotonous temporal dependence[115] and the study of such unusual phenomenon could contribute to understand systems of complex dynamic behavior.

The objective of the present thesis is to explore the kinetics of the oxidation reactions of PMS with noncomplementary reductants, such as $Fe(phen)_3^{2+}$ and $Fe(tpy)_2^{2+}$, provide a detailed mechanisms for the systems and clarify the questions[100] or contradictions[116,136] regarding the oxidation pathways of the complexes.

4) Experimental section

4.1 *Reagents and solutions*

Doubly deionized and ultrafiltered water from a Millipore Q system was used to prepare the stock solutions and samples.

Potassium peroxomonosulfate stock solutions were freshly prepared every day from Oxone ($2KHSO_5 \cdot KHSO_4 \cdot K_2SO_4$, Aldrich) and standardized by iodometric titration. These acidic stock solutions were found to be stable for at least 24 h.

1,10-Phenanthroline ($C_{12}H_8N_2 \cdot H_2O$) was purchased from POCH (Polskie Odczynniki Chemiczne), and its purity was tested by pH metric titration. 2,2':6',2"-Terpyridine was acquired from Sigma Aldrich. All chemicals utilized in this study were of analytical reagent grade, purchased from commercial sources and used as received without further purification.

The constant pH of the reaction mixtures were maintained by either using different buffer systems ($H_3PO_4/H_2PO_4^-$, CH_3COOH/CH_3COO^-, $H_2PO_4^-/HPO_4^{2-}$ and $B(OH)_3/B(OH)_4^-$) or by a sufficient amount of strong acid (H_2SO_4, $HClO_4$) or strong base (NaOH). Sodium hydroxide solutions were standardized with potassium hydrogen phtalate, and the concentrations of H_2SO_4 or $HClO_4$ solutions were determined with the standardized NaOH.

With the exception of few kinetic runs, the ionic strength was kept constant by using excess of strong acid (H_2SO_4 or $HClO_4$) or by the addition of appropriate amounts of inert salts ($NaNO_3$, $NaClO_4$ or Na_2SO_4) in all experiments.

1,10-Phenanthroline-mono-N-oxide was prepared from phenanthroline by oxidation with PMS at controlled acidity. An almost saturated aqueous solution of phenanthroline was prepared, calculated amount of PMS was added and the mixture was stirred at 40-50 °C for about 14 hours. The reaction was monitored by UV-vis spectrophotometry. The product was identified by ^{1}H-NMR analysis, which was done in D_2O and only showed the signals of the desired product. The aqueous stock solution was stable for month and was diluted to prepare the samples.

The iron(II) complexes were prepared by directly reacting iron(II) sulfate ($FeSO_4 \cdot 7H_2O$, Reanal) and the corresponding ligand at controlled acidity. The

complexes were precipitated with a large excess of perchlorate ion from the concentrated solution. The product was soluble enough in pure water to prepare samples with the concentration required in the kinetic study. The stock solutions of the iron(II) complexes were stable for months. The concentrations of these samples were standardized by UV-vis spectrophotometry using the molar absorption coefficients of the complexes: λ_{max} = 552 nm and ε = 1.222 × 10^4 $M^{-1}cm^{-1}$ for $Fe(tpy)_2^{2+}$, λ_{max} = 510 nm and ε = 1.095 × 10^4 $M^{-1}cm^{-1}$ for $Fe(phen)_3^{2+}$.

4.2 *The preparation of the Fe(III) complexes*

The tris(phen)iron(II) complex is easily prepared by mixing iron(II) and the ligand at a suitable pH. The tris(phen)iron(III) complex, however, can only be synthesized by oxidizing $Fe(phen)_3^{2+}$.[88] The typical chemical oxidants used for this purpose are lead(IV) oxide, ozone or chlorine.

Oxidation with chlorine and ozone gave much inferior results. Ozone only gave quite low yields of $Fe(phen)_3^{3+}$. Introduction of gaseous chlorine, on the other hand, turned the red $Fe(phen)_3^{2+}$ solution blue within minutes. However, excess dissolved chlorine was difficult to remove from the resulting solution and was a major source if irreproducibility. In addition, the by-product of the process chloride ion, poses a problem because PMS used in this study also oxidizes Cl^-.[1] Attempts to remove chlorine and chloride ion simultaneously are seriously hindered by the time limitations set by the decomposition of the desired product $Fe(phen)_3^{3+}$.

The use of lead(IV) oxide, however, has distinct advantages: the oxidant is solid, and the oxidation byproduct lead(II) sulfate is also insoluble in the sulfuric acid medium used for the reaction. Therefore, a reasonably pure solution of $Fe(phen)_3^{3+}$ can be obtained in this way. Two aspects are usually not emphasized in the relevant literature, although they are crucial in the process. First of all, the synthesis reaction needs to be carefully timed. The optimal reaction time depends on the initial concentration of the Fe(II) complex, acidity, overall reactor volume and stirring speed. Even a 30% deviation from the optimal reaction time could result in significant difference in the $Fe(phen)_3^{3+}$ concentration and seriously decrease the reproducibility of later kinetic experiments. The other important factor is the method of filtration. Simple decantation was not enough to obtain

reproducible results with the prepared sample because small amounts of lead(IV) oxide remained in the solutions. Thus, filtration on a glass filter was imperative. Contact with filter paper must be entirely avoided. This second criterion is quite understandable because the iron(III) complex is a strong oxidant and the filter paper is an oxidizable material. It should be pointed out that the filter material does not only influence the yield of $Fe(phen)_3^{3+}$ but also the reproducibility of the subsequent experiments.

The need for careful reaction timing is most probably necessary because $Fe(phen)_3^{3+}$ decomposes and the ligand may also be further oxidized by excess lead(IV) oxide. These processes can lead to the formation of phenanthroline-mono-N-oxide, which is involved in side reactions as it will be shown later in the dissertation (see Ch. 5. 2).

The procedure for the preparation of tris(phen)iron(III) complex: solid lead(IV) oxide (about 4 times excess) was dispersed in sulfuric acid, $Fe(phen)_3^{2+}$ was added and the mixture was intensely stirred. Under the applied conditions (~2 M H_2SO_4, 25 ºC, ~1 mM $Fe(phen)_3^{2+}$, ~2 mM PbO_2), a stirring time of 16-18 minutes was ideal.

Similar considerations are valid for the Fe(III) complex of tpy: direct mixing of the metal ion and the ligand does not result in the formation of $Fe(tpy)_2^{3+}$. However, the oxidation of the corresponding iron(II) complex is feasible in this case, too.

Two oxidants, Pb(IV) oxide and Ce(IV), were used to produce $Fe(tpy)_2^{3+}$ and each served different purposes.

Similarly to $Fe(phen)_3^{2+}$,[103] Ce(IV) oxidizes $Fe(tpy)_2^{2+}$ in a fast reaction with a rate constant of 2.0×10^5 $M^{-1}s^{-1}$. This provides a rapid and quantitative conversion of the iron(II) complex into the iron(III) one without the interference of the dissociations of the complexes. By using Ce(IV), a reliable molar spectrum of the product was easily obtained and the proton-assisted dissociation of $Fe(tpy)_2^{3+}$ was investigated in further experiments (Ch. 5.4). However, from preparative point of view this is not the most advantageous way to produce bis(terpyridine)iron(III) because the by-product of the oxidation, Ce(III), is also oxidized by PMS.[1]

Consequently, when $Fe(tpy)_2^{3+}$ is used in experiments where PMS is present, the removal of Ce(III) would have been required.

This problem can be circumvented by lead dioxide as oxidant. In the case of the oxidation by PbO_2, the excess of oxidant and the by-product of the reaction ($PbSO_4$) can be removed by filtration. In this procedure, it was necessary to use a large excess of oxidant in order to achieve shorter time for the oxidation because the rate of the dissociation of $Fe(tpy)_2^{3+}$ is significantly faster than that of $Fe(phen)_3^{3+}$. The optimal conditions found: ~0.3 M H_2SO_4, 25 ºC, ~0.4 mM $Fe(tpy)_2^{2+}$, ~35 mM PbO_2 and a stirring time of 1 minute. The filtration was carried out by a glass filter.

It should be mentioned that the yield of $Fe(tpy)_2^{3+}$ was about 80-85 % and a small amount (1-3 %) of the iron(II) complex remained unconverted. From the addition of the iron(II) complex to the acidic solution until starting to record the spectrum of the iron(III) complex, the procedure takes at least 2-2.5 minutes during which time both complexes dissociate to some extent. Thus, the smaller efficiency was most probably due to the more time-consuming procedure and the relatively fast dissociations of the complexes. Yet, to investigate the effect of $Fe(tpy)_2^{3+}$ on the reaction of $Fe(tpy)_2^{2+}$ with PMS (Ch. 5.5), this method was preferable to obtain the iron(III) complex.

The bis(tpy)iron(III) produced in this method was only used in experiments where the freshly prepared $Fe(tpy)_2^{3+}$ was added to solutions in which the initial concentration of the iron(II) complex was significantly larger compared to the $Fe(tpy)_2^{2+}$ impurity of the Fe(III) complex and merely qualitative conclusions were drawn from these measurements.

4.3 *Experimental techniques*

UV-Vis spectra and kinetic curves were recorded on *Perkin Elmer Lambda 25*, *Shimadzu UV 1800* scanning, and *HP-8543* diode-array spectrophotometers at constant temperature maintained by the use of different thermostats with the various instruments. All measurements were performed at 25.0 ± 0.1 °C except for the temperature dependence studies. Standard 1.000 cm or 0.500 cm or tandem (0.846 cm) quartz cuvettes were used.

Fast kinetic experiments were carried out in an *Applied Photophysics SX 18-MV* stopped-flow instrument. Absorbance traces were collected in an optical cell of 1.000 cm path length. The kinetic runs were repeated 3-5 times and the recorded signals were averaged to increase the signal-to-noise ratio. The oxidations of Fe(II) by $Fe(phen)_3^{3+}$ and $Fe(tpy)_2^{2+}$ by Ce(IV) were studied by this method. These reactions are not discussed in details in the thesis. Both of them follow straightforward second order kinetics and only the rate constants are shown.

The pH metric and iodometric measurements were performed with a *Metrohm 785 DMP Titrino* automatic titrator equipped with *6.0262.100* and *6.0451.100* combined electrodes, respectively. The pH electrode was calibrated by two buffers according to IUPAC recommendations.[137] The pH readings were converted to hydrogen ion concentration as described by Irving et al.[138] The procedure and the evaluation of the titrations in the temperature dependence of the pK_a of phen were carried out as described by Szabó et. al.[139]

Electrospray ionization mass spectrometric (ESI-MS) analysis and collision induced dissociation (CID) measurements were carried out by a *MicrOTOF-Q* instrument (Bruker Daltonik, Bremen, Germany) in the positive ion mode. The mass spectra were calibrated using the exact masses of the clusters generated from the electrosprayed solution of sodium trifluoroacetate (NaTFA). The spectra were analyzed with the *DataAnalysis 3.4* software from Bruker. The aim of the MS experiments was to identify the intermediates and products of the reactions in a quick and sensitive, but qualitative way.

Collision induced dissociation (CID) is a mass spectrometric technique to induce fragment of molecular ions in the gas phase. The molecular ions are usually accelerated by an electrical potential to high kinetic energy and then collide with neutral molecules (e.g. He, N_2 or Ar). The collision results in bond breakage and the fragmentation of the molecular ion into smaller fragments. The product ions produced by CID are extremely useful for the identification and characterization of the precursor ions and for complex mixture analysis.

^{1}H-NMR spectroscopic measurements were run on a *Bruker 360 MHz* spectrometer. The NMR spectra were referenced on the residual signal of the solvent (D_2O).

4.4 *Combined pH potentiometric and spectrophotometric titrations*

The pK_a of phen, phenO and PMS and the molar spectra of the species involved in the equilibria were determined by a combined pH potentiometric and spectrophotometric method. The spectra of the samples were recorded on a *HP-8453* diode array spectrophotometer at constant temperature in the 200–400 nm wavelength range. It was tested that the light source of the spectrophotometer does not induce unwanted photochemical effects in this system.[140] Standard 1.000 cm quartz cuvettes were used. Acidified solutions (ionic strength is set to the desired value) were titrated with standardized NaOH solution in a home-built flow-through titrating system (Scheme 3).

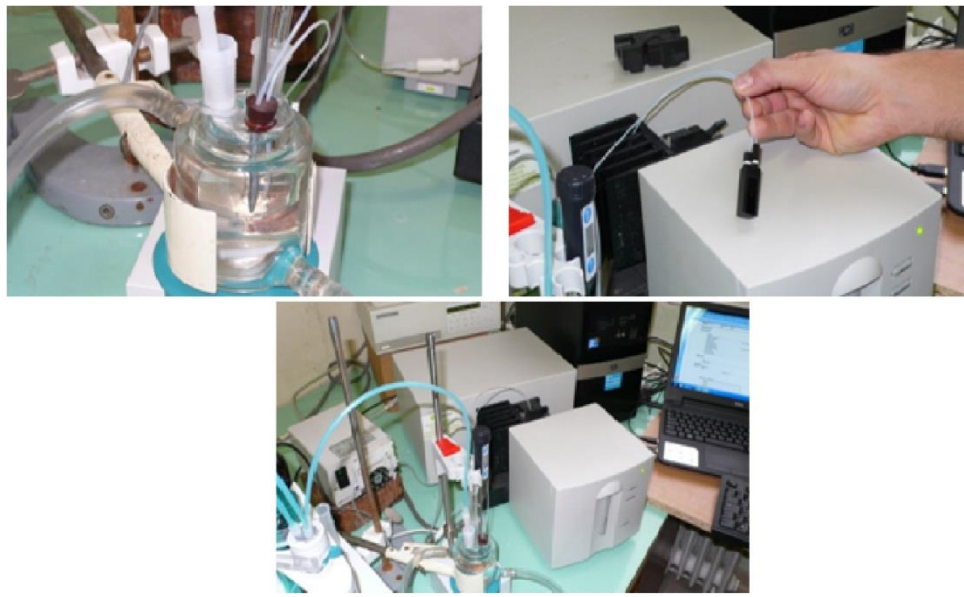

Scheme 3. The home-built flow-through titrating system. Picture 1: The thermostated closed titrating vessel with the pH electrode, the immersed nozzle of the burette and a Pt-100 thermometer. Picture 2: The flow-through optical cell. Picture 3: The complete system.

The central piece of the titrating system is a thermostated closed vessel, which is connected to a flow-through optical cell via a peristaltic pump. The liquid in the vessel is stirred with a magnetic stirrer. The combined pH electrode, a thermometer and the nozzle of the burette are immersed into the vessel. The solution is continuously circulated between the titration vessel and the optical cell,

each kept at the same temperature. After adding a sufficient aliquot of titrating solution to the sample, the pH is measured and the spectrum of the solution is recorded with the diode array spectrophotometer equipped with an HP *89090A Peltier* thermostat. Typically, 50-60 cm^3 solution was titrated and the added volume of the titrating NaOH solution was around 1 cm^3 by the end of the titration. Thus, there is a slight change in the ionic strength throughout the titration, but this is negligible for all practical purposes.

4.5 *Computation and data treatment*

The primary data sets of the measurements were processed with the instrument controlling softwares. Further necessary data manipulations were carried out with Microsoft Excel. Excel was also used for the initial rate method analysis of the kinetic data in complex systems.

Nonlinear least squares fittings of the titration curves, the kinetic traces at a given wavelength, and the pH, temperature or concentration dependence of the rate constants were performed by the software Scientist.[141] The matrix rank analysis of the time-resolved spectral changes was carried out by Matlab.[142] In some cases, the experimental kinetic traces could not be acceptably evaluated by fitting them individually to an explicit time-dependent function. Instead, multiple curves recorded under different initial conditions were simultaneously fitted on the basis of the proposed model with the program package ZiTa.[143] The data sets of the combined pH potentiometric and spectrophotometric titrations were evaluated by Specfit[144] using standard matrix algebraic calculations. Estimated parameters are always quoted in text with 1σ standard error.

4.6 *Spectral decomposition of UV-vis spectra*

The concentrations of various absorbing species were calculated by the direct linear algebraic method reported earlier,[145] which is based on an overdetermined system of simultaneous linear equations. It was convenient to use matrix formalism with the software MATLAB, i.e.:

$$\begin{pmatrix} \varepsilon_1^{\text{ferro}} & \varepsilon_1^{\text{ferri}} & \varepsilon_1^{\text{phenO}} & \varepsilon_1^{\text{phen}} \\ \varepsilon_2^{\text{ferro}} & \varepsilon_2^{\text{ferri}} & \varepsilon_2^{\text{phenO}} & \varepsilon_2^{\text{phen}} \\ \dots & \dots & \dots & \dots \\ \varepsilon_n^{\text{ferro}} & \varepsilon_n^{\text{ferri}} & \varepsilon_n^{\text{phenO}} & \varepsilon_n^{\text{phen}} \end{pmatrix} \begin{pmatrix} c_{\text{ferro}} \\ c_{\text{ferri}} \\ c_{\text{phenO}} \\ c_{\text{phen}} \end{pmatrix} = \begin{pmatrix} A_1 \\ A_2 \\ . \\ A_n \end{pmatrix} \qquad or \qquad \underline{\underline{\varepsilon}}\underline{c} = \underline{A} \qquad (8)$$

The concentration vector can be calculated using the pseudoinverse, *pinv*, of the molar absorbance matrix $\underline{\underline{\varepsilon}}$.

$$\underline{c} = pinv(\underline{\underline{\varepsilon}})\underline{A} \qquad (9)$$

Some of the columns in matrix $\underline{\underline{\varepsilon}}$ can be systematically left out in order to test whether the data could be interpreted by fewer absorbing species. The fit is characterized by the residual vector, which can be defined as

$$\underline{res} = \underline{A} - \underline{\underline{\varepsilon}}\underline{c} \qquad (10)$$

This residual matrix gives the difference between measured points and the best linear algebraic fit. The residuals themselves (as a function of wavelength) or the average of their absolute values (average deviation) can be used to characterize the goodness of fitting.

5) Results and discussion

5.1 *Reaction between PMS and phen*

5.1.1 Kinetics in strongly acidic medium

It will be shown in forthcoming subchapters that the oxidation of phen in reactions when phen is used as a ligand can play a surprisingly important role. In the PMS – $Fe(phen)_3^{2+}$ system, it was confirmed that the simultaneous oxidation of the central metal ion and the ligand results in a somewhat unusual kinetic pattern. In order to get a better understanding of the oxidation of phen, the reaction was studied independently, under metal-free conditions.

Although the oxidation of the complex was only investigated under strongly acidic conditions and at room temperature, the experiments on the phen – PMS reaction were expanded to a wide pH and temperature range.

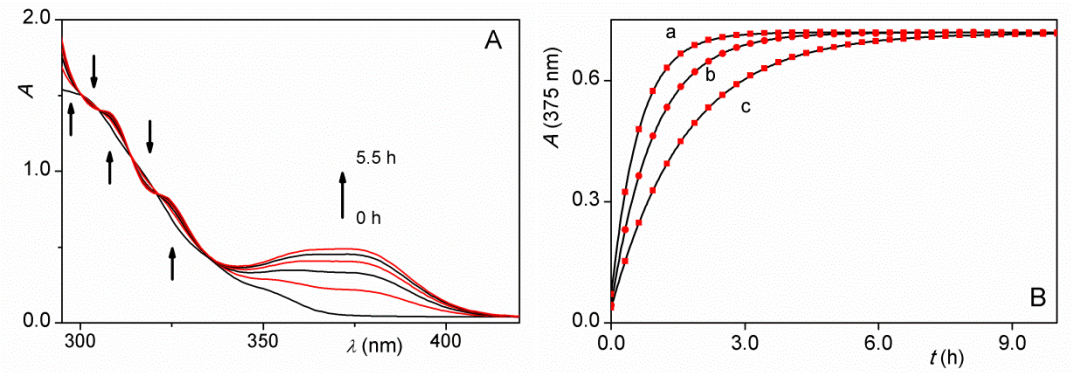

Figure 1. Reaction of 1,10-phenanthroline and PMS under strongly acidic conditions.
A: spectral changes of the reaction. $[PMS]_0$ = 27.4 mM; $[phen]_0$ = 0.234 mM; $[H_2SO_4]$ = 1.00 M; T = 25.0 °C; path length = 1.000 cm; time interval = 40 min.
B: kinetic traces obtained in the reaction. Circles: experimental points (only 10% of the recorded points are shown for clarity), continuous line: result of the fit of the data to a single exponential function. $[phen]_0$ = 0.321 mM; $[H_2SO_4]$ = 1.00 M; $[PMS]_0$ = 70.9 mM (a); 45.1 mM (b); 25.8 mM (c); T = 25.0 °C; λ = 375 nm; path length = 1.000 cm.

The spectral observations during the reaction of phen and PMS under highly acidic conditions are shown in Figure 1A. Upon mixing the reactants, the main features are the formation of a broad band in the range of 350–390 nm and the occurrence of isosbestic points. Linear algebraic decomposition of the UV-Vis

spectra[146] showed that there are two independent absorbing species during the course of the reaction. These experimental results are consistent with a simple A → B process without detectable intermediates. The two absorbing species are 1,10-phenanthroline and its oxidation product, 1,10-phenanthroline-mono-N-oxide. The product was identified by ^{1}H-NMR and ESI-MS measurements (Figure 2B). Under such acidic conditions, both methods showed only the signals of the mono-N-oxide as the final product, in agreement with the UV-Vis spectra.

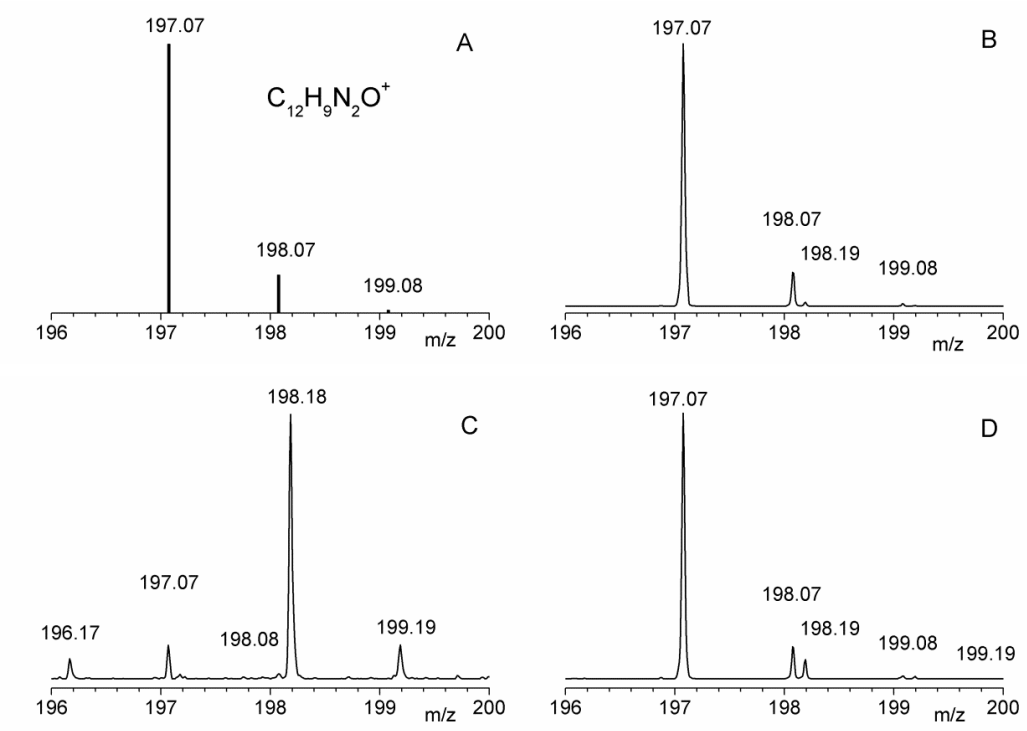

Figure 2. ESI mass spectrometric identification of 1,10-phenanthroline-mono-N-oxide in the different reaction systems.
A: calculated mass spectrum of phenO + H^+. **B**: spectrum detected during the reaction of phen with PMS. **C**: spectrum detected in the uncatalyzed decomposition of $Fe(phen)_3^{3+}$. **D**: spectrum detected during the reaction of $Fe(phen)_3^{2+}$ with PMS.

Photometric studies on the stoichiometry of the reaction are consistent with 1:1 ratio between phen and PMS in both acidic and neutral media (Figure 3). The rate equation and the calculated second order rate constant in highly acidic medium are as follows:

$$phen(H^+) + HSO_5^- \rightarrow phenO + SO_4^{2-} + (2)H^+ \qquad (11)$$

$$v = k_{11}[phen][PMS] \qquad k_{11} = (6.4 \pm 0.2) \times 10^{-3}\ M^{-1}s^{-1}$$

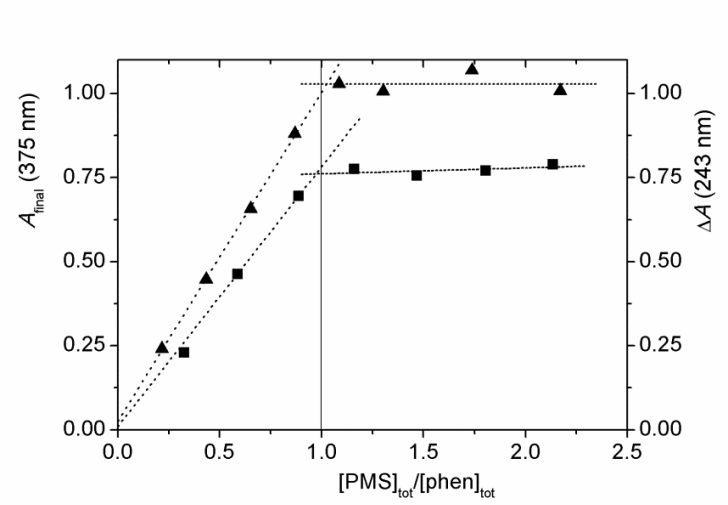

Figure 3. Spectrophotometric determination of the stoichiometry of the reaction of 1,10-phenanthroline and PMS.
Triangles (left y axis): different amounts of PMS were added to 0.462 mM phen and the final absorbance readings of the kinetic curves were plotted against the ratio of the reactants. $[H_2SO_4]$ = 1.00 M; T = 40.0 °C; λ = 375 nm; path length = 1.000 cm.
Squares (right y axis): different amounts of PMS were added to 67.7 μM phen and the difference of the initial and final absorbance readings of the kinetic curves (ΔA) were plotted against the ratio of the reactants. $[phosphate]_{tot}$ = 0.100 M; pH = 6.7; T = 25.0 °C; λ = 243 nm; path length = 1.000 cm.

The kinetics was studied at 375 nm using an excess of PMS and also under nearly stoichiometric conditions. The kinetic curves detected under pseudo-first order conditions (at least 20-fold excess of PMS over phen, shown in Figure 1B) were fitted to a single exponential function. The pseudo-first order rate constant was a linear function of the concentration of PMS with zero intercept. As expected, the constants were independent of the initial phen concentration at constant $[PMS]_0$ (kept in large excess). This is clear evidence that the reaction follows overall second order kinetics and the order with respect to both reactants is unity under the conditions applied. The second order rate constant obtained from studies at large excess of the oxidant are in excellent agreement with those gained from the fitting of kinetic curves detected under nearly stoichiometric conditions (Table 1). In the

latter experiments, 1-5-fold excess of PMS was used and the detected traces were directly fitted to the following expression:[147]

$$A_t = A_\infty + \frac{\Delta \times (A_0 - A_\infty)}{[\mathrm{PMS}]_0 \times e^{(k_{11} \times t \times \Delta)} - [\mathrm{phen}]_0} \qquad (12)$$

In this equation, A_0 and A_∞ represent the initial and the final absorbance, A_t means the absorbance at a particular time and $\Delta = [\mathrm{PMS}]_0 - [\mathrm{phen}]_0$.

Table 1. Effect of reactant concentrations on the rate of the reaction of phen and PMS. $[H_2SO_4]$ = 1.00 M; T = 25.0 °C.

$[PMS]_0$ (mM)	$[phen]_0$ (mM)	$k_{obs} \times 10^4$ (s^{-1})	$k_{11} \times 10^3$ ($M^{-1}s^{-1}$)
11.9	0.056	0.781	6.58
11.9	0.112	0.803	6.78
11.9	0.224	0.739	6.22
11.9	0.337	0.736	6.19
11.9	0.505	0.731	6.17
70.9	0.321	4.40	6.28
45.1	0.321	2.86	6.36
25.8	0.321	1.65	6.44
6.44	0.321	0.403	6.39
1.61	0.321	-	6.50
0.805	0.321	-	6.36
0.322	0.321	-	6.08
		average:	6.4 ± 0.2

Under acidic conditions, even the use of a large excess of the oxidant does not result in the formation of $phenO_2$ or any other oxidation product (Scheme 4), which is in agreement with previous literature reports.[48,65,67]

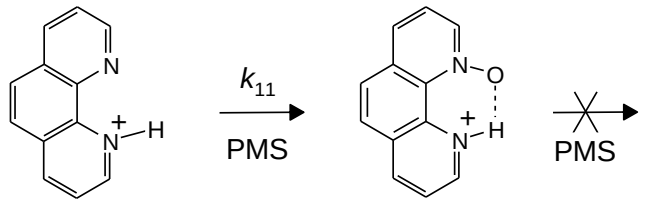

Scheme 4. Oxidation of phen by PMS under strongly acidic conditions.

5.1.2 pH and temperature dependence

The effect of pH on the initial rate of the reaction was investigated in the pH range of 1–12 by using different buffer systems ($H_3PO_4/H_2PO_4^-$, CH_3COOH/CH_3COO^-, $H_2PO_4^-/HPO_4^{2-}$ and $B(OH)_3/B(OH)_4^-$) and NaOH. In order to minimize the interference of the second order decomposition of PMS in basic medium,[39] the further oxidation of phenO or any possible side reaction of PMS with the buffers, the initial rate method was used and PMS was applied in relatively low concentrations (~5 mM, ~20-fold excess).

The initial rate was defined as the initial rate of absorbance increase at 375 nm, which is due to the formation of phenO. When the pH shifts from acidic to neutral, the formation of phenO becomes considerably faster. According to the literature, $Hphen^+$ (or $phen{\cdot}H_3O^+$) has a structure in which the H^+ (or H_3O^+) forms a bridge between the two N atoms,[148] thus offering little opportunity for the oxidative attack. Therefore, the loss of proton plays an important role in the N-oxidation process.

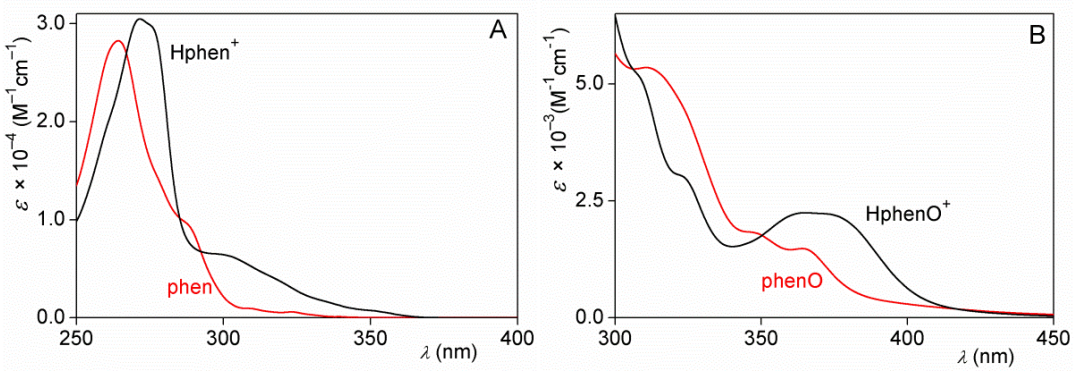

Figure 4. Molar spectra of phen and $Hphen^+$ (**A**) and phenO and $HphenO^+$ (**B**) obtained by combined pH potentiometric and spectrophotometric method.

Both the reactant (phen) and the product (phenO) are involved in acid-base equilibria in the studied pH region, which affects the absorbance change depending on the molar fraction of the protonated and deprotonated species. To determine the molar absorptivities and the pK_a, a combined pH potentiometric and spectrophotometric method was used, whereby the UV-Vis spectra of phen and phenO were recorded as a function of pH[149] (Figures 4A and 4B). The pK_a of the

N-oxide was found considerably higher (7.30 ± 0.02 in Na_2SO_4 at I = 1.00 M) than that of phen (5.12). The relative stability of the protonated form of phenO is most likely due to an intramolecular hydrogen bond (Scheme 4).[48] The literature value of pK_a of phenO is 6.63 at 22 °C,[48] which is somewhat smaller than the one determined here. Such a difference is not unexpected considering that the previous work was done at lower total electrolyte concentration (I < 0.1 M).

By using $\Delta\varepsilon$, the difference in the molar absorptivities of the reactant and the product at a given pH, and the initial analytical concentrations of the reactants, the measured initial rates were converted into apparent second order rate constants (k_{2nd}) and plotted against the pH. The rate constants of the first oxidation step pass through a maximum at about pH 6.7 (Figure 5A). Such a pH profile can be interpreted by considering the protolytic equilibria of the reactants.

$$Hphen^+ = phen + H^+ \qquad (13)$$

$$K_a^{phen} = \frac{[phen][H^+]}{[Hphen^+]}$$

$$HSO_5^- = SO_5^{2-} + H^+ \qquad (14)$$

$$K_a^{HSO5} = \frac{[SO_5^{2-}][H^+]}{[HSO_5^-]}$$

Here K_a^{phen} and K_a^{HSO5} are the acid dissociation constants of $Hphen^+$ and HSO_5^-, respectively. Thus, in principle, the redox reaction may proceed via the following parallel reaction steps:

$$Hphen^+ + HSO_5^- \rightarrow phenO + SO_4^{2-} + 2H^+ \qquad k_{15} \qquad (15)$$

$$phen + HSO_5^- \rightarrow phenO + SO_4^{2-} + H^+ \qquad k_{16a} \qquad (16a)$$

$$Hphen^+ + SO_5^{2-} \rightarrow phenO + SO_4^{2-} + H^+ \qquad k_{16b} \qquad (16b)$$

$$phen + SO_5^{2-} \rightarrow phenO + SO_4^{2-} \qquad k_{17} \qquad (17)$$

As seen in Figure 5A, the k_{2nd} values do not converge to zero in the acidic region confirming that the reaction path between $Hphen^+$ and HSO_5^- (15) is operative. The protolytic equilibria between the acidic and basic forms of the reactants are expected to be very fast, and reactions 16a and 16b are indistinguishable due to proton ambiguity.[150] Under basic conditions, k_{2nd} shows linear correlation with

decreasing $[H^+]$ in the range from pH 11 to 12 and practically becomes zero as the pH increases. This confirms that the redox reaction cannot occur between the deprotonated species (SO_5^{2-} and phen) and reaction 17 can be discarded. In accordance with these considerations, the pH dependence of k_{2nd} is given by the following equation:

$$k_{2nd} = \frac{v_0}{[\text{phen}]_0 \times [\text{PMS}]_0 \times \Delta\varepsilon} = \frac{k_{15} \times [H^+]^2 + \kappa \times [H^+]}{(K_a^{phen} + [H^+]) \times (K_a^{HSO5} + [H^+])} \qquad (18)$$

where $\kappa = k_{16a} \times K_a^{phen} + k_{16b} \times K_a^{HSO5}$

The experimental data were fitted to eq 18 by using a nonlinear least-squares algorithm and proportional weighting (the weight used for the experimental value of k_{2nd} is k_{2nd}^{-2} at each pH).[150]

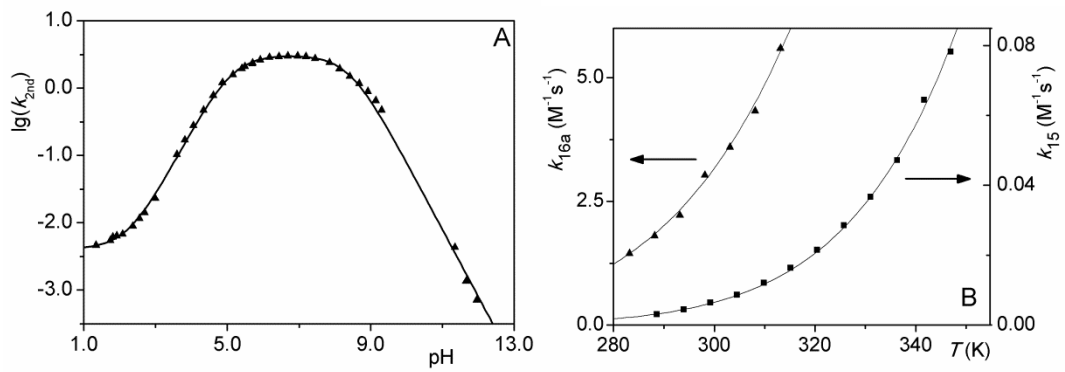

Figure 5A: The pH dependence of the apparent rate constant (k_{2nd}, $M^{-1}s^{-1}$) of the reaction of phen and PMS.
$[PMS]_0$ = 4.6-4.8 mM; $[phen]_0$ = 0.250 mM; I = 1.00 M ($NaNO_3$), $[buffer]_{tot}$ = 50.0 mM; T = 25.0 °C; λ = 375 nm. Line: result of a nonlinear fit to eq 18.
B: Temperature dependencies of the oxidation pathways of 1,10-phenanthroline and HSO_5^-. Triangles (left axis): rate constants of the oxidation of phen by HSO_5^- (16a); $[phen]_0$ = 0.242 mM; $[HSO_5^-]_0$ = 2.50 mM; $[acetate]_{tot}$ = 50.0 mM; I = 1.00 M ($NaNO_3$).
Squares (right axis): rate constants of the oxidation of $Hphen^+$ by HSO_5^- (15) $[phen]_0$ = 0.242 mM; $[H_2SO_4]$ = 1.00 M; $[HSO_5^-]_0$ = 12.1 mM. Lines: results of nonlinear fit to the Eyring equation (eq 19).

The fitted values for pK_a^{phen} = 5.12 ± 0.03 and pK_a^{HSO5} = 8.41 ± 0.03 in $NaNO_3$ at I = 1.00 M are in good agreement with the ones found in the literature at

similar ionic strength for $Hphen^+$ (5.08)[52] and the second dissociation constant of peroxomonosulfuric acid (8.43).[2] There are also literature reports on the existence of the species $H(phen)_2^+$. However, its molar fraction is relevant only in relatively concentrated solutions (higher than 7 mM).[50,51,52] The formation of such a species is not considered in this study because phen is used in significantly lower concentrations. Our spectrophotometric, pH metric and kinetic studies did not indicate the presence of $H(phen)_2^+$.

The estimated value of $k_{15} = (4.1 \pm 0.3) \times 10^{-3}$ $M^{-1}s^{-1}$ is somewhat smaller than the one found in 1.00 M H_2SO_4 (k_{11}). The difference can be interpreted in terms of medium effects. In 1.00 M H_2SO_4, the ionic strength and ionic atmosphere are slightly different from those in 1.00 M $NaNO_3$, which was used in the pH dependent study as a background electrolyte. It should be noted that the same tendency was observed in the rate constants of the oxidation reactions of 4-methyl-phenanthroline, 5-methyl-phenanthroline and 3,4,7,8-tetramethyl-phenanthroline by PMS.

The pH profile confirms that the dominant reaction path includes the acidic form of one reactant and the basic form of the other. The proton ambiguity cannot be resolved by the fitting procedure itself, only the value of $\kappa = (2.35 \pm 0.12) \times 10^{-5}$ s^{-1} can be obtained, which includes the acid dissociation constants of the reactants and the rate constants of the two indistinguishable pathways.

Yet the contribution of the two concurrent reactions (16a and 16b) can be estimated by considering the redox chemistry of the reactants. According to earlier results, HSO_5^- is much more reactive than the fully deprotonated form of the oxidant.[1,2] The protonation of phen is expected to hinder N-oxidation making the protonated form of the substrate less reactive in such reactions. Thus, it is a reasonable assumption that 16b has a minor contribution to the overall process and the main reaction occurs between the deprotonated phenanthroline (phen) and the monoprotic form of Caro's acid (HSO_5^-). This conclusion is also supported by the observation that the reaction rate at about pH 6.6 is practically independent of the ionic strength at constant initial reactant concentrations (Table 2), as expected when the charge product of the reactants is zero. By omitting the second term of κ,

the rate constant of 16a can be estimated: $k_{16a} = 3.1 \pm 0.1$ $M^{-1}s^{-1}$, which is nearly three orders of magnitude larger than k_{15}. The sluggishness of $Hphen^+$ in N-oxidation compared to phen can be interpreted by the protecting effect of the intramolecular hydrogen bond in the protonated form.[148]

Table 2. Effect of ionic strength on the rate of the reaction between phen and PMS. $[phen]_0$ = 0.212 mM; $[PMS]_0$ = 2.15 mM; $[phosphate]_{tot} = 2.00\times10^{-2}$ M; pH = 6.6; T = 25.0 °C.

I (M)	k_{16a} ($M^{-1}s^{-1}$)
0.11	2.84
0.51	2.93
0.81	2.93
1.21	2.95
1.61	3.02
average:	2.93 ± 0.06

The temperature dependencies of both oxidation pathways were studied (Figure 5B). Under strongly acidic conditions (1.00 M H_2SO_4), only the reaction via the protonated forms (HSO_5^- and $Hphen^+$, reaction 15) is operative (*cf.* eq 18). Thus, temperature effects arising from the temperature dependence of the protolytic equilibria can be neglected. However, in the case of 16a, such a simplification cannot be found. In order to determine the activation parameters of this process, the pH was set by acetate buffer because its pK_a is practically independent of the temperature between 10 and 40 °C.[137] Under slightly acidic conditions, PMS ion is present in the monoprotic form (HSO_5^-) and its decomposition can be ignored. The temperature dependence of the pK_a of phen was determined in the 10–40 °C range by conventional pH metric titration.[139] In each kinetic run, the pH was measured (and was about 4.4), the $Hphen^+$/phen ratio was determined, and then the contributions of the two oxidation pathways to the observed rate constants were calculated (Table 3).

Table 3. Temperature dependencies of the pK_a of phen and the rate constants of the two oxidation paths of the reaction between 1,10-phenanthroline and HSO_5^-. k_{15} was determined in 1.00 M H_2SO_4, in the case of the pK_a and k_{16a} the ionic strength was kept constant by using 1.0 M $NaNO_3$.

T (K)	$k_{15} \times 10^3$ ($M^{-1}s^{-1}$)	k_{16a} ($M^{-1}s^{-1}$)	pK_a (phen)
283	2.18	1.45	5.23(2)
288	3.08	1.82	5.25(2)
293	4.41	2.22	5.22(2)
298	6.35	3.03	5.14(2)
303	8.60	3.59	5.09(1)
308	12.1	4.33	5.03(2)
313	16.3	5.59	4.97(4)
318	21.4		
323	28.6		
328	36.7		
333	47.2		
338	64.4		
343	78.3		

In both series of experiments, pseudo-first order conditions were used, the kinetic traces were fitted to single exponential functions and the second order rate constants were calculated. The temperature dependencies of these constants are shown in Figure 5B. Even at high temperature, no secondary reaction was observed and the final readings of the absorbance were identical within margin of error. The activation parameters were estimated by fitting the experimental data to the Eyring equation with proportional weighting:

$$k = \frac{k_b T}{h} \exp\left(\frac{\Delta S^{\ddagger}}{R}\right) \exp\left(-\frac{\Delta H^{\ddagger}}{RT}\right) \qquad (19)$$

where k_b is the Boltzmann constant, h is the Planck constant, R is the universal gas constant, and $\Delta S^{\ddagger}$ and $\Delta H^{\ddagger}$ are the activation entropy and enthalpy, respectively. The results are listed in Table 4. The activation entropies are essentially identical large negative values. In earlier studies, it was concluded that large negative entropies of activation are characteristic for $2e^-$ oxidation reactions that involve

O-atom transfer.[1,151] Thus, it was deduced that the oxidation of phen by HSO_5^- proceeds via concerted heterolytic O−O bond cleavage and N−O bond formation via both reaction paths.

Table 4. Activation parameters of the two pathways of the phen(H^+) and HSO_5^- reaction.

Reaction	$\Delta S^{\ddagger}$ ($Jmol^{-1}K^{-1}$)	$\Delta H^{\ddagger}$ ($kJmol^{-1}$)
$Hphen^+ + HSO_5^-$ (15)	-133.8 ± 1.1	45.73 ± 0.34
$phen + HSO_5^-$ (16a)	-133.5 ± 3.0	30.58 ± 0.90

5.1.3 Formation of 1,10-phenanthroline-N,N'-dioxide under neutral conditions

Treatment of the colorless aqueous solution of phen with an equivalent amount of PMS at about pH 6.6 results in the formation of phenO, turning the mixture light yellow (featuring a broad absorbing band between 360 and 380 nm). In the presence of a slight excess of phen, the final absorbance remains stable (Figure 6A) proving that no further change occurs to phenO within the observed time interval in the absence of excess PMS.

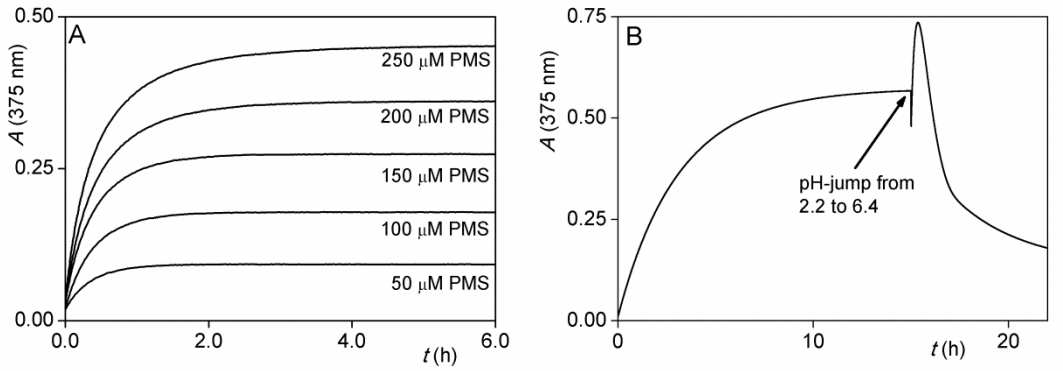

Figure 6A: Kinetic traces obtained in the reaction between 1,10-phenanthroline and PMS in the presence of excess of phen. $[phen]_0$ = 299 μM; $[phosphate]_{tot}$ = 8.00×10^{-2} M; pH = 6.7; I = 1.00 M ($NaNO_3$); T = 25.0 °C; λ = 375 nm; path length = 1.000 cm.
B: Kinetic trace demonstrating the effect of pH on the oxidation of 1,10-phenanthroline-mono-N-oxide by PMS. $[phen]_0$ = 0.256 mM; $[PMS]_0$ = 6.10 mM; $pH_{initial}$ = 2.2 (set by $HClO_4$). The pH jump was triggered by the addition of 50 μL of 0.5 M Na_2HPO_4 to 2 mL of the reaction mixture. Concentrations after dilution: [phen] = 0.250 mM; [PMS] = 5.95 mM; $[phosphate]_{tot}$ = 1.22×10^{-2} M; pH = 6.4; T = 25.0 °C; λ = 375 nm; path length = 1.000 cm.

Upon the addition of an equivalent amount of PMS to the solution of phenO, the yellowish color intensifies and not only the absorbance of the broad band increases but the absorbance maximum also shifts toward lower wavelengths (360 nm). The noted spectral change is presumably due to the oxidation of phenO by PMS. Under acidic conditions, such changes were not observed indicating that PMS is not able to oxidize the protonated form of the N-oxide (Scheme 4).

The significance of the pH in the oxidation of phenO is also demonstrated by the following experiment. The reaction of phen and PMS was initiated at pH 2.2 in the presence of about 24-fold excess of oxidant over the organic substrate. Despite the excess of PMS a one-step process is seen without further oxidation. After running the reaction for 15 h (by that time the change in the absorbance was less than 0.4% per hour) a pH jump to pH = 6.4 was induced by the addition of a sufficient amount of $H_2PO_4^-/HPO_4^{2-}$ buffer to the reaction mixture. The pH jump caused a slight decrease in the absorbance due to dilution and the deprotonation of $HphenO^+$, which has higher molar absorptivity than phenO at 375 nm. This absorbance change was followed by a relatively rapid increase. Figure 6B shows that after reaching a maximum the absorbance falls, indicating further oxidation steps, which will be discussed later.

Under acidic conditions, the internal hydrogen bond in $HphenO^+$ shields the second N atom and prevents its oxidation. This feature accounts for the stability of $HphenO^+$ in acidic medium even when a large excess of oxidant is present. When the pH is increased, the proton loss liberates the second nitrogen atom. Once $HphenO^+$ deprotonates, the second nitrogen is exposed to the oxidative attack leading to the formation of $phenO_2$. Assuming similar pH profiles for the rates of the oxidation of phen and phenO, the maximum rate is expected at about pH ~ 7.8 in the case of phenO. The ESI-MS analysis of the reaction mixture in neutral medium confirms the formation of the di-N-oxide, the intense peaks at m/z 213.06 and 235.04 belong to $HphenO_2^+$ and $\{Na{\cdot}phenO_2\}^+$**,** respectively (Figures 7A and 7B). The ^{1}H-NMR spectrum is consistent with the symmetric structure of $phenO_2$ (d, 8.52 ppm; d, 8.17 ppm; s, 7.85 ppm; dd, 7.74 ppm), and in good agreement with the results reported by Rozen and Dayan.[70]

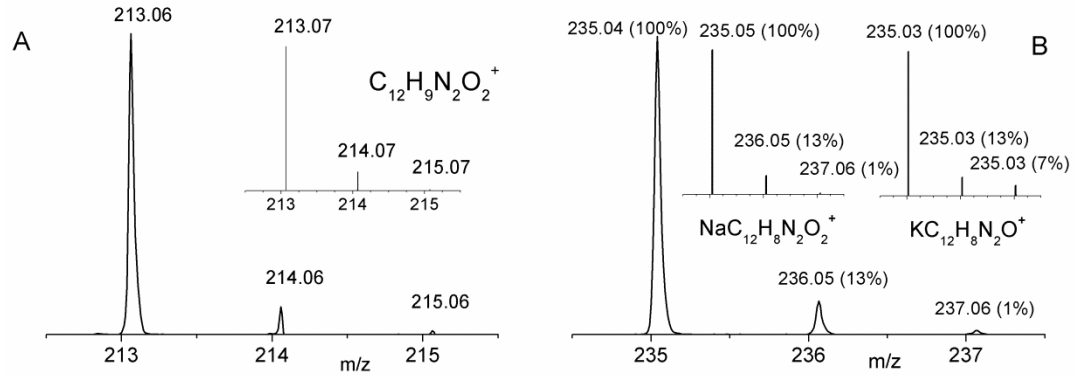

Figure 7. Electrospray ionization mass spectrometric identification of 1,10-phenanthroline-N,N'-dioxide in the reaction of 1,10-phenanthroline and PMS. **A**: identification of the protonated dioxide ($HphenO_2^+$). Inset: calculated spectrum for the formula $C_{12}H_9N_2O_2^+$.
B: identification of the dioxide ionized with sodium ion ($Na{\cdot}phenO_2^+$). Left inset: calculated spectrum for the formula $NaC_{12}H_8N_2O_2^+$. Right inset: calculated spectrum for the formula $KC_{12}H_8N_2O^+$ (monoxide ionized with potassium ion). The isotopic distribution of the peaks clearly show that although the potassium ion adduct bears peaks of similar m/z ratio, it is the $\{Na{\cdot}phenO_2\}$ cation found in the reaction mixture.

To my knowledge, there is only one report on the formation of $phenO_2$ in the previous literature, when HOF/CH_3CN mixture was used as an oxidant.[70] The results presented here confirm that there is a straightforward way to generate $phenO_2$ in aqueous solution without using extreme conditions. Apparently, the key to solving the problem is the use of appropriate (neutral) pH. However, the properties of the oxidant are also important. The oxidations of phen to the di-N-oxide with strong oxidizing agents such as O_3, H_2O_2, $S_2O_8^{2-}$ and MnO_4^- under neutral conditions were tried, but these attempts failed to produce $phenO_2$.

5.1.4 Kinetics of the overall oxidation reaction in nearly neutral medium

If a substoichiometric amount of PMS is used, the formation of phenO is the only observable reaction (Figure 6A). However, when an excess of PMS was applied in nearly neutral solutions, one maximum was seen in the kinetic curve at 375 nm. These traces cannot be fitted to a double exponential function. Thus, seemingly more than two steps occur in this system. In order to broaden the usable

wavelength range, $NaNO_3$ was discarded and only $H_2PO_4^-/HPO_4^{2-}$ buffer was applied to set both the pH and the ionic strength. Some selected wavelengths are shown in Figure 8, which clearly indicates composite kinetic behavior.

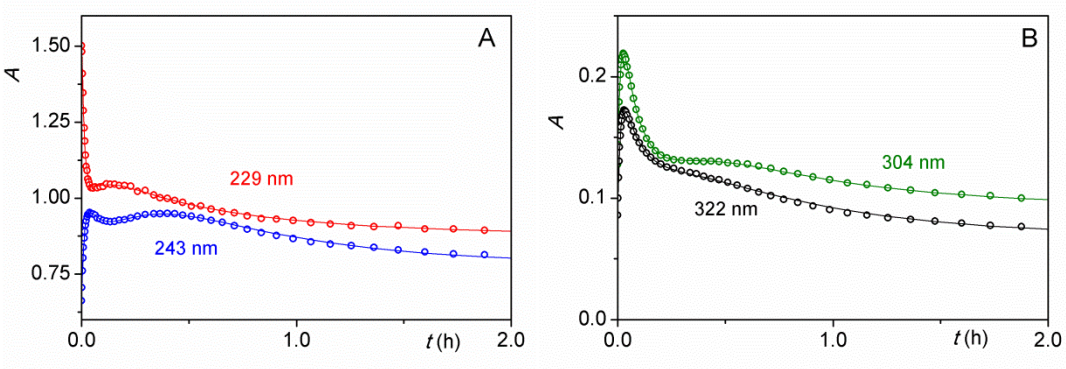

Figure 8. Kinetic traces obtained in the reaction between 1,10-phenanthroline and PMS in nearly neutral medium. $[PMS]_0$ = 7.62 mM; $[phen]_0$ = 0.100 mM; $[phosphate]_{tot}$ = 0.100 M; pH = 6.7; T = 25.0 °C; path length = 0.500 cm. **A**: λ = 229 and 243 nm. **B**: λ = 304 and 322 nm.
Open circles: experimental data. Only 20% of the recorded points are shown for clarity. Lines: results of nonlinear fit to the model described by reactions 4, 16, 20-22.

Singular value decomposition analysis was used to determine the number of the independent absorbing species in the reaction using the spectra in the 200–400 nm wavelength range.[146] By applying the method for gradually increasing reaction time, the number of absorbing species increases step by step up to 5. Thus, four well-defined reaction phases can be distinguished and the new absorbing components are presumably produced in consecutive processes (Table 5). To investigate the kinetics, 243 nm was chosen because the kinetic traces at this wavelength feature three extrema: two maxima and a minimum (Figures 8A and 9).

The noted effects were studied as the function of the concentration of the two reactants (both of them were changed by one order of magnitude). As seen in Figure 9, the maxima and minima of the curves occur at the same reaction time for all practical purposes when the initial concentration of phen is changed. This indicates that the reaction orders with respect to phen and its derivatives produced in the successive reactions are one in all steps, otherwise the positions of the extrema would depend on the concentration of the monitored species.

Table 5. The first 10 singular values (SV) of the time-resolved UV-Vis absorbance matrices of the phen – PMS reaction, recorded between 200-400 nm under the conditions given below. Only values in italics belong to real species, the other nonzero elements represent experimental error.[146] The analysis was carried out for increasing overall time range (t_{oa}) of the same spectral series.
$[phen]_0$ = 0.100 mM; $[PMS]_0$ = 7.62 mM; $[phosphate]_{tot}$ = 0.100 M; pH = 6.7; T = 25.0 °C

t_{oa} = 107.3 s SV	t_{oa} = 501.6 s SV	t_{oa} = 1495.2 s SV	t_{oa} = 10699.5 s SV
66.67	*100.5*	*119.5*	*141.9*
3.801	*5.359*	*8.610*	*17.19*
0.310	*3.473*	*5.008*	*6.374*
0.134	0.322	*2.056*	*4.159*
0.098	0.176	0.202	*1.525*
0.092	0.152	0.190	0.241
0.077	0.125	0.162	0.198
0.070	0.107	0.134	0.176
0.065	0.010	0.128	0.173
0.061	0.094	0.125	0.155

When the nearly constant contribution of PMS (which is used in large excess) is subtracted from the detected absorbance and the corrected curves are divided by the total concentration of phen, the normalized traces are practically identical within the expected error limits. This confirms again the first order dependence of the subsequent reaction steps on phen and its oxidized derivatives (Figure 9B).

The kinetic curves recorded under different initial conditions were simultaneously evaluated by considering the reactions of Scheme 5. The kinetic model consists of second order oxidation steps. This model also includes the second order decomposition of PMS. The contribution of this process to the consumption of PMS cannot be ignored completely since the applied pH (6.7) is not so far from the pH of the maximum rate of the decomposition which occurs at pH = pK_a (= 8.41).[39] Since the reaction is second order, it has more profound effect when the initial concentration of PMS is relatively high.

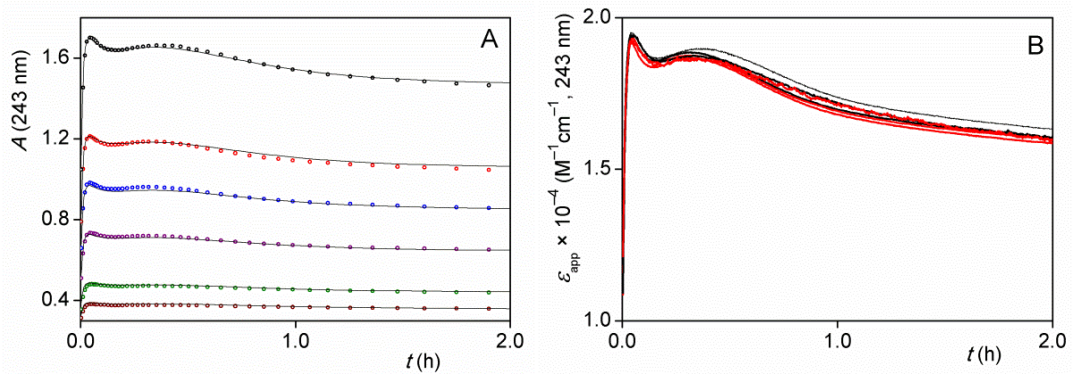

Figure 9A: Experimental kinetic curves recorded in the reaction between phen and PMS in nearly neutral medium. Circles: experimental data. Only 2% of the recorded points are shown for clarity. Lines: results of the global fit to the model described by reactions 4, 16, 20-22. $[PMS]_0$ = 9.77 mM; $[phen]_0$ = 7.5−75 μM; $[phosphate]_{tot}$ = 0.100 M; pH = 6.7; T = 25.0 °C, λ = 243 nm; path length = 1.000 cm.

B: Normalization of the 6 kinetic curves shown in Figure 9A. ε_{app} is obtained by subtracting the nearly constant contribution of PMS from the detected absorbance and the division of the residual curves by the total concentration of phen.

The kinetic model is rather complex and an explicit expression is not available for fitting or simulating the experimental kinetic traces. Thus, a comprehensive evaluation method was used which numerically solves the corresponding differential equation system and simultaneously fits the kinetic traces by using a nonlinear least squares algorithm.[143]

$$\text{phen} + HSO_5^- \rightarrow \text{phenO} + SO_4^{2-} + H^+ \qquad (16)$$

$$v = k_{16}[\text{phen}][\text{PMS}]$$

$$\text{phenO} + HSO_5^- \rightarrow \text{phenO}_2 + SO_4^{2-} + H^+ \qquad (20)$$

$$v = k_{20}[\text{phenO}][\text{PMS}]$$

$$\text{phenO}_2 + HSO_5^- \rightarrow \text{I} \qquad (21)$$

$$v = k_{21}[\text{phenO}_2][\text{PMS}]$$

$$\text{I} + HSO_5^- \rightarrow \text{P} \qquad (22)$$

$$v = k_{22}[\text{I}][\text{PMS}]$$

$$HSO_5^- + SO_5^{2-} \rightarrow 2SO_4^{2-} + O_2 + H^+ \qquad (4)$$

$$v = -\frac{1}{2} \times \frac{d[\mathrm{PMS}]}{dt} = k_4[\mathrm{PMS}]^2$$

Eleven parameters were used in these calculations: 5 rate constants and 6 molar absorptivities. Two rate constants (k_{16} and k_4) and three molar absorption coefficients (ε for phen, phenO and PMS) were determined in independent experiments and were fixed, the rest of the parameters (k_{20}, k_{21}, k_{22}, and ε for $phenO_2$, the intermediate and the product) were allowed to float. The estimated parameters are listed in Table 6.

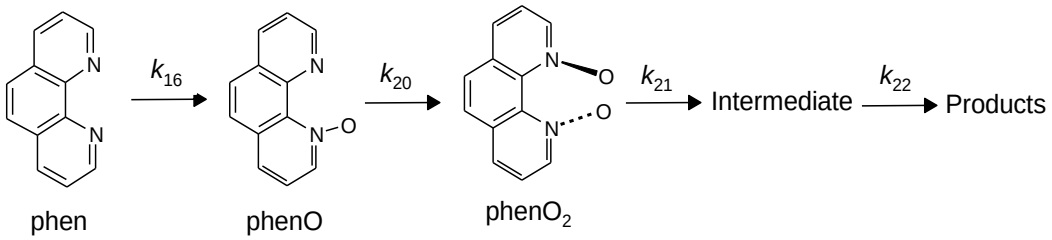

Scheme 5. Successive oxidation steps in the phen – PMS system under nearly neutral conditions. Each rate constant corresponds to an oxidation step by PMS which is used in excess.

It should be noted that the results were obtained at pH = 6.7 and the pH dependencies of the corresponding parameters were not investigated in the overall process. However, it is reasonable to assume that the rate of the individual reaction steps and the corresponding kinetic parameters are pH dependent: in the case of k_4, k_{16} and k_{20} the pH dependency is confirmed in this study or by earlier literature;[39] and k_{21} and k_{22} may also change with pH.

Using the calculated rate constants and the spectral series recorded at pH = 6.7, the apparent spectra of absorbing species, i.e. phen, phenO, $phenO_2$, the intermediate (I), the product (P) and PMS were calculated (Figure 10).[144] The apparent spectra of phen and phenO are in perfect agreement with the ones calculated from the known spectra of the protonated and deprotonated species (Figures 4A and 4B) at pH = 6.7.

Table 6. Kinetic parameters resulting from globally fitting the kinetic data of the oxidation of phen by PMS. pH = 6.7, T = 25 °C, λ = 243 nm. Parameters designated with asterisk (*) are known from independent experiments and were held fixed during the fitting procedure.

Parameter	Value	Unit
k_{16}	2.97 *	$M^{-1}s^{-1}$
k_{20}	$(4.2 \pm 0.3) \times 10^{-1}$	$M^{-1}s^{-1}$
k_{21}	$(1.7 \pm 0.2) \times 10^{-1}$	$M^{-1}s^{-1}$
k_{22}	$(4.5 \pm 0.4) \times 10^{-2}$	$M^{-1}s^{-1}$
k_4	2.5×10^{-4} *	$M^{-1}s^{-1}$
ε_{HSO5}	25.0 *	$M^{-1}cm^{-1}$
ε_{phen}	8.05×10^{3} *	$M^{-1}cm^{-1}$
ε_{phenO}	2.10×10^{4} *	$M^{-1}cm^{-1}$
ε_{phenO2}	$(1.7 \pm 0.1) \times 10^{4}$	$M^{-1}cm^{-1}$
ε_{int}	$(2.0 \pm 0.2) \times 10^{4}$	$M^{-1}cm^{-1}$
ε_{prod}	$(1.5 \pm 0.1) \times 10^{4}$	$M^{-1}cm^{-1}$

No attempt was made to isolate and identify the final products of the oxidation. The use of a large excess of oxidant probably results in the gradual cleavage of C-C and C-N bonds and the formation of smaller molecules due to the strong oxidizing ability of PMS. This feature of PMS is well known and is taken advantage in advanced oxidation processes (AOP-s).[5,6]

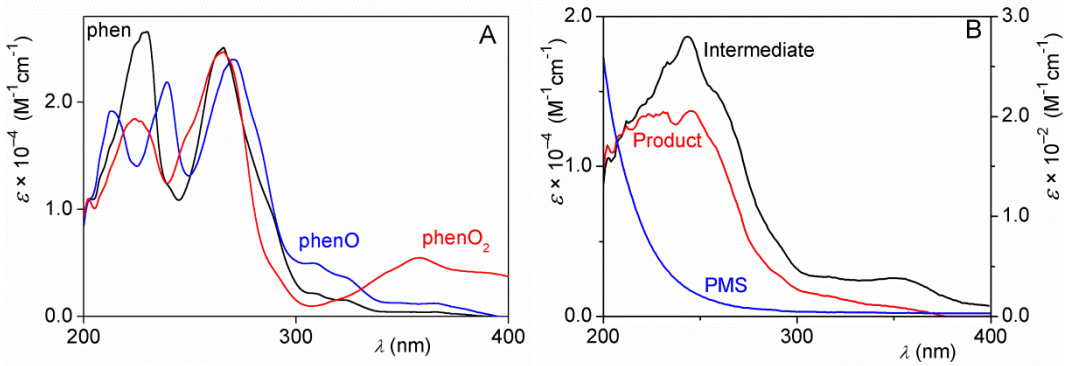

Figure 10. Calculated spectra of the species involved in the phen - PMS reaction obtained by fitting a series of spectra to the model described by reactions 4, 16, 20-22.
A: Calculated apparent spectra of phen, phenO and $phenO_2$ at pH 6.7. **B**: Left axis: Calculated apparent spectra of the intermediate (I) and the product (P). Right axis: Spectrum of PMS at pH 6.7 obtained by combined pH potentiometric and spectrophotometric method.

5.2 *Reactions of the $Fe(phen)_3^{3+}$ complex*

5.2.1 Uncatalyzed decomposition of $Fe(phen)_3^{3+}$

In the next subchapter, it will be shown that the reactions of $Fe(phen)_3^{3+}$ play a crucial role in the exotic behavior of the PMS – $Fe(phen)_3^{2+}$ system. In order to explore the details of these processes, independent studies were done on the reactions of the iron(III) tris phenanthroline complex.

$Fe(phen)_3^{3+}$, similarly to the analogous Ru^{III} and Os^{III} complexes, is able to oxidize hydroxide ion with a simple outer-sphere electron-transfer mechanism.[96,152,153] Therefore, meaningful experiments are usually limited to the acidic region. According to the literature, the formal potential of the $Fe(phen)_3^{3+}/Fe(phen)_3^{2+}$ redox pair decreases with increasing acidity and has a potential of 1.06 V in 1.0 M H_2SO_4.[89] The tris(phen)iron(III) complex is also known to undergo acid dissociation to aqueous ferric ion and the protonated ligand (24).[91,116]

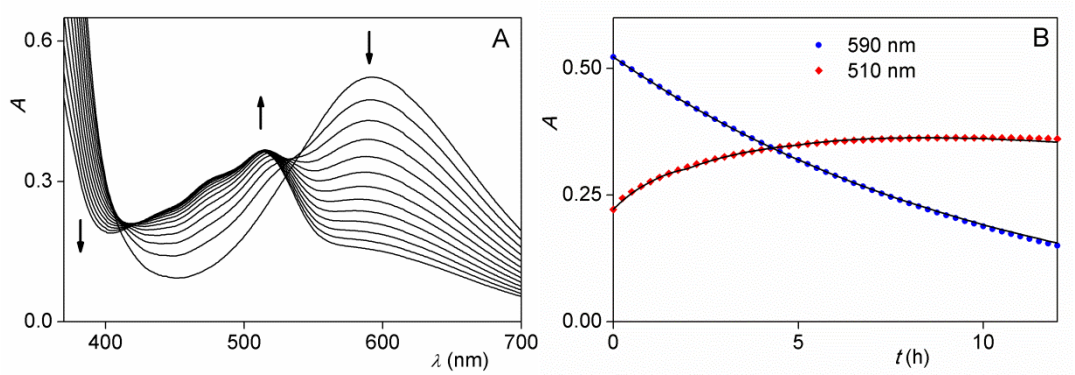

Figure 11. Spectral changes (**A**) and kinetic curves (**B**) in the decomposition reaction of $[Fe(phen)_3^{3+}]$.
$[Fe(phen)_3^{3+}]_0$ = 0.62 mM; $[H_2SO_4]$ = 1.00 M; T = 25.0 °C; path length = 1.000 cm,
A: time interval = 60 min. **B**: Points: experimental data. Lines: results of the best fit using the molar absorbances of $Fe(phen)_3^{2+}$ and $Fe(phen)_3^{3+}$ and their calculated concentration profiles based on the model described by reactions 24-28.

Spectrophotometric changes in strongly acidic medium are shown in Figure 11A. The decrease in absorbance around 590 nm is accompanied by a simultaneous increase of absorbance around 510 nm (Figure 11B). This reveals that some

$Fe(phen)_3^{2+}$ is also produced as a product of the decomposition of the corresponding iron(III) complex. Taking into account the large difference in the molar absorption coefficients (peak of $Fe(phen)_3^{3+}$, $\varepsilon_{590\ nm} = 8.35 \times 10^2\ M^{-1}cm^{-1}$, peak of $Fe(phen)_3^{2+}$, $\varepsilon_{510\ nm} = 1.095 \times 10^4\ M^{-1}cm^{-1}$), Figure 11 confirms that only a fraction of the iron(III) complex produces $Fe(phen)_3^{2+}$, and most $Fe(phen)_3^{3+}$ dissociates without redox reactions. Oxidizable impurities may be present at extremely low level in the reaction mixtures, thus, they cannot be responsible for the formation of $Fe(phen)_3^{2+}$.

The spectral observations in the reactions of $Fe(phen)_3^{3+}$ were evaluated based on the linear algebraic method described in Ch. 4.6. Figure 12A shows the relevant absorbing species of the system that were taken into consideration. For the calculation of the concentrations of the species, only those wavelengths were used where the absorbance was lower than 2 (AU). In many of the experiments, the absorbance in the UV region of the spectrum exceeded this limit and was cut off which made it difficult to obtain reliable concentrations for phen because it has substantial absorption only below 355 nm. The visible range, on the other hand, provided excellent information on the concentration profiles of $Fe(phen)_3^{3+}$ and $Fe(phen)_3^{2+}$. In addition to the kinetic traces of these species, the free iron(III) (denoted by Fe^{3+}) was also used for the evaluation of the experiments. Once Fe(III) is formed, it is not involved in further reactions and considered as a product of the reaction. The iron(II) complex produced in a redox reaction is expected to undergo proton-assisted dissociation generating free iron(II). However, Fe^{2+} is converted rapidly into Fe^{3+} by $Fe(phen)_3^{3+}$ (28) as long as the latter one is present in the solution. The concentration of Fe^{3+} was calculated by the mass balance equation (23), which is valid until the complete consumption of $Fe(phen)_3^{3+}$.

$$[Fe]_{tot} = [Fe(phen)_3^{3+}]_0 = [Fe(phen)_3^{3+}]_t + [Fe(phen)_3^{2+}]_t + [Fe^{3+}]_t \qquad (23)$$

The order of the formation of the iron(II) complex was studied by the initial rate method and a second order dependence was found with respect to the Fe(III) complex (Figure 12B). The initial rate of the loss of $Fe(phen)_3^{3+}$ and the formation of Fe^{3+}, on the other hand, showed first order dependence on the iron(III) complex. This is not unexpected because in the initial phase of the reaction, the dominant process consuming $Fe(phen)_3^{3+}$ and producing Fe^{3+} is the proton-assisted

dissociation of the complex, which is known to be first order with respect to $Fe(phen)_3^{3+}$.[91,116] In accordance with these observations, it needs to be assumed that the formation of the iron(II) complex occurs via a minor parallel reaction path.

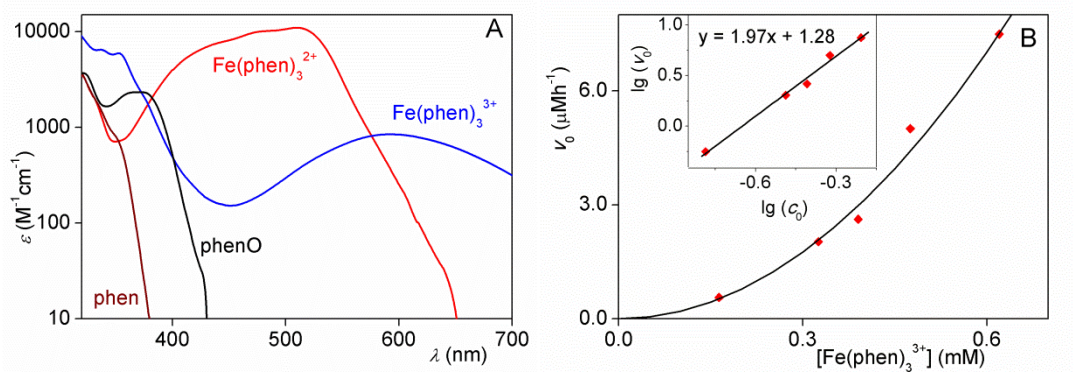

Figure 12A: Molar spectra of the relevant species in the $Fe(phen)_3^{3+}$ system. The role of phenO is discussed in Ch. 5.2.2.
B: The dependence of the initial rate of the formation of $Fe(phen)_3^{2+}$ on $[Fe(phen)_3^{3+}]_0$. $[H_2SO_4]$ = 1.00 M; T = 25.0 °C. Squares: experimental data, line: best fit to a quadratic function ($y = bx^2$). Inset: van't Hoff plot (lg v_0 vs lg $[Fe(phen)_3^{3+}]_0$) of the initial rate.

The following kinetic model was proposed to interpret the experimental data:

$$Fe(phen)_3^{3+} (+ 3H^+) \rightarrow Fe^{3+} + 3Hphen^+ \qquad (24)$$

$$v = k_{24}[Fe(phen)_3^{3+}]$$

$$2Fe(phen)_3^{3+} \rightarrow Fe(phen)_3^{2+} + Fe(phen)_3^{4+} \qquad (25)$$

$$v = k_{25}[Fe(phen)_3^{3+}]^2$$

$$Fe(phen)_3^{4+} + H_2O \rightarrow Fe^{2+} + 2phen + 2H^+ + phenO \qquad (26)$$

$$v = \text{fast}$$

$$Fe(phen)_3^{2+} (+ 3H^+) \rightarrow Fe^{2+} + 3Hphen^+ \qquad (27)$$

$$v = k_{27}[Fe(phen)_3^{2+}] \qquad k_{27} = (5.9 \pm 0.1) \times 10^{-5}\ s^{-1}$$

$$Fe^{2+} + Fe(phen)_3^{3+} \rightarrow Fe^{3+} + Fe(phen)_3^{2+} \qquad (28)$$

$$v = k_{28}[Fe(phen)_3^{3+}][Fe^{2+}] \qquad k_{28} = (2.7 \pm 0.1) \times 10^5\ M^{-1}s^{-1}$$

The rate constants of reactions 27 and 28 were determined in independent experiments and are in good agreement with the literature values.[86,99] These parameters were not allowed to float during the fitting procedure.

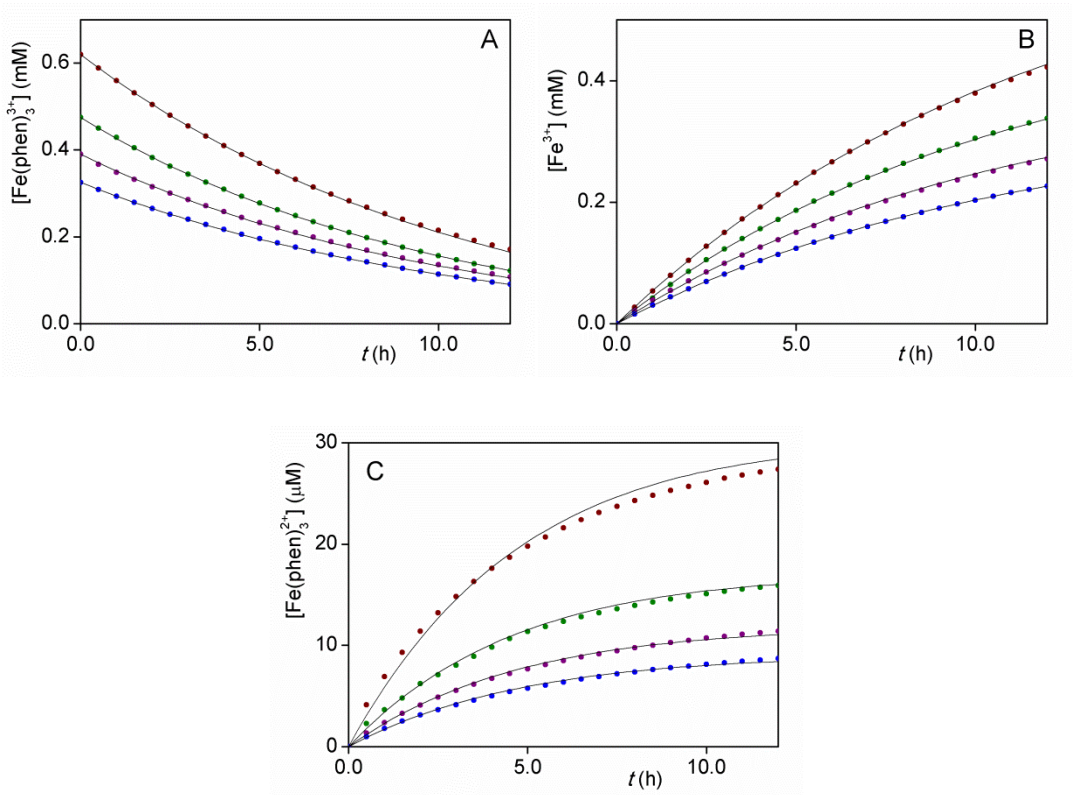

Figure 13. Concentration profiles in the uncatalyzed decomposition reaction of $Fe(phen)_3^{3+}$ at different initial concentrations of the complex. $[H_2SO_4]$ = 1.00 M; T = 25.0 °C. **A**: $Fe(phen)_3^{3+}$. **B**: Fe^{3+}. **C**: $Fe(phen)_3^{2+}$. Circles: points calculated by the molar spectra of the species and the linear algebraic method described in Ch. 4.6. Only 25% of the calculated points are shown for clarity. Lines: results of the global fit to the model described by reactions 24-28.

Reaction 25 is the disproportionation reaction of $Fe(phen)_3^{3+}$ yielding the corresponding Fe(II) and Fe(IV) complexes. The disproportionation of $Fe(phen)_3^{3+}$ was postulated earlier in order to interpret kinetic observations in the Ce(IV) – $Fe(phen)_3^{2+}$ system.[103,115] However, the appropriate experiments to test the decomposition of the Fe(III) complex were not carried out in those works. The second order rate equation (25) of the formation of $Fe(phen)_3^{2+}$ strongly suggests

that the iron(II) complex is produced in a disproportionation reaction. Beyond doubt, the $Fe(phen)_3^{4+}$ complex formed in reaction 25 is a strong oxidizing agent. The series of fast elementary steps leading to the final products are unresolved at this point. However, an oxidized product must form. There are literature reports on the formation of dioxygen and also the oxidized ligand (phenO) in the reaction of $Fe(phen)_3^{3+}$ with hydroxide ion.[96] In the present system, no effort was made to test the formation of O_2 in the reaction mixture. Yet, there is some evidence indicating the presence of phenO, which was detected by ESI mass spectrometry (Figure 2C).

Based on the model above, the differential rate equations were deduced for Fe^{3+}, $Fe(phen)_3^{3+}$ and $Fe(phen)_3^{2+}$ and the concentration profiles measured under different initial conditions were evaluated together by using proportional weighting. The measured and fitted curves are shown in Figure 13. Parameters $k_{24} = (2.55 \pm 0.11) \times 10^{-5} s^{-1}$, and $k_{25} = (2.36 \pm 0.08) \times 10^{-3}\ M^{-1}s^{-1}$ were estimated by nonlinear least squares fitting.

5.2.2 Catalytic decomposition of $Fe(phen)_3^{3+}$

It was found that the presence of the oxidized ligand (phenO) significantly influences the reaction of $Fe(phen)_3^{2+}$ with PMS (see Ch. 5.3). Since $Fe(phen)_3^{2+}$ and HSO_5^- do not react with phenO under the conditions applied, the simplest explanation for the exotic nature of the unexpected phenomenon is due to the reaction between the corresponding iron(III) complex and phenO. This reaction was studied by variation of the concentrations of phenO and $Fe(phen)_3^{3+}$. Again, spectral series were recorded and the concentration profiles of the species were calculated by the linear algebraic method (Ch. 4.6). The kinetic traces show that the addition of phenO to the iron(III) phenanthroline complex increases the rate of both the loss of $Fe(phen)_3^{3+}$ and the formation of $Fe(phen)_3^{2+}$. However, the spectral decomposition also revealed that there is no decrease in the concentration of phenO throughout the reaction which suggests catalytic behavior for the N-oxide in reaction 25. Since some phenO is produced in the uncatalyzed decomposition of $Fe(phen)_3^{3+}$, the oxidized ligand can be considered an autocatalyst.

The dependence of the initial rate of the loss of $Fe(phen)_3^{3+}$ on the reactant concentrations are shown in Figures 14A and 14B. The linear dependencies imply the following experimental rate equation for the catalytic route:

$$v = k_{29}[Fe(phen)_3^{3+}][phenO] \qquad (29)$$

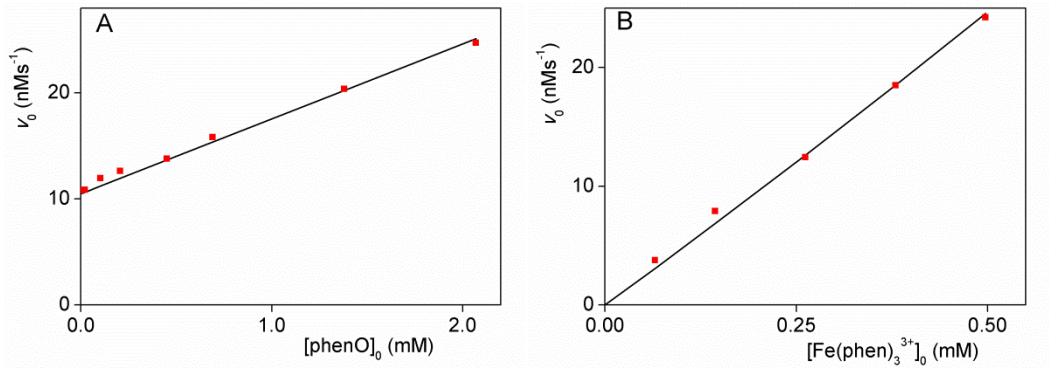

Figure 14. Initial rate of the catalytic decomposition of $Fe(phen)_3^{3+}$ as a function of the phenO and $Fe(phen)_3^{3+}$ concentrations. $[H_2SO_4]$ = 1.00 M; T = 25.0 °C.
A: dependence on phenO. $[Fe(phen)_3^{3+}]_0$ = 0.390 mM. **B**: dependence on $Fe(phen)_3^{3+}$. $[phenO]_0$ = 1.20 mM. The two sets of data were evaluated together. Lines: results of best fit to eq 30.

In Figure 14A, the initial rate has a positive intercept which gives the rate of the uncatalyzed decomposition of $Fe(phen)_3^{3+}$ including both the proton-assisted dissociation (24) and the second order redox reaction (25). In Figure 14B, there is no intercept as no reaction is possible without the presence of $Fe(phen)_3^{3+}$.

When fitting the initial rates shown in Figure 14A and 14B, the following expression was used, which is the sum of eqs 24, 25 and 29:

$$-\frac{d[Fe(phen)_3^{3+}]_0}{dt} = [Fe(phen)_3^{3+}]_0(k_{24} + 2k_{25}[Fe(phen)_3^{3+}]_0 + 2k_{29}[phenO]_0) \qquad (30)$$

Parameters determined earlier (k_{24}, k_{25}) were fixed during the fitting procedure and k_{29} = (8.5 ± 0.3) × 10^{-3} $M^{-1}s^{-1}$ was estimated by nonlinear least squares fitting. The curvature in the $Fe(phen)_3^{3+}$ dependence caused by the second order term becomes visible only at higher complex concentrations, its contribution to the overall initial rate is inferior in the concentration range of the study.

It should be mentioned that at larger reactant concentrations, the kinetic trace may have a break point that marks the complete consumption of the iron(III) complex (Figure 15A). After this reaction time, Fe^{3+} and $Fe(phen)_3^{2+}$ cannot form any longer and the only detectable change in the system is the proton-assisted dissociation of the iron(II) complex (27).

Figure 15A shows that by the time the first points were recorded, the reaction mixture already contained considerable amount of the iron(II) complex. There is significant change in the concentrations of both complexes in the beginning of the reaction which is apparently faster compared to the time resolution of the measurement. Such a reaction in the initial phase that reaches completion rapidly may imply a reactant that is consumed up. The N-oxide used in the study was prepared by oxidation of phen with stoichiometric amount of PMS. In principle, the initial fast loss of $Fe(phen)_3^{3+}$ and increase in $Fe(phen)_3^{2+}$ could be interpreted by the presence of an oxidizable impurity produced by a slight excess of PMS over phen. However, a control experiment was carried out in which 0.7 equivalent of PMS was used to prepare phenO. The results with this reactant rule out the possibility of over-oxidation of phen. In this case, the reaction was followed by a stopped-flow instrument and the detected kinetic curves (Figure 15B) confirmed an initial increase of $[Fe(phen)_3^{2+}]_0$ that cannot be attributed to a minor contaminant.

In the light of these observations, it was concluded that the rates (v_0) shown in Figure 14 and the experimentel rate equation (29) proposed indeed describe a secondary reaction because the initial absorbance change was undetectable by the time resolution used to record the spectral series. However, the model consisting of reactions 24-28 and 31-32 is in good agreement with the experimental data except for the initial stage.

The increase in the $Fe(phen)_3^{2+}$ concentration (Figure 15B) can be satisfactorily estimated by a single exponential function and the observed first order rate constant, $k_{obs} = (1.6 \pm 0.2) \times 10^{-2}$ s^{-1}, was found hardly dependent on $[phenO]_0$. However, the details of this initial process are unclear at this point. Such a reaction was not observed in the phenO-free studies (Ch. 5.2.1).

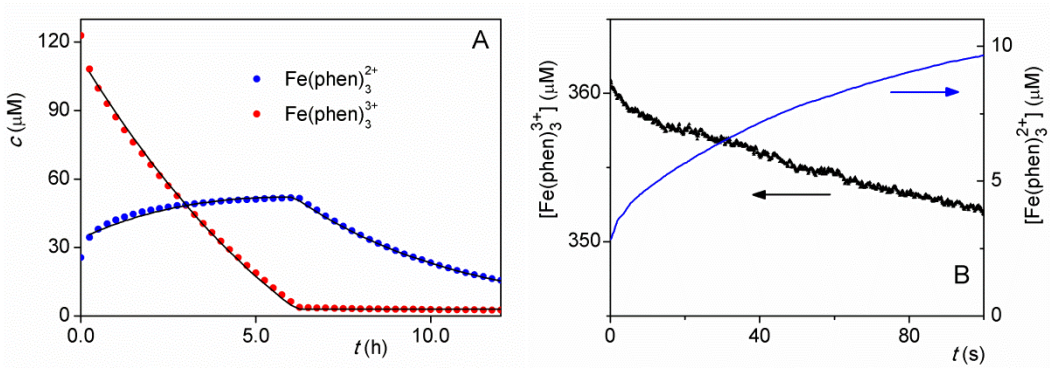

Figure 15. Concentration profiles of the iron complexes in the phenO-catalyzed decomposition of $[Fe(phen)_3^{3+}]$.
A: $[Fe(phen)_3^{3+}]_{tot}$ = 0.145 mM; $[phenO]_0$ = 1.20 mM; $[H_2SO_4]$ = 1.00 M; T = 25.0 °C. Circles: points calculated by the molar spectra of the species and the linear algebraic method described in Ch. 4.6. Only 50% of the calculated points are shown for clarity. Lines: results of the best fit by using rate equations 24-29 and ignoring the first measured points. The two curves were fitted simultaneously. Initial concentrations used for fitting $[Fe(phen)_3^{3+}]_0$ = 0.114 mM; $[Fe(phen)_3^{2+}]_0$ = 0.31 mM.
B: $[Fe(phen)_3^{3+}]_{tot}$ = 0.365 mM; $[phenO]_0$ = 0.436 mM; $[phen]_0$ = 0.197 mM; $[H_2SO_4]$ = 1.00 M; T = 25.0 °C.

The catalytic role of phenO in the decomposition reaction of $Fe(phen)_3^{3+}$ can be explained by assuming that it is oxidized to a radical by the iron(III) complex (31), which can in turn oxidize another $Fe(phen)_3^{3+}$ to $Fe(phen)_3^{4+}$(32), completing a catalytic cycle for the N-oxide in 25. After the formation of the iron(IV) species, reaction 26 proceeds.

$$Fe(phen)_3^{3+} + phenO \rightarrow Fe(phen)_3^{2+} + \{Int\} \quad (31)$$

$$Fe(phen)_3^{3+} + \{Int\} \rightarrow Fe(phen)_3^{4+} + phenO \quad (32)$$

Some experimental support for the involvement of a $Fe(phen)_3^{4+}$ species was provided by ESI-MS in the $Fe(phen)_3^{2+}$ - PMS reaction. As shown in Figure 16, a low-intensity, but clearly identifiable set of peaks was found that corresponds to the formula $FeC_{36}H_{24}N_6O_4S^{2+}$. This can be interpreted as an ion pair formed between $Fe(phen)_3^{4+}$ and SO_4^{2-}, the highest positively and negatively charged ions in the solution. In collisionally induced dissociation experiments, a loss of SO_3 was detected from this ion (Figure 16B), which shows that the sulfate moiety is intact in

$FeC_{36}H_{24}N_6O_4S^{2+}$. Adventitious oxidation during ionization is very unlikely because the ESI-MS conditions used were reductive.

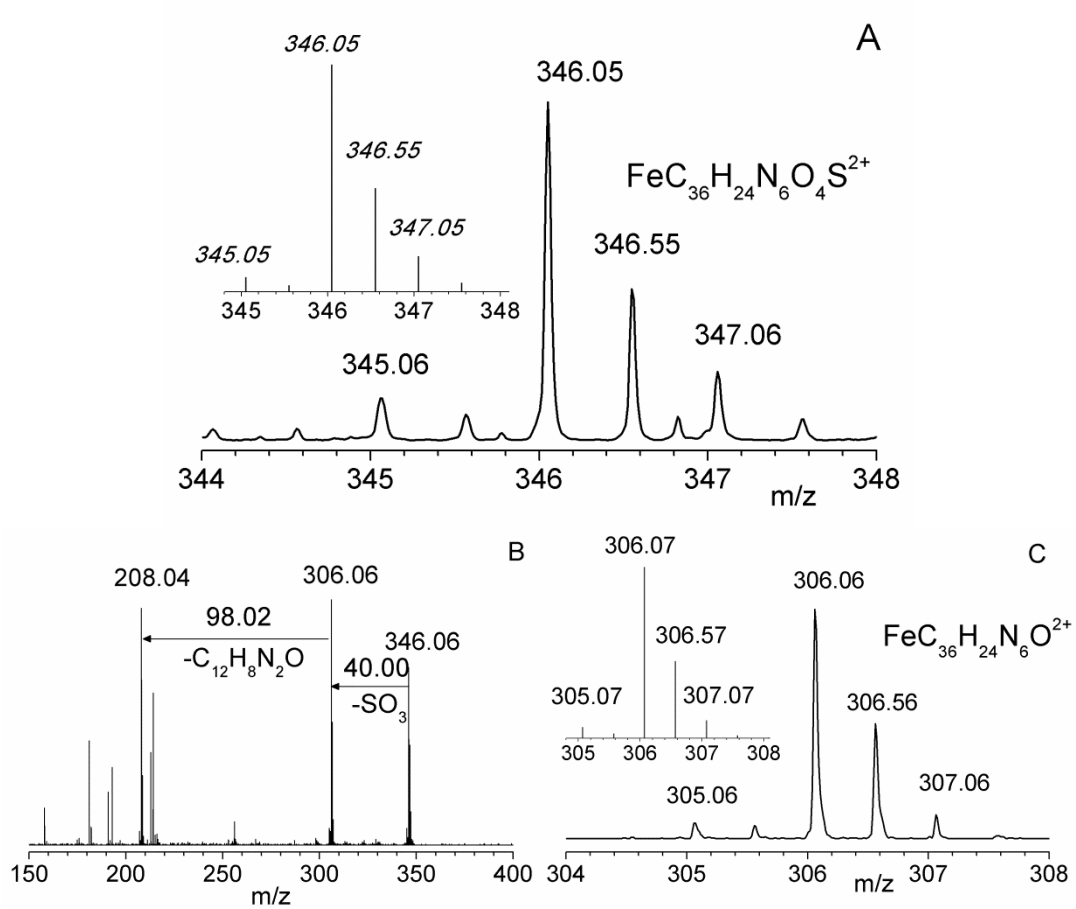

Figure 16. ESI-MS identification of $Fe(phen)_3(SO_4)^{2+}$ in the reaction between $Fe(phen)_3^{2+}$ and HSO_5^-.

A: detected and calculated spectrum for $FeC_{36}H_{24}N_6O_4S^{2+}$ = $\{Fe(phen)_3^{4+} \cdot SO_4^{2-}\}$. **B**: Collision Induced Dissociation ESI Mass Spectroscopy during the reaction of $Fe(phen)_3^{2+}$ with HSO_5^-. Parent ion: $FeC_{36}H_{24}N_6O_4S^{2+}$. Only two iron containing fragments have been identified at m/z = 306.06 and 208.04. The first is a loss of SO_3 from the parent iron, the second is a loss of $C_{12}H_8N_2O$ (phenO) from the m/z = 306.06 ion. Other fragments observable in the spectrum do not contain iron. **C**: detected and simulated spectrum of $FeC_{36}H_{24}N_6O^{2+}$.

Possible complexations between free aqueous Fe(II) and Fe(III) and the oxidized ligand, phenO, were also experimentally tested. These studies revealed that there are no spectral changes upon mixing the metal and the suspected ligand in acidic medium (Figure 17A and 17B), therefore any interference from the formation of N-oxide complexes can be ruled out. According to earlier results, $Fe(phenO)_3^{2+}$ can be prepared in solid form but the complex is not stable in aqueous solution.[96]

It should be mentioned that these experiments exclude the stepwise formation of N-oxide complexes, but does not rule out the possibility of the direct oxidation of the ligand while it is coordinated to the metal ion. Thus, N-oxide complexes of iron(II) or iron(III) may be involved in the overall mechanism.

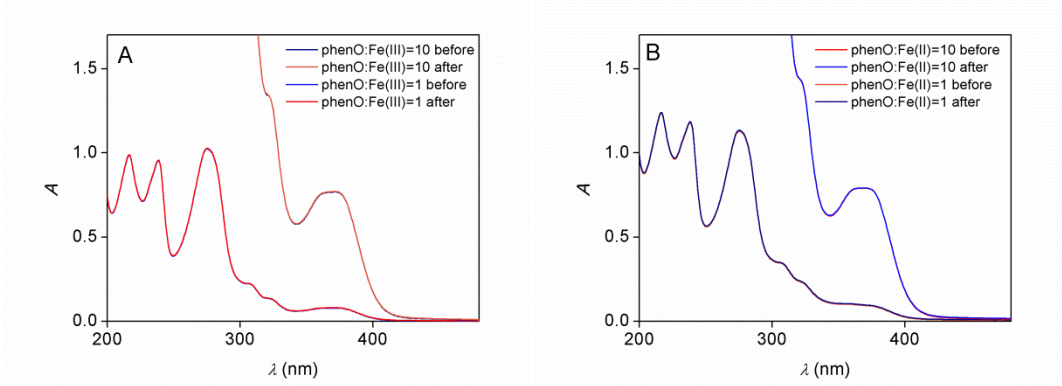

Figure 17. Absence of complex formation between phenanthroline-mono-N-oxide and Fe(II) or Fe(III) ions. The spectra before and after mixing the reactants are perfectly identical.

A: iron(III) system; $[Fe^{3+}]_0$ = 0.041 mM; $[phenO]_0$ = 0.040 or 0.40 mM; $[H_2SO_4]$ = 1.11 M; T = 25.0 °C; path length = 1.000 cm.

B: iron(II) system; $[Fe^{2+}]_0$ = 0.042 mM; $[phenO]_0$ = 0.040 or 0.40 mM; $[H_2SO_4]$ = 1.11 M; T = 25.0 °C; path length = 1.000 cm.

5.3 *Reaction between PMS and $Fe(phen)_3^{2+}$*

5.3.1 Initial stage of the reaction

Representative kinetic traces measured in the $Fe(phen)_3^{2+}$ – PMS are shown in Figure 18A. In this process, the absorbance at the absorption maxima of the Fe(II) complex (510 nm) and the Fe(III) complex (591 nm) shows nonmonotonous time dependence which is an unquestionable evidence of a multistep process. This conclusion was further strengthened by the spectral observations (Figure 18B) which will be discussed briefly in the next subchapter.

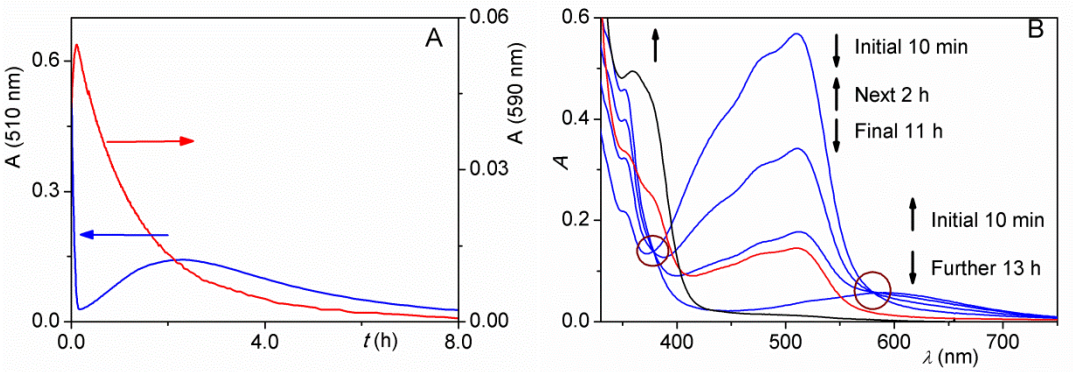

Figure 18. Kinetic traces (A) and spectral series (B) detected in the reaction between PMS and $Fe(phen)_3^{2+}$. $[PMS]_0$ = 11.4 mM; $[Fe(phen)_3^{2+}]_0$ = 75.3 μM; $[H_2SO_4]$ = 1.01×10^{-2} M; T = 25.0 °C; path length = 1.000 cm.
A: left and right axes show the absorbance change at 510 nm and 590 nm, respectively.
B: blue lines show the spectra recorded in the first 10 minutes of the reaction, red and black lines show the spectra recorded after 2.2 and 12.8 hours, respectively, circles highlight isosbestic points at the initial stage of the oxidation.

The primary reaction between $Fe(phen)_3^{2+}$ and PMS is not completely separated from subsequent processes in time. Due to this overlap, even the first segments of the detected curves could not be fitted with a single exponential function although pseudo-first order conditions were applied. Thus, the initial rate method was used, which is free from interference from later processes. The initial rate was defined as the initial rate of absorbance change at 510 nm, which is characteristic of the loss of reactant $Fe(phen)_3^{2+}$:

$$v_0 = -\frac{dA\ (510\ \text{nm})}{dt} = -\varepsilon_{510\ \text{nm}} \frac{d\left[\text{Fe(phen)}_3^{2+}\right]_0}{dt} \qquad (33)$$

Figure 19A shows the dependence of the initial rate on the concentration of PMS. The rates show saturation and a small intercept. The small intercept belongs to a chemical process that does not require the presence of the oxidant. This was experimentally confirmed in oxidant-free solutions. The $Fe(phen)_3^{2+}$-dependence of the initial reaction rate is depicted in Figure 19B. At high PMS concentrations, the rate varies linearly with the $Fe(phen)_3^{2+}$ concentration. In this case, there is no intercept as no reaction is possible without the presence of $Fe(phen)_3^{2+}$. The addition of the free ligand to the reaction mixture did not influence the initial rate at all, thus an oxidation route via the dissociation of the Fe(II) complex is ruled out.

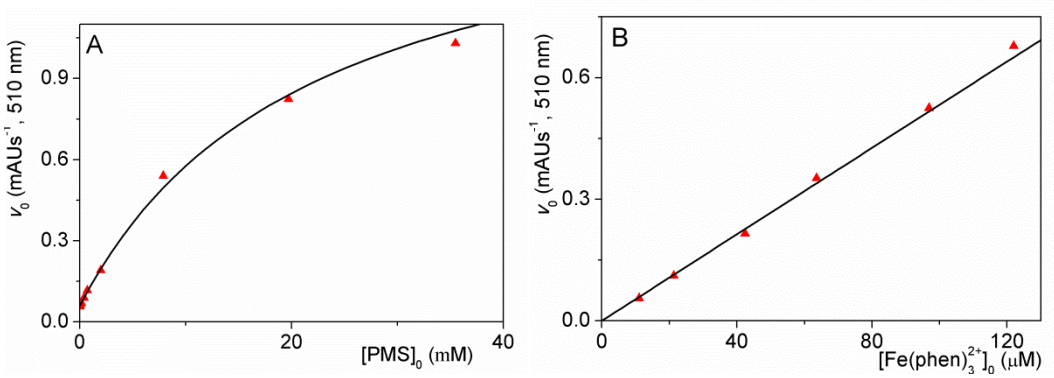

Figure 19. Dependence of the initial rate on the reactant concentrations during the reaction between $Fe(phen)_3^{2+}$ and HSO_5^-. $[H_2SO_4]$ = 1.00 M; T = 25.0 °C; path length = 1.000 cm. **A**: dependence on PMS. $[Fe(phen)_3^{2+}]_0$ = 95.5 μM. **B**: dependence on $Fe(phen)_3^{2+}$. $[PMS]_0$ = 8.22 mM. The two sets of data were evaluated together using proportional weighting (the weight used for the experimental value of v at each point is v^{-2}). Lines: results of best fit to eq 37.

The saturation tendency was explained by an adduct formation of the reactants and the findings were interpreted with the following kinetic model:

- acid catalyzed dissociation of $Fe(phen)_3^{2+}$ (27);
- the ion pair formation between the reactants that is considered a fast pre-equilibrium (34);

- the rate determining intramolecular electron transfer process followed by the dissociation of the adduct into the corresponding Fe(III) complex and sulfate ion radical($SO_4^{-\bullet}$) (35);
- fast oxidation of another Fe(II) complex by the $SO_4^{-\bullet}$ formed in the previous step (36).

$$Fe(phen)_3^{2+} (+ 3H^+) \rightarrow Fe^{2+} + 3Hphen^+ \quad (27)$$

$$v = k_{27}[Fe(phen)_3^{2+}]$$

$$Fe(phen)_3^{2+} + HSO_5^- \rightleftharpoons [Fe(phen)_3 \cdot HSO_5]^+ \quad (34)$$

$$K_{34} = \frac{[Fe(phen)_3 \cdot HSO_5^+]}{[Fe(phen)_3^{2+}][HSO_5^-]}$$

$$[Fe(phen)_3 \cdot HSO_5]^+ + H^+ \rightarrow Fe(phen)_3^{3+} + SO_4^{-\bullet} + H_2O \quad (35)$$

$$v = k_{35}[Fe(phen)_3 \cdot HSO_5^+]$$

$$Fe(phen)_3^{2+} + SO_4^{-\bullet} \rightarrow Fe(phen)_3^{3+} + SO_4^{2-} \quad (36)$$

$$v = fast$$

In this model, the proton-assisted dissociation of the complex (27) occurs simultaneously with the oxidation process and was studied independently in the absence of the oxidant. The following expression was derived for the initial rate:

$$v_0 = \varepsilon_{510\,nm}[Fe(phen)_3^{2+}]_0 \left(k_{27} + \frac{2k_{35}K_{34}[PMS]_0}{1 + K_{34}[PMS]_0}\right) \quad (37)$$

The initial rates were studied at two different acidities: in 1.00 M H_2SO_4 under which conditions the reactions of $Fe(phen)_3^{3+}$ were investigated and in 10.0 mM H_2SO_4, where the aforementioned unusual kinetic phenomenon was encountered (Figure 18). The parameters were estimated by nonlinear least squares fitting and are listed in Table 7.

Table 7. Parameters determined in the initial stage of the reaction between PMS and $Fe(phen)_3^{2+}$. $T = 25$ °C

Medium	$k_{27} \times 10^5$ (s^{-1})	$k_{35} \times 10^4$ (s^{-1})	K_{34} (M^{-1})
1.00 M H_2SO_4	5.9 ± 0.1	7.5 ± 0.5	48 ± 5
10.0 mM H_2SO_4	5.8 ± 0.3	6.5 ± 0.9	63 ± 18

The model proposed here interprets only the initial part of the reaction. It should be added that pH dependence is not discussed in detail here. It was found that varying the acidity does not change the initial stage of the kinetic curves and the corresponding parameters significantly (Table 7), which implies that the oxidation reaction does not show pH dependent kinetics. This is not unexpected as neither of the two reagents participates in any known pH dependent equilibria in the concentration range of the present study.

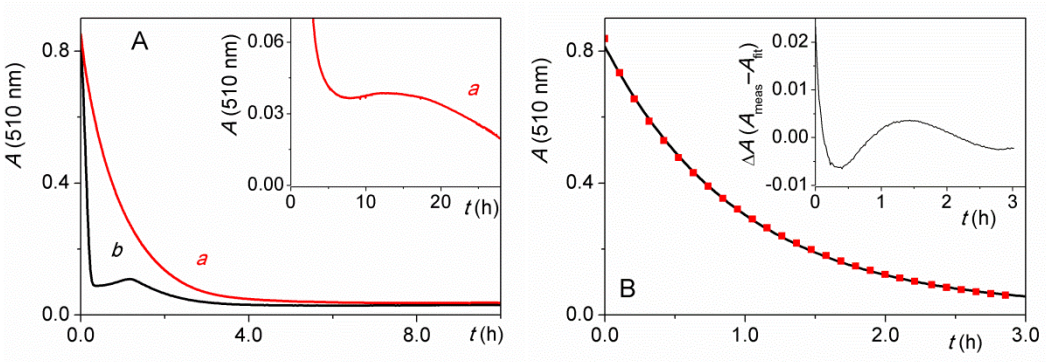

Figure 20. Kinetic traces detected at different acidity in the reaction between PMS and $Fe(phen)_3^{2+}$.
A: $[Fe(phen)_3^{2+}]_0$ = 83.9 μM; T = 25.0 °C; path length = 1.000 cm; $[PMS]_0$ = 11.7 mM; $[H_2SO_4]$ = 1.00 M (*a*); $[PMS]_0$ = 16.7 mM; $[H_2SO_4] = 1.00 \times 10^{-2}$ M (*b*). Inset: enlargement of curve *a*.
B: $[Fe(phen)_3^{2+}]_0$ = 83.9 μM; T = 25.0 °C; path length = 1.000 cm; $[PMS]_0$ = 11.7 mM; $[H_2SO_4]$ = 1.00 M. Squares: experimental points (only 15% of the recorded points are shown for clarity), continuous line: result of the fit of the data to a single exponential function. Inset: residuals from the fit; the difference between the actual and the exponentially fitted values.

The overall kinetics, on the other hand, does depend on the pH. Two kinetic curves detected at similar initial reactant concentrations but at different acidities are

shown in Figure 20A. At about pH ~ 1.8, curve (*b*) features two clearly visible extrema, meanwhile under more acidic conditions (pH ~ 0.0), seemingly the absorbance decreases monotonously (curve *a*) but a closer look at the curve (inset) reveals that this trace does have a local minimum and maximum, too. The difference in the curves can be interpreted in terms of the pH dependence of the secondary reactions, which will be discussed briefly in the subsequent subchapter.

Figure 20B demonstrates that although the exponential fit of the initial absorbance decrease detected under strongly acidic conditions may appear to be satisfactory, the careful examination of the residuals (the difference between the actual and the fitted values) clearly reveals that they do not lie randomly about the zero line (inset). The observations shown in Figure 20 confirms the multiphasic kinetics of the reaction at both pH.

An earlier study reported simple second order kinetics for the reaction of $Fe(phen)_3^{2+}$ with PMS in a similar pH range (pH = 1–3) as the one used in this study.[116] The findings regarding the initial phase of the oxidation do not reproduce those earlier published results[116] presumably for the following reasons. It was claimed that the reaction was studied under pseudo-first order conditions and it seems that the multiphasic nature of the process was completely ignored. A closer look at Figure 1 in that work reveals that the kinetic curves were not evaluated longer than a conversion of 60-70% (i. e. less than two half-lives as defined by the loss of the absorbance peak of the iron(II) complex) and never used more than 8 points per kinetic curve. The serious shortcomings of this approach were discussed in the literature.[154,155] In addition, the stoichiometric study reported there, which found a straightforward 2:1 ratio for the reactants, seems highly questionable for several reasons. The study was carried out by using $Fe(phen)_3^{2+}$ in excess and the remaining concentration of this species was determined spectrophotometrically after the completion of the process. However, the results were probably corrupted by the acid dissociation of $Fe(phen)_3^{2+}$ which undergoes on a time scale similar to that of the oxidation reaction.[91] In addition, the kinetic curves at longer reaction times (Figure 18A) clearly show a multistep process which has a complicated stoichiometry with the formation of 1,10-phenanthroline-mono-N-oxide, free

iron(III) and, at lower PMS concentrations, free phenanthroline ligand and also free iron(II).

The formation of an adduct similar to the one shown in reaction 34 was proposed in the reaction between $Fe(phen)_3^{2+}$ and $S_2O_8^{2-}$.[109] Amazingly, an ion pair was postulated in the earlier work that discusses the $Fe(phen)_3^{2+}$ – HSO_5^- reaction, too,[116] despite the fact that the rate equation reported there did not require such an assumption. The experimental basis of that proposal was a small change observed in the UV-vis spectra after mixing the reagents. Unsuccessful efforts were made to reproduce these observations. In fact, the unstructured small spectral changes (shown in the supplementary information of the earlier work)[116] may very well represent a shift in the spectral baseline. This effect could be tested based on absorbance readings in regions where the solution does not absorb. However, this test is not possible based on the published data as they were given only at wavelengths where the components have significant absorption.

The formation of an adduct between HSO_5^- and the coordinatively saturated $Fe(phen)_3^{2+}$ might seem quite puzzling. Yet, there are two independent experimental findings that support the existence of such an adduct: the rate equation found and the ESI-MS results.

The experimental data show saturation character when the initial rate is plotted as a function of PMS concentration. In principle, a sequence of reactions where $Fe(phen)_3^{2+}$ undergoes some oxidant-independent reaction first, the product of which reacts with PMS could also interpret such a saturation if there is a shift in the rate determining step. However, the dissociative pathway with the initial release of one ligand was explicitly ruled out in the studied reactions. Therefore, the association of reactants, i.e. adduct formation seems to be the simplest explanation that is in agreement with all experimental findings. The rate equation derived on this basis (E37) explains the observations very well.

The reaction mixture after about 5 minutes of reaction time was analyzed with electrospray mass spectroscopy. Figure 21 shows a part of the ESI-MS spectrum, which is characteristic of the formula $FeC_{36}H_{25}N_6O_5S^+$, equivalent to a direct adduct formed from $Fe(phen)_3^{2+}$ and HSO_5^-. In principle, this does not necessarily mean that the adduct is already present in the reaction mixture, because

it may form in the mass spectrometer during the experiments. However, this seems highly unlikely at the low operational pressure of the instrument. Additionally, HSO_4^- is present at considerably higher concentration levels in the solution than HSO_5^- and would be expected to form such an adduct if the source were only the mass spectrometric technique itself. No peaks attributable to $Fe(phen)_3^{2+}\cdot HSO_4^-$ could be identified in the mass spectrum. Therefore, it was concluded that the detected adduct must form specifically from the reactants in the solution.

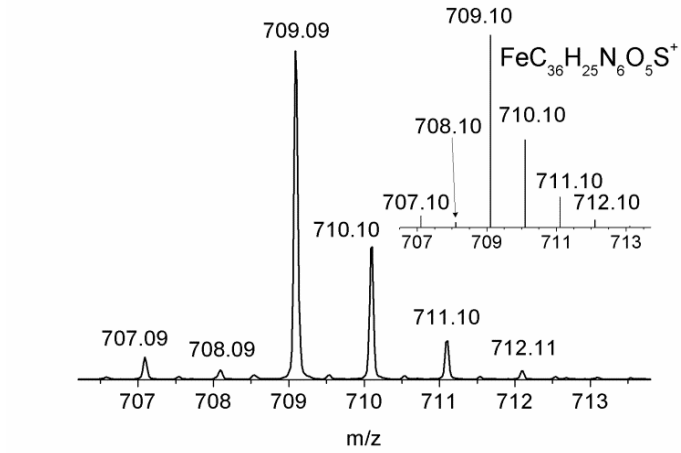

Figure 21. Electrospray ionization mass spectrometric identification of the adduct in the reaction between $Fe(phen)_3^{2+}$ and HSO_5^-. Inset: calculated spectrum for the formula $FeC_{36}H_{25}N_6O_5S^+$ = {$Fe(phen)_3^{2+}\cdot HSO_5^-$}.

The nature of the adduct remains quite unclear at this point. It is unlikely to be a simple ion pair as the association constant (K) is about an order of magnitude higher than expected from the Fuoss equation for a +2:−1 ion pair (K_{ip} = 5.2 M^{-1}).[156] Yet the UV-vis spectrum of the adduct seems to be indistinguishable from that of the parent complex. Therefore, the coordination environment in the unassociated complex must be identical to that in the adduct. Some sort of interaction between the aromatic electron cloud and the HSO_5^- ion could be envisaged as the driving force of the adduct formation, but any such proposal would be highly speculative.

5.3.2 Kinetics of the later stage of the reaction

As shown in Figures 18A and 20A, when the reaction is monitored on a longer time scale, the initial decrease in the absorbance at 510 nm is followed by an increase but after a maximum is reached, the absorbance decreases again. However, the structure of the peak during the absorbance increase (Figure 18B) clearly suggests that it is due to the re-production of the initial complex and not the formation of a new absorbing intermediate. This was also confirmed by the linear algebraic decomposition of the spectral series of the reaction mixture. The re-production of $Fe(phen)_3^{2+}$ is quite unexpected considering that the oxidizing agent is used in large excess.

In the initial phase of the reaction, mainly the oxidation of the central metal ion occurs and the primary product is the tris(phen)iron(III) complex. As Figure 18B shows, this stage features isosbestic points, which disappear as the reaction proceeds. Actually, by using the linear algebraic method applied in the previous chapter, it can be shown that there is a slight change in the linear combination of the concentrations of $Fe(phen)_3^{2+}$ and $Fe(phen)_3^{3+}$ even in the initial phase, but this is negligible for all practical purposes. As the reaction advances, there is a growing change in the linear combination implying that secondary processes occur during the course of the reaction.

The disappearance of the isosbestic points can partially be explained by the known proton-induced dissociations of the complexes. It should also be noted that isosbestic points in the initial stage are visible only in the presence of high concentration of PMS, that is, when the rate of the oxidation is superior to those of the acid dissociations. The disappearance of the isosbestic point at 378 nm, however, clearly cannot be interpreted by the dissociations of the complexes because an increase of absorbance is observed and the free ligand, free iron(III) and its sulfate complexes have lower molar absorptions[157] than those of the tris phenanthroline complexes (Figure 12A). This implies the formation of another species after the initial phase of the reaction that has higher molar absorption than $Fe(phen)_3^{2+}$ and $Fe(phen)_3^{3+}$. The formation of a new oxidation product is another interesting feature of the system. The oxidized form of the ligand was detected in the reaction mixture with ESI-MS (Figure 2D), and identified as

1,10-phenanthroline-mono-N-oxide (phenO). The N-oxide derivative of phen has characteristic band in the 360–380 nm wavelength range with higher ε than the iron(II) and iron(III) phen complexes (Figure 12A) and the calculated absorbance considering the formation of three equivalent phenO perfectly matches the measured final absorbance.

The effects of the final products of the reaction (Fe^{3+} and phenO) were tested on the oxidation. It was found that the striking minimum detected in the absorbance as a function of time (Figure 22A curve ***a***) disappears when phenO is added to the system before initiating the reaction (curve ***b***), but is not influenced by the addition of ferric ion (curve ***c***). The addition of N-oxide does not affect the proton-assisted dissociation of the Fe(II) complex at all (Figure 22B), neither can PMS further oxidize phenO under such acidic conditions (see Ch. 5.1), but increasing the amount of the N-oxide considerably slows the consumption of the iron(II) complex down when the oxidant is present (Figure 22C). This undoubtedly proves that the N-oxide influences the oxidation reaction rather than the dissociation of the complex.

These experiments confirm that the N-oxide plays a key role in the unusual kinetic behavior. The observations were interpreted by the following general model which qualitatively describes the experimental data:

- oxidation of the Fe(II) complex to the corresponding Fe(III) complex by PMS (38, the sum of reactions 34-36),
- the formation of the oxidized ligand and Fe(III), the final oxidation products of the complex (39),
- formal disproportionation reaction of the Fe(III) complex, which is (auto)catalyzed by phenO and results in the formation of the initial Fe(II) complex and the oxidized ligand (40, the sum of 25 and 26).

$$2Fe(phen)_3^{2+} + HSO_5^- + H^+ \rightarrow 2Fe(phen)_3^{3+} + SO_4^{2-} + H_2O \qquad (38)$$

$$Fe(phen)_3^{3+} + 3HSO_5^- \rightarrow 3phenO + Fe^{3+} + 3SO_4^{2-} + 3H^+ \qquad (39)$$

$$2Fe(phen)_3^{3+} + H_2O \rightarrow Fe(phen)_3^{2+} + phenO + Fe^{2+} + 2Hphen^+ \qquad (40)$$

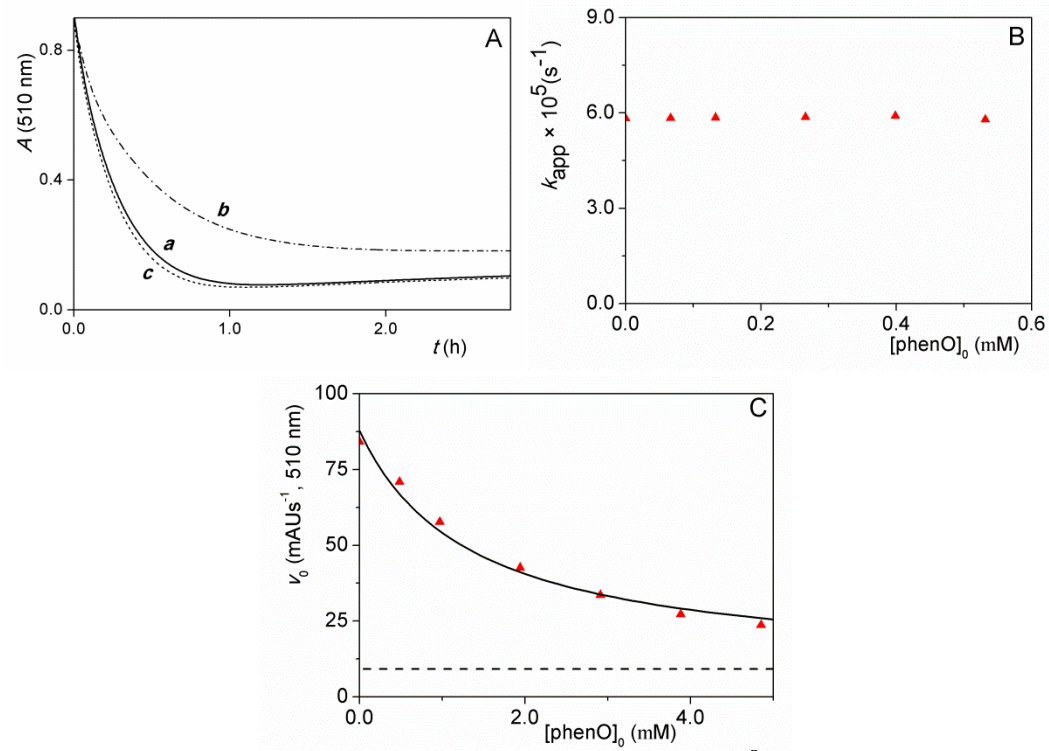

Figure 22. Effect of phenO on the reaction between $Fe(phen)_3^{2+}$ and PMS. T = 25.0 °C; path length = 1.000 cm.

A: traces detected in the reaction. $[Fe(phen)_3^{2+}]_0$ = 81 μM; $[PMS]_0$ = 30 mM; $[H_2SO_4]$ = 1.01×10^{-2} M; (a) without additional reactants; (b) 80 μM phenO added before the reaction; (c) 80 μM Fe^{3+} added before the reaction.

B: effect of phenO on the proton-assisted dissociation of $Fe(phen)_3^{2+}$. $[Fe(phen)_3^{2+}]_0$ = 83.9 μM; $[H_2SO_4]$ = 1.00 M.

C: phenO dependence of the initial rate of the reaction between $Fe(phen)_3^{2+}$ and PMS. $[Fe(phen)_3^{2+}]_0$ = 142 μM; $[PMS]_0$ = 14.6 mM; $[H_2SO_4]$ = 1.00 M. Triangles: experimental data. Continuous line: result of best fit to eq 48. Horizontal dashed line marks the rate of the proton-assisted dissociation of $Fe(phen)_3^{2+}$ under these conditions.

The proton-induced dissociation of $Fe(phen)_3^{2+}$ (27) and reaction 40 produce free iron(II), but the oxidation of Fe^{2+} by $Fe(phen)_3^{3+}$ (28) and PMS (41)[1] were confirmed to be fast (k_{28} = 2.7 × 10^5 $M^{-1}s^{-1}$ and k_{41} = 3.7 × 10^4 $M^{-1}s^{-1}$, respectively) on the time scale of the present study and these reactions ensure that Fe(II) is converted into Fe(III) rapidly as long as any of these oxidants is present.

$$Fe^{2+} + Fe(phen)_3^{3+} \rightarrow Fe^{3+} + Fe(phen)_3^{2+} \qquad (28)$$

$$2Fe^{2+} + HSO_5^- + H^+ \rightarrow 2Fe^{3+} + SO_4^{2-} + H_2O \quad (41)$$

The overall reaction 39 is obtained by combining the contributions of the proton-induced dissociation of $Fe(phen)_3^{3+}$ (24, see Ch. 5.2) and the oxidation of phen to phenO by PMS (11, see Ch. 5.1).

$$Fe(phen)_3^{3+} (+ 3H^+) \rightarrow Fe^{3+} + 3Hphen^+ \quad (24)$$

$$Hphen^+ + HSO_5^- \rightarrow phenO + SO_4^{2-} + 2H^+ \quad (11)$$

The dissociation generates Fe^{3+}, which is one of the final products of the overall reaction. The formation of the N-oxide can occur via the oxidation of the uncoordinated phen (produced in the acid dissociations of the tris complexes, and also in reaction 40), but the direct oxidation of the coordinated ligand cannot be completely ruled out, either. These steps make Fe(III) and phenO the final products of the overall reaction on a longer time scale.

The stoichiometry of the overall oxidation can be given by the following equation:

$$2Fe(phen)_3^{2+} + 7HSO_5^- \rightarrow 2Fe^{3+} + 7SO_4^{2-} + H_2O + 6phenO + 5H^+ \quad (42)$$

As shown, the mechanism involves several subsystems but most of them can be studied individually. Since some intermediates (Fe^{2+}, phen, $Fe(phen)_3^{3+}$) and one of the final products (phenO) have influence on the concentration change of $Fe(phen)_3^{2+}$ to some extent, $[Fe(phen)_3^{2+}]_t$ cannot be expressed in an explicit form.

The differential rate equations (43-47), on the other hand, can be given for the major species involved, $Fe(phen)_3^{2+}$, $Fe(phen)_3^{3+}$, Fe^{2+}, phen and phenO. The oxidant is present in large excess and its concentration is considered constant throughout the reaction.

$$\frac{d[Fe(phen)_3^{2+}]}{dt} = -k_{27}[Fe(phen)_3^{2+}] - 2[Fe(phen)_3^{2+}]\frac{k_{35}K_{34}[PMS]}{1 + K_{34}[PMS]} +$$

$$+k_{25}[Fe(phen)_3^{3+}]^2 + k_{28}[Fe(phen)_3^{3+}][Fe^{2+}] + k_{29}[Fe(phen)_3^{3+}][phenO] \quad (43)$$

$$\frac{d[Fe(phen)_3^{3+}]}{dt} = 2[Fe(phen)_3^{2+}]\frac{k_{35}K_{34}[PMS]}{1 + K_{34}[PMS]} - k_{28}[Fe(phen)_3^{3+}][Fe^{2+}] -$$

$$-k_{24}[Fe(phen)_3^{3+}] - 2k_{25}[Fe(phen)_3^{3+}]^2 - 2k_{29}[Fe(phen)_3^{3+}][phenO] \quad (44)$$

$$\frac{d[\text{phen}]}{dt} = 3k_{24}[\text{Fe(phen)}_3^{3+}] + 3k_{27}[\text{Fe(phen)}_3^{2+}] + 2k_{25}[\text{Fe(phen)}_3^{3+}]^2 + \\ +2k_{29}[\text{Fe(phen)}_3^{3+}][\text{phenO}] - k_{11}[\text{PMS}][\text{phen}] \quad (45)$$

$$\frac{d[\text{phenO}]}{dt} = k_{11}[\text{PMS}][\text{phen}] + k_{25}[\text{Fe(phen)}_3^{3+}]^2 + k_{29}[\text{Fe(phen)}_3^{3+}][\text{phenO}] \quad (46)$$

$$\frac{d[\text{Fe}^{2+}]}{dt} = k_{27}[\text{Fe(phen)}_3^{2+}] + k_{25}[\text{Fe(phen)}_3^{3+}]^2 + k_{29}[\text{Fe(phen)}_3^{3+}][\text{phenO}] - \\ - k_{28}[\text{Fe(phen)}_3^{3+}][\text{Fe}^{2+}] - 2k_{41}[\text{PMS}][\text{Fe}^{2+}] \quad (47)$$

This differential equation system includes all the processes explored in the overall oxidation reaction. By using the rate constants determined, kinetic curves and concentration dependencies can be simulated.

The process suspected to be important in the unusual kinetic behavior is the temporary re-formation of the initial iron(II) complex (40). Since free iron(II) cannot be present in the reaction mixture under the applied conditions, the only feasible way of the generation of $Fe(phen)_3^{2+}$ is by the conversion of the corresponding iron(III) complex. This cannot be a straightforward reduction due to the presence of large excess of PMS. The re-formation is considered to occur in 40 which is catalyzed by phenO. The details of this reaction were discussed in the previous chapter (Ch. 5.2). The role of this reaction in the overall mechanism can be important when a significant amount of Fe(III) is still present in the form of the tris phenanthroline complex and a considerable amount of phenO is already produced in order to exert its catalytic effect. In the early stage of the reaction, the concentrations of both phen and phenO are low and mainly 38 proceeds (see isosbestic points). It takes time for phenO to form and 40 to kick in.

When phenO is added to the initial mixture, the re-formation may proceed from the very beginning of the reaction resulting in a slower consumption of $Fe(phen)_3^{2+}$ (Figures 22A and C). The phenO-dependence of the initial rate of the oxidation was simulated by the model using the rate constants and the initial concentrations of the reactants. It was found that the deceleration of the loss of $Fe(phen)_3^{2+}$ estimated by the simulation is significantly smaller than the measured

one which implies that further steps may be operative in the overall reaction. The process in question should either rapidly consume the oxidant or contribute to the re-formation of $Fe(phen)_3^{2+}$. The former one is unlikely because PMS is present in excess compared to phenO (from 3-fold to 30-fold), minor impurities in phenO cannot cause significant change in [PMS] and PMS cannot oxidize phenO under such acidic conditions (Ch. 5.1). It seems more feasible that the missing reaction has an influence on the $Fe(phen)_3^{3+} \rightarrow Fe(phen)_3^{2+}$ conversion and may be connected to the effect shown in Figure 15.

The phenO-dependence of the initial rate of the PMS – $Fe(phen)_3^{2+}$ reaction was fitted to the following empirical expression:

$$\frac{v_0}{\varepsilon_{510\,\mathrm{nm}}[\mathrm{Fe(phen)_3^{2+}}]_0} = k_{27} + \frac{k_{48}}{1 + C[\mathrm{phenO}]_0} \qquad (48)$$

In this equation, k_{27} is the rate constant of the proton-assisted dissociation of $Fe(phen)_3^{2+}$, this parameter gives the limiting minimum rate. Figure 22B shows that the N-oxide does not affect the rate of the dissociation of the complex. Thus, it can be assumed that at large [phenO], the oxidation essentially stops but the dissociation of the complex still proceeds. The k_{48} parameter is the apparent rate constant of the $Fe(phen)_3^{2+}$ – PMS oxidation reaction. At the given $[PMS]_0$, it can be calculated by eq 37, $k_{48} = 5.7 \times 10^{-4}$ s^{-1}. At zero $[phenO]_0$, the initial rate of the reaction is the sum of the rate of the oxidation and the dissociation reaction, both of them were studied earlier (Ch. 5.3.1). The parameter in the denominator, C, is an empirical constant. The rate constant of the dissociation of $Fe(phen)_3^{2+}$ (k_{27}) was fixed during the fitting procedure, whereas $k_{48} = (5.2 \pm 0.3) \times 10^{-4}$ s^{-1} and $C = (7.4 \pm 0.8) \times 10^2$ M^{-1} were estimated by nonlinear least squares fitting. The fitted rate constant of the oxidation is in good agreement with the apparent rate constant calculated by eq 37.

It should also be mentioned that the detailed kinetic studies were carried out in 1.00 M H_2SO_4, however, the noted phenomena were more distinct at slightly higher pH (Figures 18A and 20A). Some of the kinetic parameters are found (k_{27}, k_{28}, k_{35}, k_{41}, K_{34}) or expected (k_{24}) to be practically pH independent, k_{11} is known to be larger at higher pH, meanwhile some rate constants are expected to increase with increasing pH but were only determined in strongly acidic medium (k_{25}, k_{29}).

5.4 *Dissociation of the $Fe(tpy)_2^{3+}$ complex*

It was discussed in the experimental section (Ch. 4.2) that two oxidants were used to produce $Fe(tpy)_2^{3+}$ from the corresponding iron(II) complex.

By using PbO_2, the excess of oxidant and the by-product of the reaction ($PbSO_4$) were easily removed by filtration, but lower yield (80-85%) was achieved by this method and a small amount of the initial complex (1-3%) remained in the solution.

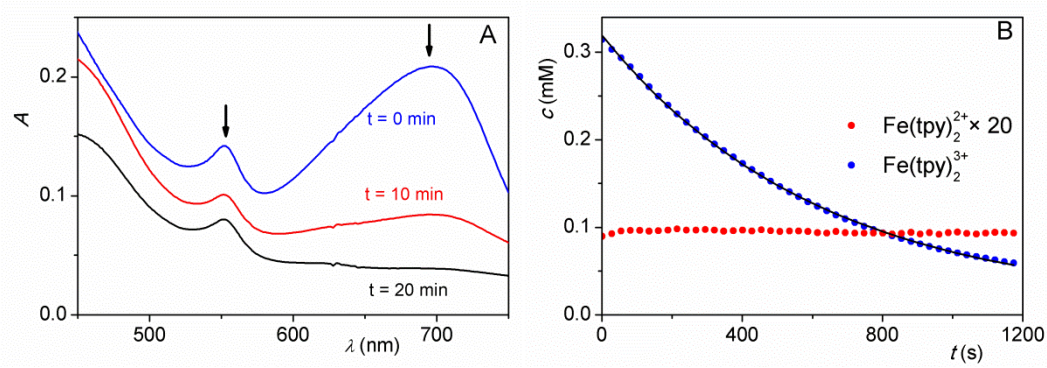

Figure 23. Spectral changes (**A**) and kinetic curves (**B**) in the decomposition reaction of $[Fe(tpy)_2^{3+}$. The initial concentration of $Fe(tpy)_2^{2+}$ to produce the iron(III) complex was 389 μM; $[H_2SO_4]$ = 0.323 M, pH = 0.42; T = 25.0 °C; path length = 1.000 cm.
A: time interval = 10 min. **B**: calculated concentration profiles of the iron complexes. Calculated initial concentrations after filtration: $[Fe(tpy)_2^{3+}]_0$ = 315 μM; $[Fe(tpy)_2^{2+}]_0$ = 4.5 μM. Circles: points calculated by the molar spectra of the species and the linear algebraic method described in Ch. 4.6. Only 25% of the calculated points are shown for clarity. Line: best fit to a single exponential function.

The spectral change of the filtered solutions was recorded (Figure 23A) and the linear algebraic method (Ch. 4.6) was used to calculate the concentration profiles of the iron complexes (Figure 23B). The spectra clearly show that some iron(II) complex (characteristic peak at 552 nm, ε = 1.222 × 10^4 $M^{-1}cm^{-1}$) is present in the beginning of the reaction, but most of the iron is in the form of $Fe(tpy)_2^{3+}$ (absorption maximum at 702 nm, ε = 7.05 × 10^2 $M^{-1}cm^{-1}$). In contrast to the decomposition reaction of $Fe(phen)_3^{3+}$ (Ch. 5.2), there is no increase in the absorption band of the reduced complex. Actually, Figure 23B demonstrates that the $Fe(tpy)_2^{2+}$ concentration is practically constant throughout the reaction. These

observations can be interpreted by a similar model to the one used to describe the uncatalyzed decomposition of $Fe(phen)_3^{3+}$ (Ch. 5.2). The only difference between the models is that the second one lacks the second order disproportionation reaction of the iron(III) complex.

$$Fe(tpy)_2^{3+} (+ 4H^+) \rightarrow Fe^{3+} + 2H_2tpy^{2+} \quad (49)$$

$$v = k_{49}[Fe(tpy)_2^{3+}] \qquad k_{49} = (1.6 \pm 0.1) \times 10^{-3}\ s^{-1}$$

$$Fe(tpy)_2^{2+} (+ 4H^+) \rightarrow Fe^{2+} + 2H_2tpy^{2+} \quad (50)$$

$$v = k_{50}[Fe(tpy)_2^{2+}] \qquad k_{50} = (4.0 \pm 0.1) \times 10^{-4}\ s^{-1}$$

$$Fe^{2+} + Fe(tpy)_2^{3+} \rightarrow Fe^{3+} + Fe(tpy)_2^{2+} \quad (51)$$

$$v = k_{51}[Fe(tpy)_2^{3+}][Fe^{2+}]$$

According to the model, the iron(II) complex does dissociate (50) but it is re-produced quantitatively in reaction 51 as long as $Fe(tpy)_2^{3+}$ is present in the reaction mixture. Reaction 50 was studied in independent experiments and will be briefly discussed in the next subchapter (Ch. 5.5). Reaction 51 is an electron transfer reaction between the iron(III) complex and ferrous ion, which is very fast on the time scale of the studied reaction ($k_{51} = 7.4 \times 10^5\ M^{-1}s^{-1}$).[99]

Due to the initial presence of the iron(II) complex, there are two reactions, 49 and 51, that consume $Fe(tpy)_2^{3+}$. However, the lower $[Fe(tpy)_2^{2+}]_0$, the smaller the contribution of 51 to the overall consumption of the iron(III) complex. In these experiments, the initial concentration of $Fe(tpy)_2^{2+}$ was about 1-3% of $[Fe(tpy)_2^{3+}]_0$. Consequently, reaction 49 is superior to 51.

The proton-assisted dissociation of $Fe(tpy)_2^{3+}$ without the interference of reaction 51 was studied by the method described earlier in the literature.[128] Cerium(IV) was used to produce the iron(III) complex and an excess of oxidant ensured the absence of $Fe(tpy)_2^{2+}$. The Ce(IV) - $Fe(tpy)_2^{2+}$ reaction is fast ($2.0 \times 10^5\ M^{-1}s^{-1}$) and quantitative, and the product iron(III) complex dissociates without participating in any redox reactions. These kinetic runs provided the pseudo-first order rate constant (k_{49}) of the dissociation of $Fe(tpy)_2^{3+}$ at the given acidity.

5.5 *Reaction between PMS and $Fe(tpy)_2^{2+}$*

5.5.1 Initial stage of the oxidation of $Fe(tpy)_2^{2+}$ by PMS

The complex is known to undergo proton-assisted dissociation (50) in acidic medium.[126,127] The observations taken under oxidant-free conditions were consistent with earlier reports: the dissociation follows first order kinetics with respect to $Fe(tpy)_2^{2+}$ (50) and the pseudo-first order rate constant, k_{obs}, increases with decreasing pH. It was also found that $Fe(tpy)_2^{2+}$ is stable above pH = 2.5. However, below pH ~ 0.7, the dissociation of the complex goes to completion. Most of the experiments were done under the latter conditions (at pH = 0.42, in 0.323 M H_2SO_4).

Typical kinetic curves in the presence and absence of the oxidant are shown in Figure 24A. The most notable feature of the traces is the linear shape of the curves at higher initial PMS concentrations. The curves in the presence of large excess of oxidant are not exponential and the observations cannot be interpreted in terms of a straightforward pseudo-first order approximation. The almost perfectly linear concentration change of $Fe(tpy)_2^{2+}$ implies that the order with respect to the Fe(II) complex becomes zero at this stage of the reaction. This clearly suggests a somewhat complex mechanism.

Similarly to the oxidation of $Fe(phen)_3^{2+}$, the initial rate method was used, which is free from interference from later processes. The initial rate was derived from the initial rate of absorbance change at 552 nm, which is the absorption maximum of the iron(II) complex, and was defined as follows:

$$v_0 = -\frac{dA\ (552\ \text{nm})}{dt} \times \frac{1}{\varepsilon_{552\ \text{nm}}} = -\frac{d\left[\text{Fe(tpy)}_2^{2+}\right]_0}{dt} \qquad (52)$$

Figure 24B shows the dependence of the initial rate on the concentration of PMS. The rates show saturation with an intercept. The intercept gives the rate of the proton-assisted dissociation of the complex (50).

The $Fe(tpy)_2^{2+}$-dependence of the initial reaction rate is represented in Figure 24C. In the presence of large excess of PMS, the rate varies linearly with the $Fe(tpy)_2^{2+}$ concentration. In this case, there is no intercept as no reaction is possible without the iron(II) complex.

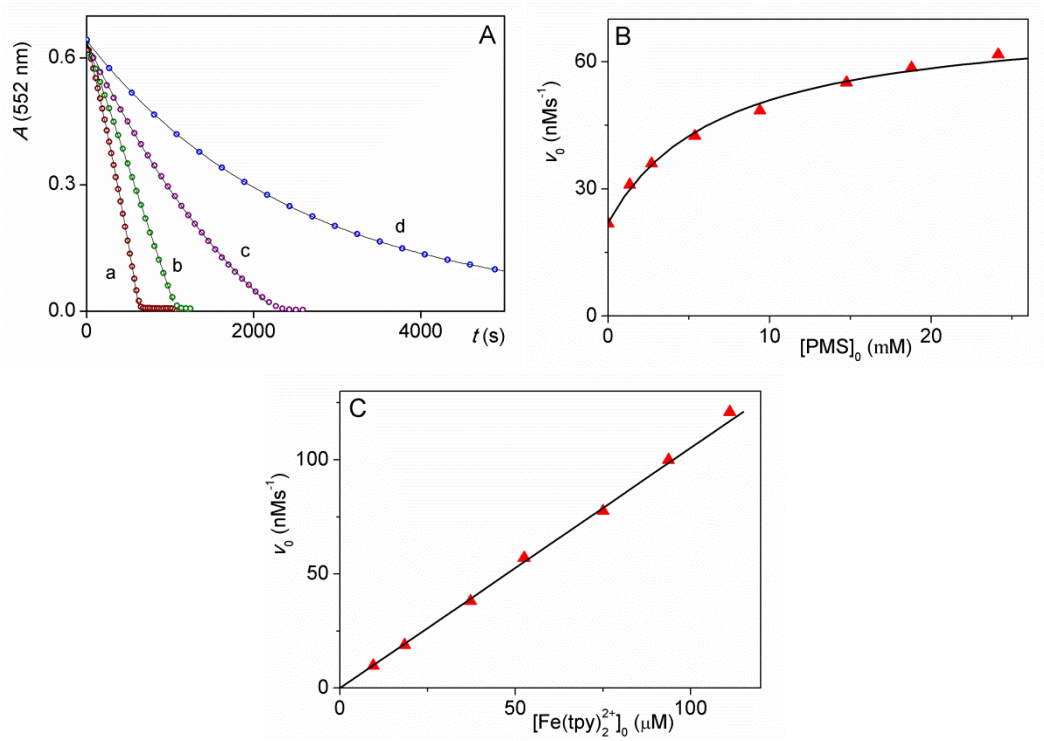

Figure 24A. Kinetic traces detected in the reaction between $Fe(tpy)_2^{2+}$ and PMS. Circles: experimental data. Only 4% of the recorded points are shown for clarity. Lines: results of the fit of the curves to eqs 60 and 61. $[Fe(tpy)_2^{2+}]_0$ = 52.3 μM; $[PMS]_0$ = 24.1 mM (a); 9.39 mM (b); 2.68 mM (c); no PMS is added (d); $[H_2SO_4]$ = 0.323 M; T = 25.0 °C; λ = 552 nm; path length = 1.000 cm.

24B and **24C**: dependence of the initial rate on the reactant concentrations. $[H_2SO_4]$ = 0.323 M; T = 25.0 °C; λ = 552 nm; path length = 1.000 cm. **B**: dependence on PMS. $[Fe(tpy)_2^{2+}]_0$ = 52.3 μM. **C**: dependence on $Fe(tpy)_2^{2+}$. $[PMS]_0$ = 14.8 mM. The two sets of data were evaluated together using proportional weighting. Lines: results of best fit to eq 56.

The saturation tendency was explained by the same kinetic model as in the case of the oxidation of $Fe(phen)_3^{2+}$ by PMS. The model includes the acid catalyzed dissociation of the complex (50), an adduct formation of the reactants (53), the rate determining dissociation of the ion pair (54) and a fast oxidation step by $SO_4^{-\bullet}$ (55):

$$Fe(tpy)_2^{2+} (+ 4H^+) \rightarrow Fe^{2+} + 2H_2tpy^{2+} \qquad (50)$$

$$v = k_{50}[Fe(tpy)_2^{2+}]$$

$$Fe(tpy)_2^{2+} + HSO_5^- \rightleftharpoons [Fe(tpy)_2 \cdot HSO_5]^+ \quad (53)$$

$$K_{53} = \frac{[Fe(tpy)_2 \cdot HSO_5^+]}{[Fe(tpy)_2^{2+}][HSO_5^-]}$$

$$[Fe(tpy)_2 \cdot HSO_5]^+ (+ H^+) \rightarrow Fe(tpy)_2^{3+} + SO_4^{-\bullet} + H_2O \quad (54)$$

$$v = k_{54}[Fe(tpy)_2 \cdot HSO_5^+]$$

$$Fe(tpy)_2^{2+} + SO_4^{-\bullet} \rightarrow Fe(tpy)_2^{3+} + SO_4^{2-} \quad (55)$$

$$v = fast$$

In accordance with the model, the following expression was derived for the initial rate:

$$v_0 = [Fe(tpy)_2^{2+}]_0 \left(k_{50} + \frac{2k_{54}K_{53}[PMS]_0}{1 + K_{53}[PMS]_0} \right) \quad (56)$$

The rate constant of the proton-assisted dissociation of the complex was determined under oxidant-free conditions, $k_{50} = (4.0 \pm 0.1) \times 10^{-4}$ s^{-1}. The further parameters were estimated by nonlinear least squares fitting: $k_{54} = (4.8 \pm 0.2) \times 10^{-4}$ s^{-1} and $K_{53} = 129 \pm 18$ M^{-1}.

In light of the oxidation of similar complexes, tris(phenanthroline)iron(II) and tris(bipyridine)iron(II), by PMS, such a rate equation is not unexpected and an oxidation pathway that occurs via an ion pair formation between the reactants seems to be feasible. Attempts were made to identify the ion pair by ESI-MS method. The peaks of the oxidation product, $Fe(tpy)_2^{3+}$ were found in the spectrum, however, the proposed adduct could not be detected. Although in the $Fe(phen)_3^{2+}$ - PMS reaction, the corresponding ion pair gave identifiable peaks, such adduct is supposed to be a reactive intermediate and expected to be present in very low concentrations.

5.5.2 Kinetic studies on the further stage of the reaction

The traces of the $Fe(tpy)_2^{2+}$-dependence study are shown in Figure 25. A closer look at the curves demonstrates that there is an initial acceleration in the rate and then the decrease of absorbance becomes linear.

The only absorbing species at 552 nm is $Fe(tpy)_2^{2+}$ in this system, thus, in Figure 25, the horizontal red line marks the reaction times at which the concentrations of the reactants can be considered identical for all practical purposes (since PMS is used in large excess, its concentration is very close to constant during the whole kinetic run). Yet, the higher the initial $Fe(tpy)_2^{2+}$ concentration, i.e. the more the reaction proceeded until the intersection, the higher the rate is. The simplest explanation for this observation is autocatalysis.

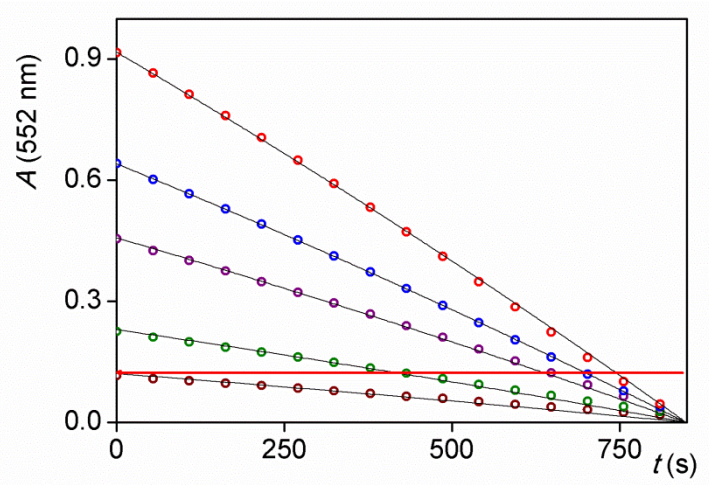

Figure 25. Kinetic traces detected in the reaction between $Fe(tpy)_2^{2+}$ and PMS. Circles: experimental data. Only 4% of the recorded points are shown for clarity. Lines: results of the fit of the curves to eqs 60 and 61. [PMS] = 14.8 mM; $[Fe(tpy)_2^{2+}]_0$ = 9.34 - 74.7 μM; $[H_2SO_4]$ = 0.323 M; T = 25.0 °C; λ = 552 nm; path length = 1.000 cm. Along the horizontal red line, the $Fe(tpy)_2^{2+}$ concentrations are the same in each kinetic trace.

This assumption was tested in the following experiment: the reaction was allowed to reach completion (cycle *1*), then the consumed amounts of Fe(II) complex, oxidant and H^+ was added to the aged solution in order to have identical initial conditions except for the oxidation products (cycle *2*). This procedure was

repeated as many times as the volume of the cuvette enabled us to do so (up to cycle *5*). As Figure 26A shows, the reaction is faster in every successive cycle than the previous ones owing to the increasing amount of oxidation products. This clearly proves the autocatalytic feature of the reaction.

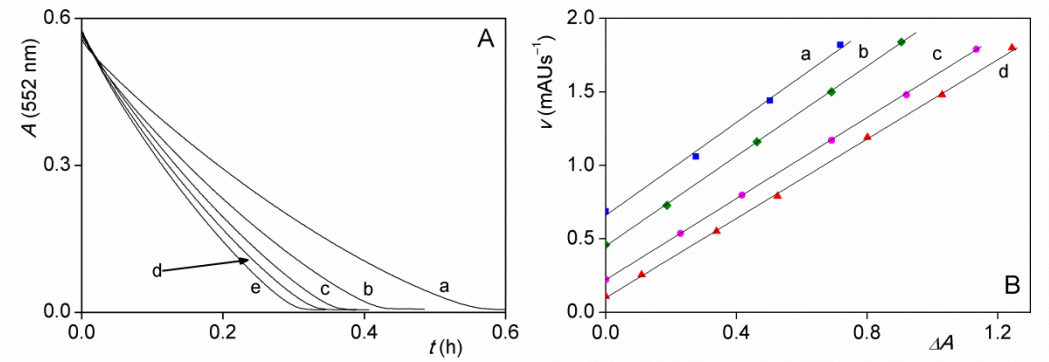

Figure 26. Study of the autocatalysis in the reaction between $Fe(tpy)_2^{2+}$ and PMS.
$[H_2SO_4]$ = 0.323 M; T = 25.0 °C; λ = 552 nm; path length = 1.000 cm.
A: effect of increasing amount of aged reaction mixture on the oxidation. a: cycle *1*, b: cycle *2*; c: cycle *3*; d: cycle *4*; e: cycle *5*. See details in the text. $[PMS]_0$ = 45.0 mM; $[Fe(tpy)_2^{2+}]_0$ = 47.2 μM.
B: dependence of the rate of the autocatalyzed process on the autocatalyst and the $Fe(tpy)_2^{2+}$ complex. $[PMS]_0$ = 14.8 mM; $[Fe(tpy)_2^{2+}]_0$ = 52.3 μM (a); 37.4 μM (b); 18.7 μM (c); 9.34 μM (d).

Further conclusions can be drawn regarding the autocatalytic reaction by considering Figure 25. Since the iron(II) complex is the only absorbing species at 552 nm, the absorbance change (defined as $\Delta A = A_{initial} - A_t$) is directly proportional to the consumed $Fe(tpy)_2^{2+}$. Supposing that the catalyst is formed according to a well-defined stoichiometry, its concentration can also be estimated by the absorbance change ($\Delta A \sim [Fe(tpy)_2^{2+}]_{consumed} \sim [cat]_{produced}$).

In Figure 25, at the intersections of the horizontal red line and the traces, the difference in the rates is due to the different amounts of autocatalyst formed up to those reaction times. The rate of the absorbance change (which is directly proportional to the overall rate) was determined at each intersection, then it was plotted against ΔA. The result is shown in Figure 26B: a straight line was obtained, that is the order with respect to the autocatalyst is unity. At zero ΔA, the intercept

represents the rate of the noncatalytic reactions (the sum of the noncatalytic oxidation and the proton-assisted dissociation of the complex) under the given initial conditions. Intersecting the kinetic traces of Figure 25 at distinct absorbance values (thus varying the concentration of the Fe(II) complex) and repeating the plot (v versus ΔA), a straight line was obtained in each case and the lines were practically parallel (with identical slopes within the usual margin of error) regardless of the actual $Fe(tpy)_2^{2+}$ concentration.

The independence of the slope from the actual $Fe(tpy)_2^{2+}$ concentration suggests that the autocatalytic process is zeroth order with respect to the $Fe(tpy)_2^{2+}$. This conclusion is in line with the linear shape of the kinetic curves and the presence of break points at the final stage of the oxidation, since the autocatalytic process is most probably superior to the noncatalytic ones close to the completion of the reaction.

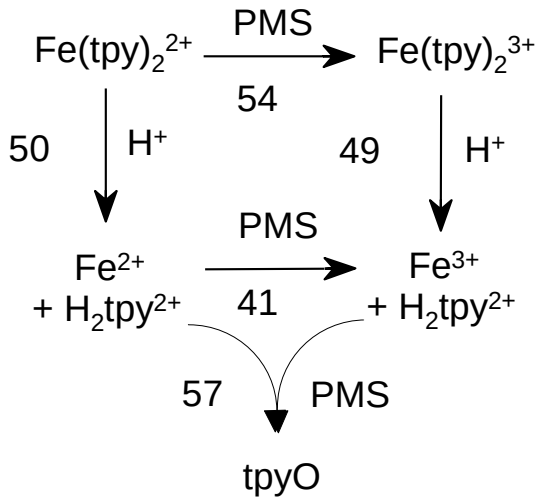

Scheme 6. Summary of the processes in the PMS – $Fe(tpy)_2^{2+}$ reaction system under acidic conditions

The possible pathways of the reaction system are summarized in Scheme 6. The proton-assisted dissociation of $Fe(tpy)_2^{2+}$ (50) was shortly discussed earlier and under the applied acidity it has a half-life of approximately 30 minutes. The $Fe(tpy)_2^{3+}$ complex undergoes dissociation (49), too, and its half-life under such acidic conditions is about 7 minutes. Both reactions produce protonated ligand (under such acidic conditions, mainly H_2tpy^{2+}). When the free ligand was added to

the initial reaction mixture, it did not influence the rate at all. This observation rules out that the ligand is the autocatalyst.

The oxidation of Fe^{2+} by PMS (41) was confirmed to be fast on the time scale of the present study ($k_{41} = 3.7 \times 10^4$ $M^{-1}s^{-1}$)[1] and this reaction ensures that Fe(II) cannot accumulate as long as excess PMS is present. This excludes the presence of iron(II) in the aged solution, thus it cannot be the autocatalyst, either.

Since the oxidation of the ligand plays a significant role in the $Fe(phen)_3^{2+}$ – PMS reaction, the formation of N-oxide(s) was taken into consideration in this system as well (57). However, it was found in metal-free solutions that the oxidation of tpy by PMS is practically does not occur in strongly acidic medium, at 25 °C (see Ch. 5.5.3). The effect of the oxidized ligand (tpyO) on the oxidation of $Fe(tpy)_2^{2+}$ was tested, but no acceleration was observed.

Both the dissociation of $Fe(tpy)_2^{3+}$ and the oxidation of Fe(II) (49 and 41) result in the formation of Fe^{3+}. As a potential product of the reaction, it was added to the initial reaction mixture, but it did not enhance the rate of the reaction, either.

To sum up, the free ligand (H_2tpy^{2+}), the oxidized ligand (tpyO), Fe(II) and Fe(III) were excluded as autocatalysts.

Although the bis(terpyridine)Fe(III) complex ($Fe(tpy)_2^{3+}$) is the primary product of the oxidation (54), on a longer time scale it is, in fact, an intermediate. However, it should also be considered as the catalyst of the main reaction in focus. At 702 nm, it has a significantly lower molar absorption maximum ($\varepsilon = 7.05 \times 10^2$ $M^{-1}cm^{-1}$) than that of the corresponding Fe(II) complex at 552 nm ($\varepsilon = 1.222 \times 10^4$ $M^{-1}cm^{-1}$). By properly choosing the concentration of $Fe(tpy)_2^{2+}$, both peaks can be monitored simultaneously (Figure 27A). By using the molar spectra of the complexes and the linear algebraic method (Ch. 4.6), the time-dependent concentration profiles of $Fe(tpy)_2^{2+}$ and $Fe(tpy)_2^{3+}$ were calculated. Figure 27B shows that the initial formation of the iron(III) complex is followed by a decrease due its proton-assisted dissociation (49). The increase of $[Fe(tpy)_2^{3+}]$ ceases when the iron(II) complex is completely consumed, as indicated by break points in the kinetic traces at the same instant.

The spectra feature characteristic isosbestic points as long as the oxidation proceeds (Figure 27A). The spectral changes after the oxidation are due to the

dissociation of $Fe(tpy)_2^{3+}$. Isosbestic points imply that a linear combination of the concentrations of two absorbing species (the tpy complexes of Fe^{2+} and Fe^{3+}) is constant throughout the oxidation. It should be added that this can only be observed at larger initial PMS concentrations, that is, when the rate of oxidation of the iron(II) complex (54) is superior to the proton-assisted dissociations of the complexes (49 and 50).

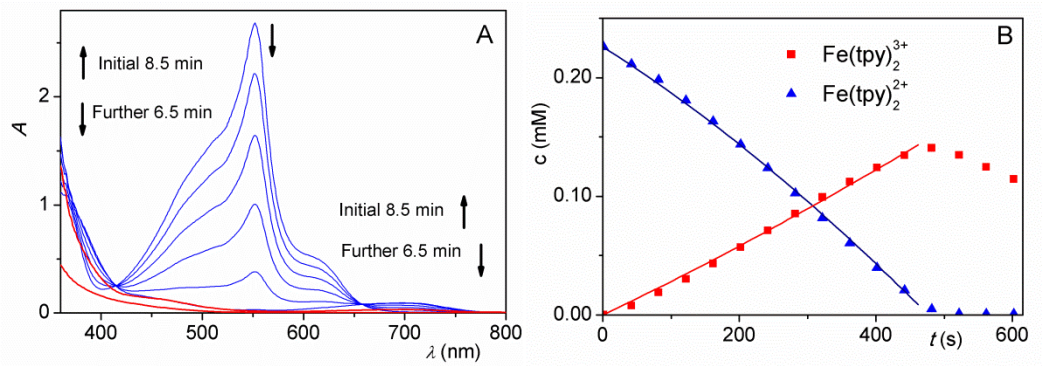

Figure 27A. Spectral changes in the reaction between $Fe(tpy)_2^{2+}$ and PMS. Blue spectra were recorded before the break point (time interval = 100 s), red spectra were recorded after the break point (time interval = 300 s). $[Fe(tpy)_2^{2+}]_0$ = 234 μM; $[PMS]_0$ = 26.8 mM; $[H_2SO_4]$ = 0.323 M; T = 25.0 °C; path length = 1.000 cm.

Figure 27B. Concentration profiles of the tpy complexes in the reaction between $Fe(tpy)_2^{2+}$ and PMS. Points: experimental data; only 10% of the recorded points are shown for clarity. Lines: results of the simultaneous fit of the two curves to eqs 60 and 61 (only the points before the break point were fitted). $[Fe(tpy)_2^{2+}]_0$ = 234 μM; $[PMS]_0$ = 26.8 mM; $[H_2SO_4]$ = 0.323 M; T = 25.0 °C.

In order to test the possible role of $Fe(tpy)_2^{3+}$ as an autocatalyst of the oxidation process, the complex was prepared by the oxidation of the corresponding iron(II) complex using solid PbO_2 (Ch. 3.3). Figure 28A clearly shows that the presence of $Fe(tpy)_2^{3+}$ accelerates the disappearance of the absorbance peak of the bis(terpyridine)iron(II) complex. The dependence of the initial rate on $[Fe(tpy)_2^{3+}]$ was also studied and the results are shown in Figure 28B. The points give a straight line, which confirms earlier assumptions, namely that the order with respect to the autocatalyst is unity. The intercept represents the rate of the noncatalytic reactions

(the sum of the noncatalytic oxidation, 54, and the proton-assisted dissociation of the complex, 50) under the given initial conditions.

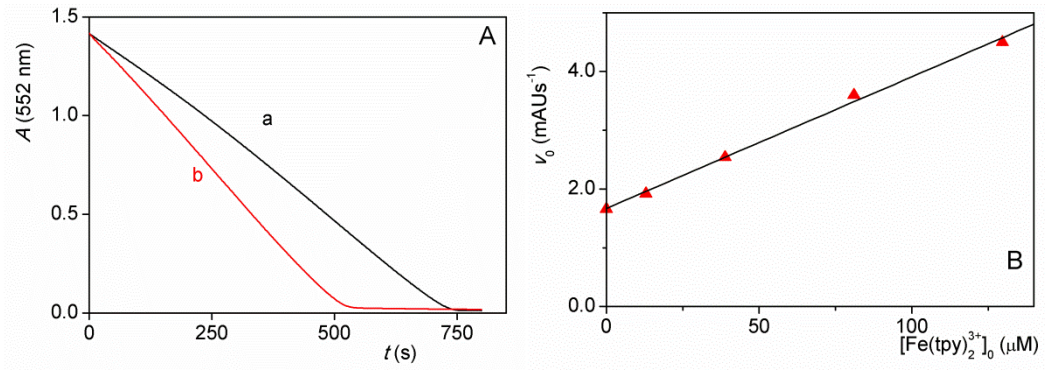

Figure 28. The effect of $Fe(tpy)_2^{3+}$ on the reaction between $Fe(tpy)_2^{2+}$ and PMS. $[H_2SO_4]$ = 0.323 M; T = 25.0 °C; λ = 552 nm; path length = 1.000 cm.
A: kinetic traces in the presence (b) and absence (a) of $Fe(tpy)_2^{3+}$. $[Fe(tpy)_2^{2+}]_0$ = 117 μM; $[PMS]_0$ = 321 mM, (a) without additional reactants; (b) 39 μM $Fe(tpy)_2^{3+}$ added before the reaction.
B: dependence of the initial rate on the $Fe(tpy)_2^{3+}$ concentration. $[Fe(tpy)_2^{2+}]_0$ = 117 μM; $[PMS]_0$ = 321 mM.

These results clearly confirm that the autocatalysis is caused by the formation of $Fe(tpy)_2^{3+}$. Taking into consideration the discussed experimental observations and the reactions of the initial phase, the following simplified model was used to describe the autocatalytic oxidation. Excess of oxidant ($[PMS]_0$ >> $[Fe(tpy)_2^{2+}]_0$) was used and in the expressions, A and B stand for $Fe(tpy)_2^{2+}$ and $Fe(tpy)_2^{3+}$, respectively.

$$\mathrm{A} \rightarrow \mathrm{B} \qquad v = k_{\mathrm{obs1}}[\mathrm{A}] \tag{58}$$

$$\mathrm{A} + \mathrm{B} \rightarrow 2\mathrm{B} \qquad v = k_{\mathrm{obs2}}[\mathrm{B}] \tag{59}$$

where k_{obs1} and k_{obs2} are the pseudo-first order rate constants of the noncatalytic and autocatalytic pathways of the oxidation, respectively. The concentration change of $Fe(tpy)_2^{2+}$ is as follows:

$$\frac{d[\mathrm{A}]}{dt} = -k_{50}[\mathrm{A}] - k_{\mathrm{obs1}}[\mathrm{A}] - k_{\mathrm{obs2}}[\mathrm{B}] \tag{60}$$

Whereas, the differential rate equation for B by taking into account its consumption in the proton-assisted dissociation (49):

$$\frac{d[\mathrm{B}]}{dt} = k_{\mathrm{obs1}}[\mathrm{A}] + k_{\mathrm{obs2}}[\mathrm{B}] - k_{49}[\mathrm{B}] \qquad (61)$$

The kinetic traces were fitted by the differential rate equation system of eqs 60 and 61 using a nonlinear least squares algorithm. During the fitting procedure, k_{49}, k_{50} and k_{obs1} were held fixed and only k_{obs2} was allowed to float. The value of k_{obs1} was calculated in each run by the use of $[\mathrm{PMS}]_0$ and the parameters determined for the initial phase of the reaction. Eqs 60 and 61 can describe the concentration profiles before the breakpoint. Thus, the experimental data were used until ~90-95% consumption of the initial complex.

When the curves in Figure 25 were evaluated individually, the fitted constants were found independent of the initial complex concentration and were identical within the margin of error. The continuous lines in Figure 25 are the result of the simultaneous fit of the traces.

The PMS-dependence of k_{obs2} was studied by fitting the curves of Figure 24A. Similarly to k_{obs1}, the rate constant of the catalytic route exhibits saturation tendency (Figure 29A). The experimental data were fitted by the following expression:

$$k_{\mathrm{obs2}} = \frac{k_{64}K_{63}[\mathrm{PMS}]_0}{1 + K_{63}[\mathrm{PMS}]_0} \qquad (62)$$

The parameters were estimated by nonlinear least squares fitting: $k_{64} = (4.9 \pm 0.2) \times 10^{-3}\ \mathrm{s}^{-1}$ and $K_{63} = 87 \pm 10\ \mathrm{M}^{-1}$.

Both the noncatalytic and the catalytic pathways of the oxidation are likely to proceed via the formation of an adduct from the reactants (53 and 63). This is the simplest interpretation of the saturation of the apparent rate constants.

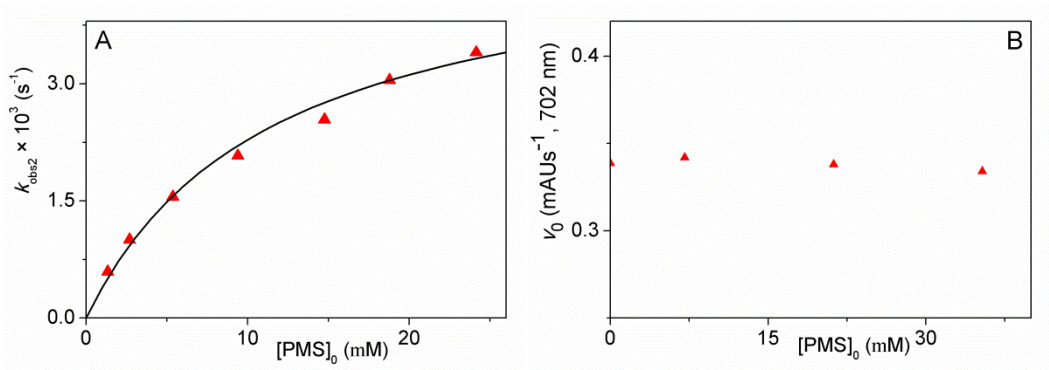

Figure 29A: Dependence of the observed rate constant (k_{obs2}) of the autocatalytic pathway on the PMS concentration. $[Fe(tpy)_2^{2+}]_0$ = 52.3 μM; $[H_2SO_4]$ = 0.323 M; T = 25.0 °C; path length = 1.000 cm. Line: result of best fit to eq 62.
B: Dependence of the initial rate of the loss of $Fe(tpy)_2^{3+}$ on the $[PMS]_0$. $[Fe(tpy)_2^{3+}]_0$ = 290 μM; $[H_2SO_4]$ = 0.323 M; λ = 702 nm; path length = 1.000 cm; T = 25.0 °C.

The catalytic route of the oxidation is zeroth order with respect to the initial complex. This can only be possible if the $Fe(tpy)_2^{2+}$-consuming process occurs after the rate-determining step (64) of the autocatalytic pathway. The saturation in k_{obs2} can be interpreted by an equilibrium prior to the rate-limiting step. In this process, a reversible reaction occur between PMS and $Fe(tpy)_2^{3+}$ (63) which results in the formation of an adduct similar to that of the initial reactants.

When the reaction was monitored on a longer time scale, it was observed that after the break point (Figure 27B), the rate of the consumption of the $Fe(tpy)_2^{3+}$ does not depend on the PMS concentration. Similarly, when PMS was added to the freshly prepared iron(III) complex, the initial rate of the loss of $Fe(tpy)_2^{3+}$ was independent of $[PMS]_0$ (Figure 29B). According to these observations, in the rate-determining step of the autocatalytic pathway, there is a reaction between the autocatalyst ($Fe(tpy)_2^{3+}$) and the oxidant (PMS), but in the absence of the iron(II) complex, the PMS does not increase the rate of the decomposition of $Fe(tpy)_2^{3+}$. This can be interpreted by assuming that the ion pair formed between the oxidant and the autocatalyst (63) dissociates in an other equilibrium step (64). This equilibrium is shifted strongly to the left side and the proposed products, an iron(IV) species and sulfate ion radical rapidly recombine unless $Fe(tpy)_2^{2+}$ is

present. As long as the iron(II) complex is in the reaction mixture, both powerful oxidants readily react with $Fe(tpy)_2^{2+}$ (55 and 65).

$$Fe(tpy)_2^{3+} + HSO_5^- \rightleftharpoons [Fe(tpy)_2 \cdot HSO_5]^{2+} \quad (63)$$

$$K_{63} = \frac{[Fe(tpy)_2 \cdot HSO_5^{2+}]}{[Fe(tpy)_2^{3+}][HSO_5^-]}$$

$$[Fe(tpy)_2 \cdot HSO_5]^{2+} (+ H^+) \overset{k_{64}}{\rightleftharpoons} Fe(tpy)_2^{4+} + SO_4^{-\bullet} + H_2O \quad (64)$$

$$v = k_{64}[Fe(tpy)_2 \cdot HSO_5^+]$$

$$Fe(tpy)_2^{2+} + SO_4^{-\bullet} \rightarrow Fe(tpy)_2^{3+} + SO_4^{2-} \quad (55)$$

$$v = fast$$

$$Fe(tpy)_2^{2+} + Fe(tpy)_2^{4+} \rightarrow 2Fe(tpy)_2^{3+} \quad (65)$$

$$v = fast$$

ESI-MS measurements were carried out in order to identify the intermediates and products of the reaction. It should be noted that the mass spectrometric instrument do not facilitate such acidic conditions under which the kinetics was studied. In the reaction mixture prepared for the ESI-MS, the only H^+ source was the HSO_4^- content of oxone and the estimated pH was about 3.5-4. Under these conditions, the oxidation of the ligand is much more probable than in strongly acidic medium (see Ch. 5.5.3). The N-oxide derivative of the ligand, tpyO was detected in traces among the oxidation products, but it is reasonable to assume that merely the higher pH gave rise to its formation.

The primary oxidation product, $Fe(tpy)_2^{3+}$ was also found by ESI-MS, but neither the proposed ion pairs, nor any Fe(IV) complex was detected.

5.5.3 Reaction between PMS and tpy

The oxidation of tpy was studied because of its relevance in the $Fe(tpy)_2^{2+}$ – PMS system. Under strongly acidic conditions and at 25.0 °C, the reaction was found rather slow even in the presence of large (more than 220-fold) excess of oxidant over tpy (inset of Figure 30A).

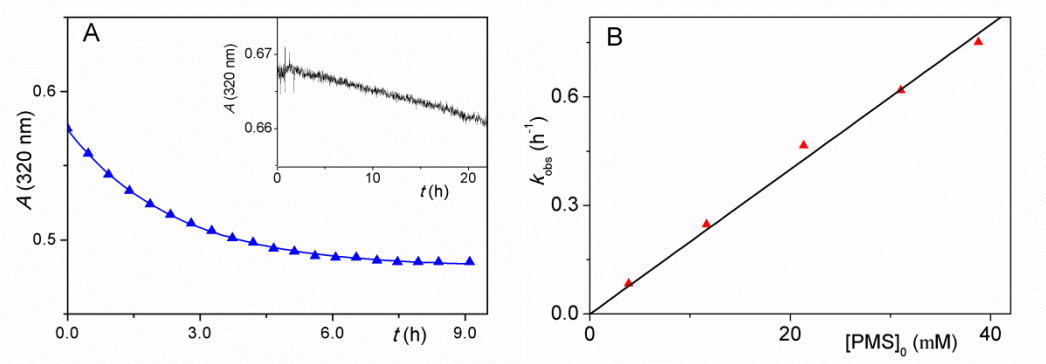

Figure 30. Study of the reaction between tpy and PMS at elevated temperature.
A: experimental kinetic curve. $[tpy]_0$ = 31.4 μM; $[PMS]_0$ = 6.78 mM; $[H_2SO_4]$ = 1.00 M; T = 60.0 °C; λ = 320 nm; path length = 1.000 cm. Triangles: experimental points (only 10% of the recorded points are shown for clarity), continuous line: result of the fit of the data to a single exponential function. Inset: experimental kinetic curve detected at 25 °C. $[tpy]_0$ = 35.3 μM; $[PMS]_0$ = 7.87 mM; $[H_2SO_4]$ = 0.10 M; path length = 1.000 cm; λ = 320 nm.
B: dependence of the pseudo-first order rate constants on $[PMS]_0$. $[tpy]_0$ = 31.4 μM; $[H_2SO_4]$ = 1.00 M; T = 60.0 °C.

In order to observe considerable change in the absorbance, the reaction was run at 60.0 °C. Under pseudo-first order conditions ($[PMS]_0$ >> $[tpy]_0$), a one-step process was observed, exponential curves were detected (Figure 30A) and the k_{obs} showed linear dependence on the initial oxidant concentration (Figure 30B). When $[PMS]_0$ was kept constant (and in large excess) and the tpy dependence was studied, as expected, the pseudo-first order constant was independent of $[tpy]_0$. This implies that the reaction follows second order kinetics and the order with respect to both reactants is one (57).

$$tpy + HSO_5^- \rightarrow tpyO + HSO_4^- \qquad (57)$$

$$v = k_{57}[\text{tpy}][\text{PMS}]$$

The second order rate constants obtained from the two series of experiment were in good agreement, $k_{57} = (5.4 \pm 0.4) \times 10^{-3}$ $M^{-1}s^{-1}$. The corresponding rate constant of the oxidation of phen by PMS at the same temperature is nearly an order of magnitude larger ($k_{11} = 4.7 \times 10^{-2}$ $M^{-1}s^{-1}$). Although the flexibility and the nucleophilicity of the molecule would favor the oxidation of tpy compared to phen, seemingly these are not the key factors. According to the literature, the doubly protonated tpy, which is the dominant species in 1.00 M H_2SO_4, is in the symmetric form ($H_2tpy^{2+}{}_s$) and the asymmetric species ($H_2tpy^{2+}{}_a$) is present in ignorable concentration.[77] Previous reports also states that the N-oxidation of the nitrogen atom of the central aromatic ring is sterically hindered: the symmetric mono-N-oxide ($tpyO_s$) can only be obtained by a coupling reaction and the direct oxidation of the parent molecule always results in the asymmetric product ($tpyO_a$).[83] In line with these observations, it is reasonable to assume that in the PMS – tpy reaction, the primary oxidation product is $tpyO_a$, whose formation is highly unfavorable due to the protonation of both nitrogen atoms of the nonadjacent rings. In the phen molecule, on the other hand, one of the nitrogens is free of H^+ and the deprotonation is not a requisite condition of the oxidation.

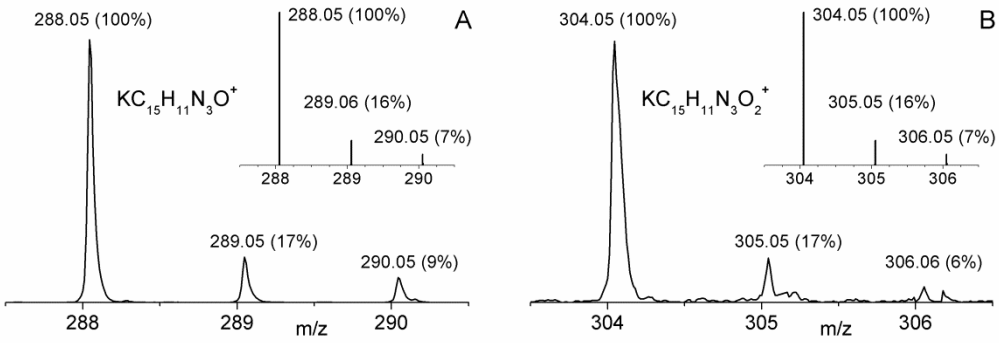

Figure 31. Electrospray ionization mass spectrometric (ESI-MS) identification of terpyridine-N-oxides in the reaction mixture of tpy and PMS.
A: identification of the mono-N-oxide ionized with potassium ion ($K{\cdot}tpyO^+$). Inset: calculated spectrum for the formula $KC_{15}H_{11}N_3O^+$.
B: identification of the di-N-oxide ionized with potassium ion ($K{\cdot}tpyO_2^+$). Inset: calculated spectrum for the formula $KC_{15}H_{11}N_3O_2^+$.

The oxidation products of the reaction were identified by ESI-MS method. Although the detailed concentration dependence was studied in 1.00 M H_2SO_4, the MS measurements were carried out under moderately acidic conditions (the pH was about 4) due to the limitations of the technique. Apart from the mono-N-oxide, the di-N-oxide ($tpyO_2$) derivative of terpyridine was also detected in small amounts when slight excess of oxidant was used (Figure 31).

The pH dependence of the oxidation rate was studied but only qualitative conclusions were drawn from the data. The tendency is very similar to the pH profile of the oxidation of phen: the rate of the reaction (defined by the absorbance decrease at 320 nm) increases by shifting the pH from acidic to neutral medium, then decreases as the medium gets more basic (Figure 32A). Such a pH profile can be interpreted by considering the protolytic equilibria of the reactants and their reactivities. Under acidic conditions, the protonation of the substrate (pK_{a1} = 3.7, pK_{a2} = 4.7)[52] hinders the N-oxidation. Under basic conditions, the less reactive form of the oxidant, SO_5^{2-} becomes the predominant species (pK_a = 8.4)[2] which decelerates the oxidation.

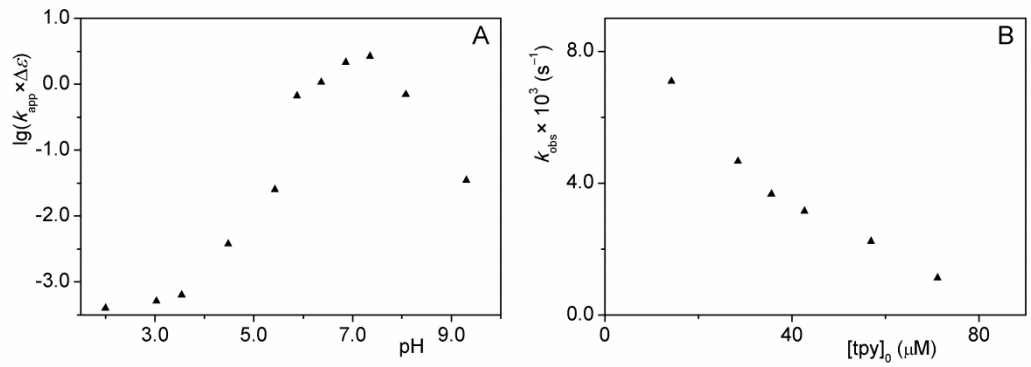

Figure 32A: The pH dependence of the rate of the reaction of tpy and PMS.
$[PMS]_0$ = 0.80 mM; $[tpy]_0$ = 0.039 mM; I = 1.00 M ($NaClO_4$), $[buffer]_{tot}$ = 50.0 mM; T = 25.0 °C; λ = 320 nm.
B: dependence of the pseudo-first order rate constants on $[tpy]_0$, the limiting reactant. $[PMS]_0$ = 500 μM; $[phosphate]_{tot}$ = 0.10 M; pH = 6.6, T = 25.0 °C.

The initial rate method was used to study the pH dependence. In order to estimate the apparent rate constants, the difference of the molar absorptions of the primary oxidation product and the reactant ($\Delta\varepsilon = \varepsilon_{tpyO} - \varepsilon_{tpy}$) is needed at each pH.

However, the pH dependent apparent molar absorption of tpyO (which takes into account the actual ε values and the molar fractions of the differently protonated species) was not determined. Thus, Figure 32A reflects the pH dependence of the $k_{app} \times \Delta\varepsilon$ product and does not provide quantitative information regarding the actual rate constants of the possible, parallel oxidations pathways. Furthermore, there is every indication that also the mechanism changes with the pH. The concentration dependence of the reaction was studied in nearly neutral medium, too. Under pseudo-first order conditions ($[PMS]_0 >> [tpy]_0$), the curves can be satisfactorily fitted to single exponential function but the value of k_{obs} significantly decreases with the concentration of the limiting reactant (Figure 32B). This clearly suggests that the straightforward second order kinetics does not apply in neutral medium. The decreasing tendency might be a result of some kind of product inhibition but any such proposal would be highly speculative at this point.

The main objective of the study of the tpy – PMS reaction was to explore its possible role in the oxidation of $Fe(tpy)_2^{2+}$. At room temperature and in strongly acidic medium, PMS oxidizes tpy to tpyO in a slow, one-step process, and it is of negligible significance in the oxidation of the complex.

6) Summary

In this dissertation, the kinetics and mechanism of the oxidation reactions of coordinatively saturated iron(II) complexes ($Fe(phen)_3^{2+}$ and $Fe(tpy)_2^{2+}$) and the corresponding N-heteroaromatic ligands (phen and tpy) by peroxomonosulfate ion (PMS) are discussed.

During the oxidations of $Fe(phen)_3^{2+}$ and $Fe(tpy)_2^{2+}$, unusual kinetic behaviour was observed. The proton-assisted dissociation of the Fe(II) complexes is a common side reaction in the systems, but neither of the oxidations occur via the dissociative pathway, instead, they result in the formation of $Fe(phen)_3^{3+}$ and $Fe(tpy)_2^{3+}$, as the primary oxidation products.

The initial rate method was chosen to study the early phase of the reactions. All of our findings in the two different systems were interpreted with a common kinetic model that includes *i)* the acid catalyzed dissociation of the Fe(II) complex; *ii)* the formation of an intermediate, a 1:1 adduct between the reactants which is considered a fast pre-equilibrium; *iii)* the rate determining intramolecular electron transfer process followed by the dissociation of the adduct into the corresponding Fe(III) complex and sulfate ion radical and *iv)* the fast oxidation of another Fe(II) complex by the $SO_4^{-\bullet}$. In the $Fe(phen)_3^{3+}$ – PMS reaction, the adduct was identified by ESI-MS method.

In the later stage of the oxidation, the two systems feature significant differences. The ligand and the $Fe(phen)_3^{2+}$ complex are oxidized on a similar time scale. The oxidation of phen yields the corresponding N-oxide. This product inhibits the oxidation of $Fe(phen)_3^{2+}$ probably by inducing the temporary re-formation of the iron(II) complex from $Fe(phen)_3^{3+}$.

The oxidation of $Fe(tpy)_2^{2+}$, on the other hand, is autocatalytized by $Fe(tpy)_2^{3+}$. A model was proposed for the catalytic pathway which is likely to proceed via the formation of an adduct between HSO_5^- and the autocatalyst, $Fe(tpy)_2^{3+}$. The dissociation of the ion pair yields reactive oxidizing agents ($Fe(tpy)_2^{4+}$ and $SO_4^{-\bullet}$), which consume the iron(II) complex in rapid steps. These fast processes occur after the rate-determining step of the autocatalysis which interprets the linear decrease of $[Fe(tpy)_2^{2+}]$ in the final stage of the oxidation.

In the $Fe(tpy)_2^{2+}$ – PMS reaction, seemingly the N-oxide derivative of the ligand (tpyO) does not have any effect on the oxidation of the complex, most probably due to its very slow formation under the strongly acidic conditions of the study.

It was shown that the decomposition reactions of the iron(III) complexes proceed via slightly different routes. It was found that $Fe(tpy)_2^{3+}$ dissociates only in the acid-catalyzed pathway without participating in any redox reactions. It was revealed, on the other hand, that a small fraction of $Fe(phen)_3^{3+}$ produces $Fe(phen)_3^{2+}$. The oxidized ligand (phenO) is also a product of the redox decomposition of $Fe(phen)_3^{3+}$ and phenO had an autocatalytic effect on the reaction producing it. The mechanism is proposed to involve $Fe(phen)_3^{4+}$ as a minor intermediate.

It was shown that phenO plays a more crucial role in the reactions of the iron-phen complexes than the N-oxide derivatives of tpy play in the oxidation of $Fe(tpy)_2^{2+}$. This is the reason why the N-oxidation of phen gained more attention. Under strongly acidic conditions, both ligands are oxidized by PMS in one-step reactions, which give the mono-N-oxides derivatives and follow net second-order kinetics (the order with respect to both reactants are one).

The rates of both oxidation reactions feature complex pH dependence and show similar tendency: the rate shows maximum close to the neutral pH region. This pH dependence can be interpreted by considering that the protonation of the substrate gives less opportunity for the oxidative attack on the nitrogen atom under acidic conditions. Under basic conditions, the deprotonation of HSO_5^- decelerates the oxidation because SO_5^{2-} is much less reactive than the monoprotonated form.

According to the pH dependence of the phen – PMS reaction, two oxidation pathways can be distinguished. The temperature dependencies of both paths were studied and it was found that they are more likely to proceed via oxygen atom transfer. At excess PMS, four consecutive oxidation steps were found in nearly neutral solution. In the early stage of the reaction, the stepwise oxidation results in the formation of phenO, then 1,10-phenanthroline-N,N'-dioxide ($phenO_2$). In contrast to earlier assumptions, the results confirm that special experimental

conditions are not required to produce $phenO_2$, it may form in aqueous solution by using a common oxidant.

Similarly, ESI-MS measurements revealed that the di-N-oxide derivative of tpy ($tpyO_2$) also forms under not strongly acidic conditions and in the presence of slight excess of PMS. However, the kinetics of the overall oxidation reaction was not studied in detail.

7) Összefoglalás

Munkám során a peroxomonoszulfát-ion (PMS) redoxireakcióit tanulmányoztam nitrogéntartalmú heteroaromás ligandumokkal (1,10-fenantrolinnal, phen és 2,2':6',2''-terpiridinnel, tpy) és a megfelelő vas(II)-komplexekkel ($Fe(phen)_3^{2+}$ és $Fe(tpy)_2^{2+}$).

A komplexek reakciói összetett kinetikai viselkedést mutatnak. Közös jellemzője a két rendszernek, hogy egyik oxidáció sem disszociatív úton megy végbe, mindkét esetben a megfelelő vas(III)-komplex ($Fe(phen)_3^{3+}$ és $Fe(tpy)_2^{3+}$) a primer termék, azonban az oxidációkkal párhuzamosan a savkatalizált bomlás is fogyasztja a kiindulási komplexeket.

A reakciók kezdeti szakaszát közös modellel sikerült értelmezni, mely tartalmazza *i)* a vas(II)-komplex savkatalizált bomlását; *ii)* egy ionpár képződését a kiindulási komplexből és az oxidálószerből gyors előegyensúlyi folyamatban; *iii)* az ionpár sebességmeghatározó lépésben történő redoxibomlását a megfelelő Fe(III)-komplexre és szulfátiongyökre; *iv)* valamint egy újabb Fe(II)-komplex $SO_4^{-\bullet}$ általi, gyors oxidációját. Az adduktumot sikerült kimutatni ESI-MS módszerrel a $Fe(phen)_3^{2+}$ – PMS reakcióban.

A reakciók további szakaszában lényeges eltérések mutatkoznak. A $Fe(phen)_3^{2+}$ oxidációjától időben nem különül el a ligandum oxidációja. A fenatrolinból PMS hatására a szerves szubsztrát mono-N-oxidja (phenO) képződik, melyet ESI-MS technikával azonosítottunk. Az oxidált ligandum lassítja a komplex oxidációját (autoinhibítor) és fontos szerepet játszik a szokatlan kinetikai viselkedés kialakulásában feltehetően azért, mert elősegíti a kiindulási komplex átmeneti visszaképződését.

Ezzel szemben a $Fe(tpy)_2^{2+}$ és a PMS reakciója autokatalitikus és a primer oxidációs termék ($Fe(tpy)_2^{3+}$) az autokatalizátor. A kísérleti tapasztalatok alapján feltételezhető, hogy a katalitikus útvonal is egy ionpáron keresztül játszódik le, mely a peroxomonoszulfát-ionból és az autokatalizátorból ($Fe(tpy)_2^{3+}$) alakul ki. Az adduktum bomlása erős oxidálószerek ($Fe(tpy)_2^{4+}$ and $SO_4^{-\bullet}$) képződésével jár, melyek gyors lépésben reagálnak a Fe(II)-komplexszel. Ezek a gyors oxidációs folyamatok a sebességmeghatározó lépés után történnek, azaz a katalitikus oxidáció a $Fe(tpy)_2^{2+}$ komplexre nézve nulladrendű kinetika szerint fogyasztja a

$Fe(tpy)_2^{2+}$ iont. Ezzel a modellel értelmezhető, hogy a kiindulási komplex koncentrációcsökkenése az oxidáció végső fázisában lineáris időfüggést mutat.

A $Fe(tpy)_2^{2+}$ és a PMS közötti reakcióban, jelenlegi ismereteink szerint nem játszik fontos szerepet a ligandum oxidációja. Ennek egyik oka az lehet, hogy az alkalmazott, erősen savas körülmények között a PMS csak rendkívül lassan oxidálja a terpiridint.

Megmutattuk, hogy a Fe(III)-komplexek bomlási útjai kissé eltérnek egymástól. Míg a $Fe(tpy)_2^{3+}$ fogyása csak savkatalizált úton megy végbe, addig a $Fe(phen)_3^{3+}$ egy kis része redoxireakcióban alakul át, melyben a mind $Fe(phen)_3^{2+}$, mind phenO képződik. A képződő phenO autokatalizátora a folyamatnak. A kísérleti tapasztalatokat leíró modellben az egyik köztitermék egy Fe(IV)-tartalmú részecske, melyet ESI-MS módszerrel sikerült kimutatni.

A phenO lényegesen jelentősebb szerepet játszik a $Fe(phen)_3^{2+}/Fe(phen)_3^{3+}$ komplexek reakcióiban, mint a terpiridin-N-oxidok a $Fe(tpy)_2^{2+}/Fe(tpy)_2^{3+}$ rendszerben, ezért előbbi ligandum képződését tanulmányoztuk alaposabban. Erősen savas közegben mindkét ligandum oxidációja csak mono-N-oxidot eredményez bruttó másodrendű kinetikájú lépésben (mely elsőrendű mindkét reaktánsra nézve) és nem történik további oxidáció.

A ligandumok oxidációjának sebessége összetett pH-függést mutat és maximum van a semlegeshez közeli pH-tartományban. Savas körülmények között a protonált szubsztrát nitrogénatomján történő támadás gátolt, és így az N-oxidáció lehetősége lényegesen kisebb. Lúgos közegben pedig a HSO_5^- deprotonálódása lassítja a reakciót, ugyanis a képződő SO_5^{2-} anion kevéssé reaktív oxidációs reakciókban.

A phen – PMS reakció pH-függése alapján két párhuzamos oxidációs út különíthető el. Megvizsgáltuk mindkét oxidációs út hőmérsékletfüggését és meghatároztuk az aktiválási paramétereket. A kapott aktiválási entrópiák gyakorlatilag megegyeznek és nagy negatív értékek, melyek tipikusak a PMS oxigénatom-transzferrel történő reakcióiban. A közel semleges körülmények között végzett kinetikai vizsgálatok során négy konszekutív folyamatot figyeltünk meg, melynek első két lépésében a fenantrolin mono-(phenO) és di-N-oxidja ($phenO_2$)

képződik. Korábban eddig csak egy, extrém körülményeket igénylő módszerrel sikerült előállítani a di-N-oxidot.

Hasonlóképpen a terpiridinből is előállítható a di-N-oxid ($tpyO_2$), melyet ESI-MS módszerrel sikerült azonosítani. Képződéséhez oxidálószer-feleslegre van szükség és kerülni kell az erősen savas közeget, ahol a mono-N-oxid továbbalakulása gátolt.

8) List of publications

Papers related to the thesis

4. Gábor Bellér, Gábor Lente, István Fábián
Detailed kinetics and mechanism of the autocatalytic oxidation of bis(terpyridine)-iron(II) by peroxomonosulfate ion in acidic medium
(beküldésre előkészítve – to be submitted)

3. Gábor Bellér, Gábor Lente, István Fábián
Unexpected formation of 1,10-phenantroline-di-N-oxide under mild conditions: the kinetics and mechanism of the oxidation of 1,10-phenanthroline by peroxomonosulfate ion
(submitted)

2. Gábor Bellér, Gabriella Bátki, Gábor Lente, István Fábián
Unexpected adduct formation in the reaction of peroxomonosulfate ion with the tris-(2,2′-bipyridine)iron(II) and tris-(1,10-phenanthroline)iron(II) complexes
Journal of Coordination Chemistry, **2010,** *63*, 2586-2597.
DOI: 10.1080/00958972.2010.493213; IF: 1.932

1. Gábor Bellér, Gábor Lente, István Fábián
Central role of phenanthroline mono-N-oxide in the decomposition reactions of tris(1,10-phenanthroline)iron(II) and -iron(III) complexes
Inorganic Chemistry, **2010**, *49*, 3968-3970.
DOI: 10.1021/ic902554b; IF: 4.326

UNIVERSITY OF DEBRECEN
UNIVERSITY AND NATIONAL LIBRARY

Registry number: DEENK/173/2015.PL
Subject: Ph.D. List of Publications

Candidate: Gábor Bellér
Neptun ID: O1K6MD
Doctoral School: Doctoral School of Chemistry

List of publications related to the dissertation

Foreign language scientific article(s) in international journal(s) (2)

1. **Bellér, G.**, Bátki, G., Lente, G., Fábián, I.: Unexpected adduct formation in the reaction of peroxomonosulfate ion with the tris-(2,2 '-bipyridine)iron(II) and tris-(1,10-phenanthroline)iron(II) complexes.
   J. Coord. Chem. 63 (14/16), 2586-2597, 2010. ISSN: 0095-8972.
   DOI: http://dx.doi.org/10.1080/00958972.2010.493213
   IF:1.932

2. **Bellér, G.**, Lente, G., Fábián, I.: Central Role of Phenanthroline Mono-N-oxide in the Decomposition Reactions of Tris(1,10-phenanthroline)iron(II) and -iron(III) Complexes.
   Inorg. Chem. 49 (9), 3968-3970, 2010. ISSN: 0020-1669.
   DOI: http://dx.doi.org/10.1021/IC902554b
   IF:4.325

Total IF of journals (all publications): 6,257
Total IF of journals (publications related to the dissertation): 6,257

The Candidate's publication data submitted to the iDEa Tudóstér have been validated by DEENK on the basis of Web of Science, Scopus and Journal Citation Report (Impact Factor) databases.

03 September, 2015

Address: 1 Egyetem tér, Debrecen 4032, Hungary Postal address: Pf. 39. Debrecen 4010, Hungary
Tel.: +36 52 410 443 Fax: +36 52 512 900/63847 E-mail: publikaciok@lib.unideb.hu, ▫ Web: www.lib.unideb.hu

9) References

[1] G. Lente, J. Kalmár, Z. Baranyai, A. Kun, I. Kék, D. Bajusz, M. Takács, L. Veres, I. Fábián, *Inorg. Chem.*, **2009**, *48*, 1763-1773.

[2] J. Kalmár, G. Lente, I. Fábián, *Inorg. Chem.*, **2013**, *52*, 2150-2156.

[3] H. Hussain, I. R. Green, I. Ahmed, *Chem. Rev.*, **2013**, *113*, 3329-3371.

[4] W. Zhaohui, R. T. Bush, L. A. Sullivan, C. Chuncheng, L. Jianshe, *Environ. Sci. Technol.*, **2014**, *48*, 3978-3985.

[5] G. P. Anipsitakis, D. D. Dionysiou. *Environ. Sci. Technol.*, **2003**, *37*, 4790-4797.

[6] X.-Y. Lou, Y.-G. Guo, D.-X. Xiao, Z.-H. Wang, S.-Y. Lu, J.-S. Liu, *Environ. Sci. Pollut. Res.*, **2013**, *20*, 6317-6323.

[7] R. J. Durante, S. J. Lee, T. P. Tufano, Y. C. Park, J. W. Lee, S. Y. Lee, H. K. Lee, Y. J. Lee, S. H. Jang, US20100252530, 2010.

[8] F. Melin, S. Choua, M. Bernard, P. Turek, J. Weiss, *Inorg. Chem.*, **2006**, *45*, 10750-10757.

[9] T. Dhanalakshmi, M. Bhuvaneshwari, M. Palaniandavar, *J. Inorg. Biochem.*, **2006**, *100*, 1527-1534.

[10] E. Kianmehr, M. Rezaeefard, M. R. Khalkhali, K. M. Khan, *RSC Adv.*, **2014**, *4*, 13764-13767.

[11] J. Chen, N. Takenaka, *Chem. Eur. J.*, **2009**, *15*, 7268-7276.

[12] M. MacCoss, E. K. Ryu, R. S. White, *J. Org. Chem.*, **1980**, *45*, 788-794.

[13] A. F. Martins, S. V. Eliseeva, H. F. Carvalho, J. M. C. Teixeira, C. T. B. Paula, P. Hermann, C. Platas-Iglesias, S. Petoud, É. Tóth, C. F. G. C. Geraldes, *Chem. Eur. J.*, **2014**, *20*, 14834-14845.

[14] D. E. Chavez, M. A. Hiskey, D. L. Naud, *Propellants Explos. Pyrotech.*, **2004**, *29*, 209-215.

[15] Q. Wu, W. Zhu, H. Xiao, *RSC Adv.*, **2014**, *4*, 53000-53009.

[16] M. D. Farahani, B. Honarparvar, F. Albericio, G. E. M. Maguire, T. Govender, P. I. Arvidsson, H. G. Kruger, *Org. Biomol. Chem.*, **2014**, *12*, 4479-4490.

[17] F. Epifano, M. C. Marcotullio, M. Curini, *Trends Org. Chem.*, **2003**, *10*, 21-34.

[18] A. Chrobok, *Tetrahedron.* **2010**, *66*, 6212-6216.

[19] B. R. Travis, B. P. Ciaramitaro, B. Borhan, *Eur. J. Org. Chem*. **2002**, *20*, 3429-3434.

[20] B. M. Trost, R. Braslau, *J. Org. Chem*. **1988**, *53*, 532-537.

[21] W. Zhu, W. T. Ford, *J. Org. Chem.* **1991**, *56*, 7022-7026.

[22] T. Balakrishnan, S. Damodarkumar, *J. Appl. Polym. Sci.*, **2000**, *76*, 1564-1571.

[23] R. S. Kannas, M. S. Ramachandran, *Int. J. Chem. Kinet.*, **2003**, *35*, 475-483.

[24] G. Ragukumar, P. Andal, M. Murugavelu, C. Lavanya, M.S. Ramachandran, *J. Mol. Cat. A-Chem.*, 2014, 390, 22-28.

[25] R. J. Kennedy, A. M. Stock, *J. Org. Chem*. **1960**, *25*, 1901-1906.

[26] S. E. McKay, J. A. Sooter, S. G. Bodige, S. C. Blackstock, *Heterocycl. Commun.*, **2011**, 7, 307-312.

[27] C. E. Mixan, R. G. Pews, *J. Org. Chem*. **1977**, *42*, 1869-1871.

[28] T. W. Bell, Y.-M. Cho, A. Firestone, K. Healy, J. Liu, R. Ludwig, S. D. Rothenberger, *Org. Synth.* **1990**, *69*, 226-237.

[29] M. Göbel, K. Karaghiosoff, T. M. Klapötke, D. G. Piercey, J. Stierstorfer, *J. Am. Chem. Soc.*, **2010**, *132*, 17216-17226

[30] A. Agrawal, R. Sailani, B. Gupta, C. L. Khandelwal, P. D. Sharma, *J. Korean Chem. Soc.*, **2012**, 56, 212-216.

[31] N. N. Greenwood, A. Earnshaw: *Chemistry of the Elements*, 2nd Ed., Butterworth-Heinemann, Oxford, UK, **1997**, p. 713.

[32] W. V. Steele, E. H. Appelman, *J. Chem. Thermodynamics*, **1982**, *14*, 337-344.

[33] J. M. Anderson, J. K. Kochi, *J. Am. Chem. Soc*. **1970**, *92*, 1651-1659.

[34] R. C. Thompson, P. Wieland, E. H. Appelman, *Inorg. Chem.* **1979**, *18*, 1974-1977.

[35] E. A. Betterton, *Environ. Sci. Technol.* **1992**, *26*, 527-532.

[36] C. Gella, È. Ferrer, R. Alibés, F. Busqué, P. de March, M. Figueredo, J. Font, *J. Org. Chem.*, **2009**, *74*, 6365-6367.

[37] R. C. Thompson, *Inorg. Chem*. **1981**, *20*, 3745-3748.

[38] B. C. Gilbert, J. K. Stell, *J. Chem. Soc., Perkin Trans. 2*, **1990**, *8*, 1281-1288.

[39] D. L. Ball, J. O. Edwards, *J. Am. Chem. Soc.*, **1956**, *78*, 1125-1129.

[40] E. Koubek, J. E. Welsch, *J. Org. Chem*., **1968**, *33*, 445-446.

[41] D. F. Evans, M. W. Upton, *J. Chem. Soc. Dalton Trans.*, **1985**, 1151-1153.

[42] R. C. Thomson, *Inorg. Chem*., **1981**, *20*, 1005-1010.

[43] B. C. Gilbert, J. K. Stell, *J. Chem. Soc., Faraday Trans*., **1990**, *86*, 3261-3266.

[44] G. P. Anipsitakis, D. D. Dionysiou, *Environ. Sci. Technol*., **2004**, *38*, 3705-3712.

[45] L. Pochtarenko, I. Zilbermann, D. Shamir, D. Meyerstein, *J. Coord. Chem*., **2013**, *66*, 4355-4362.

[46] J. A. McCleverty, T. J. Meyer: *Comprehensive Coordination Chemistry II.*, vol. 1, Elsevier, Oxford, UK, **2003**, pp. 25-39.

[47] A. Bencini, V. Lippolis, *Coord. Chem. Rev.*, **2010**, *254*, 2096-2180.

[48] E. J. Corey, A. L. Borror, T. Foglia, *J. Org. Chem.*, **1965**, *30*, 288-290.

[49] R. H. Beer, J. Jimenez, R. S. Drago, *J. Org. Chem.*, **1993**, *58*, 1746-1747.

[50] M. J. Fachsel, C. V. Banks, *J. Am. Chem. Soc.*, **1966**, *88*, 878-884.

[51] S. Ishiguro, H. Wada, H. Ohtaki, *Bull. Chem. Soc. Jpn*., **1985**, *58*, 932-937.

[52] C. Bretti, F. Crea, C. De Stefano, S. Sammartano, *Fluid Phase Equilib.*, **2008**, *272*, 47-52.

[53] D. W. Margerum, R. I. Bystroff, C. V. Banks, *J. Am. Chem. Soc.*, **1956**, *78*, 4211-4217.

[54] S. Anbu, S. Shanmugaraju, M. Kandaswamy, *RSC Adv.*, **2012**, *2*, 5349-5357.

[55] T. S. Lobana, S. Indoria, H. Kaur, D. S. Arora, A. K. Jassal, J. P. Jasinski, *RSC Adv.*, **2015**, *5*, 14916-14936.

[56] J. Shakeri, H. Farrokhpour, H. Hadadzadeh, M. Joshaghani, *RSC Adv.*, **2015**, *5*, 41125-41134.

[57] Y. N. Chen, Y. Fan, J. Ni, *Dalton Trans.*, **2008**, *5*, 573-581.

[58] F. Linsker, R. L. Evans, *J. Am. Chem. Soc.*, **1946**, *68*, 403.

[59] J. E. Dickeson, L. A. Summers, *Aust. J. Chem.*, **1970**, *23*, 1023-1027.

[60] F. L. Wimmer, S. Wimmer, *Org. Prep. Proced. Int.*, **1983**, *15*, 368-369.

[61] R. Kumar, P. Mathur, *RSC Adv.*, **2014**, *4*, 33190-33193.

[62] M. V. Mirífico, E. L. Svartman, J. A. Caram, E. J. Vasini, *J. Electroanal. Chem.*, **2004**, *566*, 7-13.

[63] R. Balicki, J. Golinski, *Synt. Comm.*, **2000**, *30*, 1529-1534.

[64] I. Murase, *Nippon Kagaku Zasshi*, **1956**, *77*, 682-685.

[65] D. Wenkert, R. B. Woodward, *J. Org. Chem.*, **1983**, *48*, 283-289.

[66] F. H. Case, *J. Org. Chem.*, **1962**, *27*, 640-641.

[67] G. Maerker, F. H. Case, *J. Am. Chem. Soc.*, **1958**, *80*, 2745-2748.

[68] R. D. Gillard, *Inorg. Chim. Acta*, **1981**, *53*, 173.

[69] R. D. Gillard, *Inorg. Chim. Acta*, **1989**, *156*, 155.

[70] S. Rozen, S. Dayan, *Angew. Chem.*, **1999**, *38*, 3471-3473.

[71] M. Carmeli, S. Rozen, *J. Org. Chem.*, **2005**, *70*, 2131-2134.

[72] R. G. Panari, A. L. Harihar, S. T. Nandibewoor, *J. Phys. Org. Chem.*, **1999**, *12*, 340-346.

[73] P. D. Pol, R. T. Mahesh, S. T. Nandibewoor, *React. Kinet. Catal. Lett.*, **2004**, *81*, 113-119.

[74] U. S. Schubert, A. Winter, G. R. Newkome: *Terpyridine-based Materials: For Catalytic, Optoelectronic and Life Science Applications*, Wiley-VCH, Weinheim, Germany, **2011**.

[75] R. B. Martin, J. A. Lissfelt, *J. Am. Chem. Soc.*, **1956**, *78*, 938-940.

[76] D. I. Bullock, P. V. G. Simpson, *J. Chem. Soc., Faraday Trans I.*, **1981**, *77*, 1991-1997.

[77] P. O'D. Offenhartz, P. George, G. P. Haight, *J. Phys. Chem.*, **1963**, *67*, 116-118.

[78] E. C. Constable, *Chem. Soc. Rev.*, **2007**, *36*, 246-253.

[79] E. C. Constable, *Adv. Inorg. Chem. Radiochem.*, **1986**, *30*, 69-121.

[80] J. C. Tomkinson, R. J. P. Williams, *J. Chem. Soc.*, **1958**, 2010-2018.

[81] W. W. Brandt, J. P. Wright, *J. Am. Chem. Soc.*, **1954**, *76*, 3082-3083.

[82] R. P. Thummel, Y. Jahng, *J. Org. Chem.*, **1985**, *50*, 3635-3636

[83] R. A. Fallahpour, M. Neuburger, *Eur. J. Org. Chem.*, **2001**, 1853-1856.

[84] W. L. Wong, W. S. Lee, H. L. Kwong, *Tetrahedron-Asymmetr.*, **2002,** *13*, 1485-1492.

[85] T. S. Lee, I. M. Kolthoff, D. L. Leussing, *J. Am. Chem. Soc.*, **1948**, *70*, 2348-2352.

[86] T. S. Lee, I. M. Kolthoff, D. L. Leussing, *J. Am. Chem. Soc.*, **1948**, *70*, 3596-3600.

[87] T. S. Lee, I. M. Kolthoff, D. L. Leussing, *J. Am. Chem. Soc.*, **1950**, *72*, 2173-2177.

[88] W. W. Brandt F. P. Dwyer, E. C. Gyarfas, *Chem. Rev.*, **1954**, *54*, 959-1017.

[89] G. F. Smith, F. P. Richter, *Ind. Eng. Chem. Anal. Ed.*, **1944**, *16*, 540-541.

[90] D. W. Margerum, *J. Am. Chem. Soc.*, **1957**, *79*, 2728-2733.

[91] J. E. Dickens, F. Basolo, H. M. Neumann, *J. Am. Chem. Soc.*, **1957**, *79*, 1286-1290.

[92] M. Kimura, G. Wada, *Inorg. Chem.*, **1978**, *17*, 2239-2242.

[93] J. Grodkowski, P. Neta, C. J. Schlesener, J. K. Kochi, *J. Phys. Chem.*, **1985**, *89*, 4373-4378.

[94] J. H. Penn, R. C. Plants, A. Liu, *Chem. Commun.*, **1999**, 2359-2360.

[95] L. Hegedűs, H. D. Försterling, L. Onel, M. Wittman, Z. Noszticziusz, *J. Phys. Chem. A*, **2006**, *110*, 12839-12844.

[96] G. Nord, B. Pedersen, E. Bjergbakke, *J. Am. Chem. Soc*., **1983**, *105*, 1913-1919.

[97] E. Eichler, A. C. Wahl, *J. Am. Chem. Soc.*, **1958**, *80*, 4145-4149.

[98] N. Sutin, B. M. Gordon, *J. Am. Chem. Soc.*, **1961**, *83*, 70-73.

[99] M. H. Ford-Smith, N. Sutin, *J. Am. Chem. Soc.*, **1961**, *83*, 1830-1834.

[100] B. Z. Shakhashiri, G. Gordon, *J. Am. Chem. Soc.*, **1969**, *91*, 1103-1107.

[101] B. Z. Shakhashiri, G. Gordon, *Inorg. Chem*., **1968**, *7*, 2454-2456.

[102] R. J. Campion, N. Purdie, N. Sutin, *Inorg. Chem*., **1964**, *3*, 1091-1094.

[103] G. Dulz, N. Sutin, *Inorg. Chem.*, **1963**, *2*, 917-921.

[104] H. Diebler, N. Sutin, *J. Phys. Chem.*, **1964**, *68*, 174-180.

[105] A. A. Green, J. O. Edwards, P. Jones, *Inorg. Chem*., **1966**, *5*, 1858-1862.

[106] M. Cyfert, *Inorg. Chim. Acta*, **1985**, *98*, 25-28.

[107] J. H. Espenson, E. L. King, *J. Am. Chem. Soc*., **1963**, *85*, 3328-3333.

[108] J. Burgess, R. H. Prince, *J. Chem. Soc. A*, **1966**, 1772-1775.

[109] S. Raman, C. H. Brubaker, *J. Inorg. Nucl. Chem.*, **1969**, *31*, 1091-1099.

[110] J. Burgess, R. H. Prince, *J. Chem. Soc. A*, **1970**, 2111-2113.

[111] E. Kőrös, M. Burger, A. Kis, *React. Kinet. Catal. L.*, **1974**, *1*, 475-480.

[112] A. B. Rovinskii, A. M. Zhabotinskii, *React. Kinet. Catal. L.*, **1979**, *11*, 205-208.

[113] K. Showalter, *J. Phys. Chem.*, **1981**, *85*, 440-447.

[114] V. A. Vavilin, P. V. Gulak, A. M. Zhabotinskii, A. N. Zaikin, *Izv. Akad. Nauk SSSR, Ser. Khim.*, **1969**, *18*, 2467.

[115] M. Melichercik, J. Treindl, *J. Phys. Chem.*, **1989**, *93*, 7654-7659.

[116] M. Mehrotra, R. N. Mehrotra, *Polyhedron*, **2008**, *27*, 2151-2156.

[117] L. H. N. Cooper, *Proc. Roy. Soc. B*, **1935**, *118*, 419-438.

[118] H. Hofmeier, U. S. Schubert, *Chem. Soc. Rev*., **2004**, *33*, 373-399.

[119] D. J. Robinson, C. H. L. Kennard, *Aust. J. Chem*., **1966**, *19*, 1285-1286.

[120] W. M. Reiff, N. E. Erickson, W. A. Baker, *Inorg. Chem*., **1969**, *8*, 2019-2021.

[121] J. A. Broomhead, F. P. Dwyer, *Aust. J. Chem*., **1961**, *14*, 250-252.

[122] R. H. Holyer, C. D. Hubbard, S. F. A. Kettle, R. G. Wilkins, *Inorg. Chem*., **1966**, *5*, 622-625.

[123] K. Kamata, A. Suzuki, Y. Nakai, H. Nakazawa, *Organometallics*, **2012**, *31*, 3825−3828.

[124] A. M. Tondreau, C. C. H. Atienza, J. M. Darmon, C. Milsmann, H. M. Hoyt, K. J. Weller, S. A. Nye, K. M. Lewis, J. Boyer, J. G. P. Delis, E. Lobkovsky, P. J. Chirik, *Organometallics*, **2012**, *31*, 4886-4893.

[125] W. M. Reiff, W. A. Baker, N. E. Erickson, *J. Am. Chem. Soc*., **1968**, *90*, 4794-4780.

[126] R. Farina, R. Hogg, R. G. Wilkins, *Inorg. Chem.*, **1968**, *7*, 170-172.

[127] J. Burgess, M. V. Twigg, *J. Chem. Soc. Dalton Trans.*, **1974**, 2032-2036.

[128] Y. W. D. Chen, K. S. V. Santhanam, A. J. Bard, *J. Electrochem. Soc*., **1981**, *128*, 1460-1467.

[129] H. Tomiyasu, G. Gordon, *Ozone Sci. Eng*., **1989**, *11*, 59-68.

[130] T. Satyanarayana, N. R. Anipindi, V. Subbiah, M. W. Pandit, *Ind. J. Chem. A*, **1992**, *31*, 125-127.

[131] T. Satyanarayana, N. R. Anipindi, *React. Kinet. Catal. Lett.*, **1992**, *47*, 111-118.

[132] T. Satyanarayana, N. R. Anipindi, *Transition Met. Chem.*, **1992**, *17*, 533-534.

[133] T. Satyanarayana, N. R. Anipindi, *React. Kinet. Catal. Lett.*, **1992**, *47*, 333-341.

[134] R. N. Reddy, T. Satyanarayana, A. N. Rao, *Oxid. Commun.*, **2010**, *33*, 864-869.

[135] R. N. Reddy, T. Satyanarayana, N. R. Anipindi, *Oxid. Commun.*, **2011**, *34*, 533-539.

[136] K. V. Reddy, T. Satyanarayana, N. R. Anipindi, R. N. Reddy, *Oxid. Commun.*, **2011**, *34*, 38-43.

[137] A. K. Covington, R. G. Bates, R. A. Durst, *Pure Appl. Chem.*, **1985**, *57*, 531-542.

[138] H. Irving, G. Miles, L.D. Pettit, *Anal. Chim. Acta*, **1967**, *38*, 475-488.

[139] K. Szabó, I. Nagypál, I. Fábián, *Talanta*, **1983**, *30*, 801-804.

[140] I. Fábián, G. Lente, *Pure Appl. Chem.*, **2010**, *82*, 1957-1973.

[141] Scientist, Version 2.0, Micromath Software, Salt Lake City, UT, USA, **1995**.

[142] MatLab for Windows, Version 4.2c1, The Mathworks, Inc., Natick, MA, USA, **1994**.

[143] G. Peintler, ZiTa: A comprehensive program package for fitting parameters of chemical reaction mechanisms, version 4.1; Institute of Chemistry JATE: Szeged, Hungary, **1997**.

[144] Specfit/32^{TM}, Global Analysis System, Version 3.0, Spectrum Software Associates, Marlborough, MA, USA

[145] I. Kerezsi, G. Lente, I. Fábián, *Dalton Trans.*, **2006**, 955-960.

[146] G. Peintler, I. Nagypál, A. Jancsó, I. R. Epstein, K. Kustin, *J. Phys. Chem. A*, **1997**, *101*, 8013-8020.

[147] J. H. Espenson. *Chemical Kinetics and Reaction Mechanisms*, 2nd Edn., McGraw-Hill, New York, USA, **1995**, pp. 20-25.

[148] L. A. Summers, *Adv. Heterocyclic Chem.*, **1978**, *22*, 1-69.

[149] A. Simon, Cs. Ballai, G. Lente, I. Fábián, *New J. Chem.*, **2011**, *35*, 235-241.

[150] G. Lente. *Deterministic Kinetics in Chemistry and Systems Biology*, Springer, New York, Heidelberg, Dordrecht, London, **2015,** pp 48-53, 78-79.

[151] M. Galajda, T. Fodor, M. Purgel, I. Fábián, *RSC Adv.*, **2015**, *5*, 10512-10520.

[152] G. Nord, O. Wernberg, *J. Chem. Soc., Dalton Trans.*, **1972**, 866-868.

[153] G. Nord, O. Wernberg, *J. Chem. Soc., Dalton Trans.*, **1975**, 845-849.

[154] E. T. Urbansky, *J. Chem. Educ.*, **2001**, *78*, 921-923.

[155] G. Lente, *J. Chem. Educ.*, **2004**, *81*, 32.

[156] R. M. Fuoss, *J. Am. Chem. Soc.*, **1958**, *80*, 5059-5061.

[157] B. Kormányos, G. Peintler, A. Nagy, I. Nagypál, *Int. J. Chem. Kinet.*, **2008**, *40*, 114-124.